DEPOSITION OF TRACE METAL-CONTAINING AEROSOLS ON SMOOTH, FLAT SURFACES AND ON WILD OAT GRASS (*Avena fatua*)

Thesis by
Cliff Ian Davidson

In Partial Fulfillment of the Requirements

for the Degree of

Doctor of Philosophy

California Institute of Technology

Pasadena, California

1977

(Submitted April 25, 1977)

to Megan

ACKNOWLEDGMENTS

My foremost acknowledgment is extended to Professor Sheldon Friedlander, for his continual inspiration and technical assistance. His willingness to spend hour after hour in technical discussion is greatly appreciated; without such guidance, this research would not have been possible.

Also appreciated is the assistance and advice of Drs. James Huntzicker and Clair Patterson. Their suggestions were invaluable during the initial phases of this work.

The following individuals are also thanked for their valuable technical assistance: Drs. Karl Bell, John Brock, Patrick Delattre, Rick Flagan, Steve Heisler, Susanne Hering, Rudy Husar, Gary Leal, Toni Miguel, Jim Morgan, Paul Roberts, John Seinfeld and Warren White. Thanks are also due to Messrs. Ken Bencala, Glen Cass, Don Kuehne, Howard Liljestrand, Larry McClellan, Pete McMurry, Alan Moskowitz, Jim Pankow, Tom Peterson, Daryl Roberts, Stan Sander, Jim Taylor, and Mmes. Sylvia Garcia, Pam McMurry, and Joan Roach.

The assistance of Messrs. Dave Byrum, Elton Daly, and Joe Fontana in equipment construction and technical drawing is greatly appreciated.

Thanks are due Mmes. Megan Davidson, Helen Fabel, Elaine Granger, and Carol Storm for typing assistance. Mmes. Rayma Harrison and Diane Masumoto are also thanked for their help in the Keck reference room.

A special acknowledgment is made to my officemates, Ms. Lisa Anderson and Mr. Pete McMurry, for their delightful (and sometimes necessary) distracting conversations.

The efforts of those who were instrumental in obtaining funding for this research are greatly appreciated, including Drs. F.S. Buffington, Sheldon Friedlander and Jack McKee. This work was supported by U.S. Environmental Protection Agency Grant No. 68-03-0434 and by U.S. Public Health Service Grant No. 5-T01-ES0004.

I would also like to thank my parents, and my brothers and their wives for their continual encouragement.

Finally, I would like to thank my wife Megan for her love and especially for her friendship which were so needed during the darkest hours and the brightest days of this project.

ABSTRACT

A new model for the dry deposition of aerosol particles on fields of vegetation has been developed. The model, which includes diffusion, sedimentation, and impaction as transport mechanisms, has been applied to deposition on a field of wild oat grass, Avena fatua. The model was tested experimentally for the diffusion range, and applied to predict the deposition of lead for all mechanisms for typical wind conditions. Inputs to the model include the airborne chemical species distribution with respect to particle size, the windfield above and within the canopy, and details of the vegetation elements.

Deposition is considered to be a two-step process, namely transport from the open atmosphere into the vegetation followed by filtration by the vegetation elements. Each step is described by an expression for particle flux. The equation for transport from the atmosphere relates the flux to the sedimentation velocity and the Brownian and eddy diffusivities. This relation is assumed to apply both above and within the canopy. The filtration equation is used only within the canopy, incorporating either convective diffusion or impaction. The two equations are solved simultaneously for the effective concentration sink and particle flux.

According to the model, the deposition of unit density, spherical particles with diameters smaller than 0.001 μm and larger than 10 μm is controlled by the rate at which particles are delivered to the canopy. For particles with diameters between these values, the rate of

deposition is controlled by relatively inefficient filtration within the canopy.

The model was tested by measuring profiles of condensation nuclei above a field of Avena fatua. The atmospheric transport equation was used with the profiles to determine the flux. This value compared well with fluxes calculated by solving the equations for atmospheric transport and filtration simultaneously. The latter calculation used only one concentration measurement at a known height rather than the entire profile.

The deposition of lead, zinc, and cadmium on flat, smooth surfaces exposed to the free atmosphere was also measured. Simultaneous isokinetic measurements of the airborne size distributions of these trace metals provided data which were used to calculate the sedimentation fluxes. About 70% of the total mass deposition of each trace metal was due to sedimentation of particles with aerodynamic diameter greater than 10 μm. The airborne fractions of these large particles for lead, zinc, and cadmium were 17%, 32%, and 37%, respectively. Because large airborne particles controlled the mass deposition, isokinetic sampling was essential.

The isokinetically measured distribution of lead with respect to particle size was used to calculate deposition on a field of Avena fatua. Ninety percent of the lead deposition resulted from impaction of particles greater than 10 μm. As with the flat, smooth surfaces, the relatively high concentrations of small airborne

lead particles did not contribute significantly to mass deposition.

Comparing the smooth surface data with the calculations for Avena fatua fields suggested that the deposition of lead on such fields is two to three times greater than on a flat, smooth surface.

TABLE OF CONTENTS

		Page
INTRODUCTION		1
CHAPTER I	A FILTRATION MODEL FOR AEROSOL DRY DEPOSITION: APPLICATION TO TRACE METAL DEPOSITION FROM THE ATMOSPHERE	5
	Abstract	5
	Introduction	6
	Theory	12
	Region 1 Transport	14
	Region 2 Transport	17
	Steady-State Transport	19
	Experimental Measurements	22
	Flat Plate Experiments	23
	Cylinder Experiments	24
	Grassy Field Experiments: Condensation Nuclei Profiles	27
	Deposition Velocity Curves	33
	Deposition in Fields of Avena fatua: Comparison with Experiment	35
	Conclusions	42
	Appendix: Description of Avena fatua	44
CHAPTER II	THE DEPOSITION OF TRACE METAL-CONTAINING PARTICLES ON FLAT, SMOOTH SURFACES IN THE LOS ANGELES AREA	46
	Abstract	46
	Introduction	47
	Theory	48
	Source Size Distributions: A Literature Survey	50

Page

Lead 50

Zinc and Cadmium 50

Ambient Size Distributions: A Literature Survey 51

Lead 51

Zinc and Cadmium 51

Ambient Size Distributions: Isokinetic Experiments 52

Deposition of Trace Metals 59

Conclusions 66

APPENDIX I: CALIBRATION OF THE MODIFIED ANDERSEN IMPACTOR 69

APPENDIX II: THE DEPOSITION OF SULFATES 79

Introduction 79

Theory 80

Experiments: Presentation of Data 89

Flat Surface Experiments 89

Pipe Experiments 94

Size Distributions 96

Experiments: Discussion of Data 96

Conclusions 106

APPENDIX III: TRACE METAL AND CONDENSATION NUCLEI DEPOSITION DATA 107

Deposition of Lead, Zinc, and Cadmium on the Keck Laboratory Roof 107

Deposition of Nickel and Vanadium on the Keck Laboratory Roof 111

Deposition of Trace Metals Throughout Southern California 117

Page

Condensation Nuclei Concentration Data 130

APPENDIX IV: RESUSPENSION EXPERIMENTS 132

APPENDIX V: WIND PROFILES 138

APPENDIX VI: EXPERIMENTAL ERRORS 144

CONCLUSIONS 151

REFERENCES 153

LIST OF TABLES

		Page
Table I-1	Calculated and measured trace metal fluxes on vertically oriented cylinders.	26
Table I-2	Result of simultaneous solutions of Equations I-2 and I-14 by an iterative technique for the flux J and concentration sink z_s.	32
Table I-3	Calculated deposition fluxes of Pb on Avena fatua.	37
Table II-1	Percentage of mass greater than 10 μm aerodynamic diameter for nonisokinetic runs (1972, 1974) and isokinetic runs (1975).	55
Table II-2	Dry deposition velocities for lead from several investigations.	60
Table II-3	Calculated and measured fluxes to flat surfaces on the roof of W. M. Keck Laboratory at Caltech.	63
Table II-4	Airborne concentrations during the two isokinetic impactor experiments.	65
Table A I-1	Values of mass mean cutoff diameters d_{pm} and the standard deviations, for the Andersen impactor efficiency curves.	73
Table A II-1	Deposition of sulfates on flat surfaces facing upward and downward, as a function of capacitor charging voltage.	93
Table A II-2	Deposition of sulfates during day and night, and on electrically grounded and ungrounded strips.	95
Table A II-3	Description and results of sulfate pipe deposition experiments.	97
Table A II-4	Sulfate size distribution data for July 27, 1976.	101
Table A II-5	Calculated and measured deposition fluxes for the July 1976 sulfate pipe deposition experiment.	104
Table A III-1	Deposition of Pb, Zn, and Cd on flat teflon plates during several experiments on the Keck Laboratory roof.	108
Table A III-2	Size distribution information for the May 1975 and July 1975 sedimentation experiments.	112

Page

Table A III-3 Measured and calculated deposition fluxes for nickel and vanadium on flat teflon plates for the July 1975 experiment. 118

Table A III-4 Deposition of Ni and V on flat teflon plates during the July 1975 experiment. 119

Table A III-5 Deposition of lead, zinc, cadmium, nickel, and iron on flat teflon plates at several Southern California sites. 125

Table A III-6 Estimates of the lead flux in three regions contiguous to Los Angeles, due only to automotive traffic within each region. 129

Table A III-7 Condensation nuclei concentration data above a field of Avena fatua. 131

Table A IV-1 Concentrations of large particles as functions of height above a field of 2 cm tall grass. 135

LIST OF FIGURES

		Page
Figure I-1	Deposition may be considered a two-step process.	13
Figure I-2	Hypothetical curves of concentration versus height.	15
Figure I-3	Airborne concentration of condensation nuclei as a function of height above the ground in a residential area of Los Angeles near Occidental College, June 1974.	29
Figure I-4	The points of Figure I-3 plotted on a logarithmic scale.	30
Figure I-5	Calculated values of deposition velocity as a function of particle size for heights of 150 cm and 400 cm above the ground, for a field of Avena fatua, wild oat grass.	34
Figure I-6	Particles deposited on a 0.2 cm diameter stem of Avena fatua, 40 cm above the ground.	38
Figure I-7	Particles deposited on a small stalk connecting seed pods with the main stem.	39
Figure I-8	Fine hairs on the seed pods, which are efficient particle collectors.	40
Figure I-9	Close-up view of the seed pod hairs of Figure I-8.	41
Figure I-10	A typical specimen of Avena fatua, wild oat grass.	45
Figure II-1	Normalized size distributions for lead, zinc, and cadmium for the May 1975 experiment.	56
Figure II-2	Normalized size distributions for lead, zinc, and cadmium for the July 1975 experiment.	57
Figure A I-1	Efficiency of collection versus particle diameter for the Andersen impactor, stages 0 through 7.	70
Figure A I-2	Number and mass distributions for stage A of the modified Andersen impactor.	75
Figure A I-3	Number and mass distributions for stage B of the modified Andersen impactor.	76

		Page
Figure A I-4	Number and mass distributions for stage 1 of the regular Andersen impactor	77
Figure A II-1	Deposition of particles on a smooth, horizontal plate from a horizontal wind.	81
Figure A II-2	Deposition of particles on a smooth, horizontal plate from a vertical wind.	83
Figure A II-3	Mounting scheme for stainless steel strips for measuring sulfate deposition.	90
Figure A II-4	The recovery of two standard solutions of sulfate as a function of capacitor charging voltage.	91
Figure A II-5	Ambient size distribution data for sulfates, obtained on July 27, 1976 on the Keck Laboratory roof.	100
Figure A III-1	Deposition of lead and zinc on flat teflon plates as a function of height above the roof of Keck Laboratory.	110
Figure A III-2	Airborne size distributions for nickel and vanadium.	116
Figure A III-3	Deposition measurement sites.	123
Figure A IV-1	Variations of large particle concentration with height above the Caltech athletic field.	136
Figure A V-1	Wind profile above a field of 65 cm tall Avena fatua, located in a residential area of Los Angeles near Occidental College.	139
Figure A V-2	Wind profile above a field of 50 cm tall Avena fatua in Ernest Debs Park, Los Angeles.	140
Figure A V-3	Wind profile above the Caltech athletic field, obtained during one of the resuspension experiments.	141
Figure A V-4	Wind profile above the roof of the Keck Laboratory penthouse.	142

INTRODUCTION

The deposition of trace metal-containing particles from the atmosphere has not been previously studied in detail. Some trace metal deposition data exist in the literature, but these studies have presented only limited data from which it is difficult to generalize. It is important, however, to obtain accurate information on the transport of trace metals to surfaces. For example, information on particle residence time in the atmosphere can be obtained from deposition studies. The effects of sources on downwind regions is linked to deposition rates. Trace metal deposition on vegetation can harm animals feeding on the plants. Deposition rates are also useful when setting up tracer studies.

Although thorough trace metal deposition studies have not been undertaken, the deposition of other particles has been examined. Most of these studies can be divided into two categories:

1) controlled wind tunnel experiments using monodisperse particles, and
2) field experiments where little data have been obtained on the particle size distribution or the detailed structure of the surface.

Studies of the first type have yielded empirical and theoretical models for particle deposition under controlled conditions. There has been little verification of these theories for the free atmosphere. Studies of the second type have not provided sufficient information to generalize to the wide variety of ambient conditions.

This research involves field experiments where sufficient data were obtained to allow development of a theoretical predictive model. Inputs to this model include the windfield, the particle size distribution, and details of the surface structure. The surface structure is especially important, and many previous models attempted to describe the deposition using only gross features of the surface roughness.

The work about to be described incorporates two basic topics. First, the deposition from the free atmosphere of particles on Avena fatua, wild oat grass, is discussed. A model is presented in which deposition is viewed as a two-step process: atmospheric transport into the vegetated canopy followed by filtration by the roughness elements of the vegetation. Experimental data incorporating lead and condensation nuclei are presented.

Second, detailed ambient size distribution data for lead, zinc, and cadmium are used to predict the deposition of these elements on smooth, flat surfaces. Experimental deposition data are also presented. It is expected that these smooth surface deposition fluxes will be lower limits to the fluxes on natural surfaces.

Chapters I and II present the information on the two major topics. In addition to these research studies, several minor experiments have been conducted. These experiments, as well as additional detailed data from the first two chapters, are discussed in the appendices.

Appendix I describes the calibration of the Andersen impactor, which was used to obtain the trace metal size distributions. The deposition of sulfates, which was briefly examined, is discussed in

Appendix II. Detailed data for the trace metal and condensation nuclei measurements are presented in Appendix III, along with some additional discussion. Appendix IV presents some limited data and discussion of resuspension. Wind profile measurements are presented in Appendix V, while experimental uncertainties are discussed in Appendix VI.

The most important experimental results are the trace metal size distribution data, obtained isokinetically. These distributions show considerable mass in particles larger than 10 microns aerodynamic diameter. Data in the literature on trace metals were obtained nonisokinetically, and show very little mass in these large particles due to inaccurate sampling. These particles are also the most important contributors to total trace metal mass deposition on smooth and vegetated surfaces. Since only a fraction of the total airborne concentration of the trace metals contributes significantly to deposition, the traditional concept of applying a deposition velocity to the total concentration may lead to inaccurate predictions of the deposition. It is necessary to consider only those particle sizes which are important to the deposition process.

Other important experimental results are the measurements of condensation nuclei concentration profiles above a field of Avena fatua. These data show that the flux equation can be used to predict the transport of small particles from the atmosphere to a grassy field. The assumption of particle eddy diffusivity equal to the air eddy diffusivity was seen to be reasonable even within the canopy.

The most novel conceptual aspect of this research is the filtration model for particle deposition on Avena fatua. At this point,

the model cannot be readily adapted to calculate deposition on all natural vegetation, because of uncertainties concerning the airflow through such canopies. However, the feasibility and importance of incorporating filtration mechanisms into a predictive deposition model have been demonstrated.

CHAPTER I

A FILTRATION MODEL FOR AEROSOL DRY DEPOSITION: APPLICATION TO TRACE METAL DEPOSITION FROM THE ATMOSPHERE

ABSTRACT

The dry deposition of Pb, Zn, and Cd-containing particles from the atmosphere was studied by comparing theory with experiment for two types of surfaces: 1) smooth, flat teflon plates mounted on a smooth building roof, and 2) fields of Avena fatua, wild oat grass, about 50 cm tall. Gravitational sedimentation controlled the dry deposition of these trace metals on flat surfaces, while inertial impaction was the controlling mechanism for the vegetated surfaces. Convective diffusion to the grassy surfaces controlled the deposition of particles smaller than about 0.1 microns (condensation nuclei) over the grassy fields; this mechanism contributed little to total trace metal deposition. Theories for these three mechanisms were then used to construct a plot of deposition velocity versus particle diameter for Avena. The model incorporates a novel two-step deposition process: 1) eddy diffusion and sedimentation from the atmosphere to the grassy field, followed by 2) filtration by the grass elements. The results of the calculations compared well with literature data for lead deposition on fields of Avena.

INTRODUCTION

Many previous investigators have examined aerosol deposition on surfaces from a turbulent gas flow parallel to the surface. These studies have generated curves of deposition velocity versus particle size based on the experimental data. For the most part, empirical models have been developed to describe these curves. A thorough physical understanding of the deposition processes has not been achieved.

Many ideas have been proposed concerning the physical processes. Most investigators agree that air eddies bring the particles from the region far above the surface into the momentum boundary layer. However, there are a number of different concepts of particle transport in the region close to the surface.

Friedlander and Johnstone (1957) examined deposition of micron-sized particles to smooth pipe walls under turbulent flow conditions. They assumed that the eddy diffusivity of the particles was equal to the eddy diffusivity of the air, and that the particles were carried by air eddies to within one stopping distance of the wall. This stopping distance represents the free-flight distance of the particles, propelled by their own inertia through the viscous sublayer. The expressions for the eddy diffusivities of the air are empirical but have been well-established. The radial velocity of the particles at the start of the free-flight region was assumed to be equal to the mean fluctuating air velocity just outside the boundary layer.

Owen (1960) and Davies (1966) considered the same problem but made different assumptions concerning the velocity of the particles

at the beginning of the free-flight region. Beal (1970a, 1970b) generalized this approach by including diffusion of small particles as well as inertial transport of larger particles through the viscous sublayer.

A different approach was conceived by Sehmel (1970) in examination of the same problem. He assumed that the effective sink was at one particle radius from the wall. Particle deposition data were then used to obtain empirical expressions for the effective eddy diffusivities of the particles at various distances from the surface.

Another concept was introduced by Kitamoto and Takashima (1974a, 1974b) for the smooth surface deposition problem. These investigators assumed a sink at one particle radius from the surface, and then developed a new expression for particle eddy diffusivity. This expression incorporated their particle deposition data, but also utilized the basic form of the established expression for air eddy diffusivity.

Many investigations have also involved deposition on rough surfaces. As with the smooth surface studies, the models differ in their treatment of particle behavior near the surface. For example, Chamberlain (1966b) assumed equal eddy diffusivities for particles and for air, and used his deposition data to empirically determine the height of the effective particle sink. Sehmel (1972) approached the rough surface problem similarly to the smooth surface case, by assuming an effective sink at one particle radius and using deposition data to calculate particle eddy diffusivities.

In addition to model development, there is a wealth of aerosol deposition data available in the literature. For example, Chamberlain (1966b) obtained data on the transport of spores to grassy surfaces in a wind tunnel and in the field. Gregory (1961) performed similar experiments on smooth and rough surfaces. Sehmel (1973) and Sehmel et al. (1973) used monodisperse particles generated in the laboratory to investigate deposition on a number of surfaces in a wind tunnel.

In contrast with the models mentioned above, which did not include details of the surface structure, the use of a filtration model for aerosol scavenging by vegetation has been suggested by Gregory (1961), Davies (1966), Hidy (1972), Slinn (1976), and Hidy and Heisler (1977). The concept of filtration has not, however, been previously used to predict aerosol deposition from the free atmosphere in natural vegetated canopies. A convective diffusion model was used by Chamberlain (1960; 1966a; 1968; 1974a) to predict the transport of small particles and gases to vegetation in wind tunnel experiments. A summary of this research is given by Chamberlain (1975). These diffusion models for mass transport are derived by analogy with heat transfer models developed by Owen and Thomson (1963).

Filtration models for the deposition of large particles on vegetation based on impaction have not been verified, either in wind tunnels or in field experiments. However, the data suggest that bounceoff becomes a problem for particles large enough to

have appreciable impaction efficiencies (Chamberlain, 1966b; Chamberlain and Chadwick, 1972).

The importance of including details of the surface structure in a deposition model was brought out by Wells and Chamberlain (1967). These investigators measured the deposition of micron-sized particles to two aerodynamically smooth surfaces, brass and filter paper. In spite of comparable values of friction velocity, the net deposition on the filter paper was orders of magnitude greater than on the brass surface. This was attributed to the role of small fibers protruding from the surface of the filter paper. These fibers assisted in capturing and preventing reentrainment of the particles.

Two different natural surfaces might have similar friction velocities and roughness heights, yet greatly differing deposition characteristics. For example, a gravel surface may have airflow patterns comparable to a field of short grass. However, deposition on the latter surface might be considerably greater due to relatively efficient filtration by the grass blades.

A problem in applying filtration theory to natural vegetation is that the complex geometry of the vegetation makes it difficult to describe the airflow near the surface. In this respect, it is fortunate that fields of Avena fatua, common in the Los Angeles area, can be modeled as collections of vertical cylinders (Appendix of this chapter). It is thus a relatively simple matter to apply previously-established models for deposition on cylindrical filter fibers to ambient aerosol deposition.

The physical processes controlling trace metal deposition from the atmosphere have not been investigated in detail because of a lack of data on the size distributions as well as difficulties in characterizing natural surfaces. However, there are considerable data in the literature on trace metal deposition rates. Most of these studies have focused on lead-containing particles. Rabinowitz (1972) measured the lead content of wild oat grass in urban and nonurban areas of Southern California. This lead was shown to be deposited airborne material rather than soil lead. Patterson and Settle (1974), Huntzicker et al. (1975) and Davidson et al. (1974) examined the deposition of lead on flat teflon plates which were placed in cities as well as in the mountain, desert, and coastal areas of Southern California. Similar studies involving the lead deposition on artificial surfaces were conducted by Atkins in Palo Alto (1969) and by Servant in France (1976). Chamberlain (1974b) summarized the results of several lead deposition studies.

The deposition of automobile-emitted lead depositing on soil and vegetation near roadways has been examined by several investigators. Kloke and Riebartsch (1964) measured a high lead content in grass growing near busy streets. Heichel and Hankin (1972) identified large lead particles deposited on trees near a roadway. The lead content of soil near a highway was compared with lead in soil samples obtained near a battery smelter and from a greenhouse soil supply by Marten and Hammond (1966). Rapid decreases in the lead content of vegetation with increasing distance from highways have been measured by several experimenters (Rolfe and Haney, 1975;

Cannon and Bowles, 1962; Cholak et al.,1968; Chow, 1970; Page et al., 1971). Other researchers have examined several varieties of plants with high lead content growing near roads, investigating whether the lead is deposited airborne material or translocated from the soil (Dedolph et al., 1970; Leh, 1966; Motto et al., 1970; Shuck and Locke, 1970; Ter Haar, 1970; Rabinowitz, 1972).

The deposition of other trace metals has also been examined. Peirson et al. (1973) studied the deposition of several elements in England. Lagerwerff and Specht (1970) measured the lead, zinc, nickel, and cadmium content of soil and grass at various distances from roadways in Eastern and Midwestern U.S. They found a decrease in metal content with increasing distance from the road. Similar gradients were also measured by Huntzicker and Davidson (1975) near a Los Angeles freeway. In other studies, Huntzicker et al. (1974) measured the deposition of zinc, nickel, and cadmium on flat teflon plates in Southern California.

The present study examines trace metal deposition in terms of a new deposition model. Deposition velocity curves based on filtration and sedimentation are constructed and compared with field measurements of lead, zinc, cadmium, and condensation nuclei deposition. The accomplishments of this research are thus twofold. First, deposition data and theories have been used to derive and verify a model which can be applied to the deposition of aerosols in general. The input data needed for this model include the aerosol size distribution, characteristics of the windfield, and characteristics of the

surface. Second, the data are useful in predicting the transport and deposition of trace metals of public health interest.

The model can be applied to any vegetated surface where the filtration efficiency of the vegetation is known, and where the windfield is known. For example, Avena fatua has been adequately characterized to permit application of the model. The particle size distribution must also be accurately known, especially for the large particle end of the spectrum.

THEORY

The overall deposition process can be considered to incorporate two steps. During the first step, particles are transported from the atmosphere into the vegetated canopy. The second step involves transport inside the canopy, where the winds may be very small, onto the surface of the vegetation or the soil. Figure I-1 illustrates the two regions. Note that sedimentation and eddy diffusion control the transport in region 1, while sedimentation, impaction, and eddy and Brownian diffusion are the applicable mechanisms for region 2.

At any given location in the field, it is assumed that a steady state exists with the local rate of transport through region 1 equal to the rate of deposition in region 2. The shape of the distribution of particle concentration with height yields information on where there is resistance to mass transport. For example, if the profile is nearly constant with height in region 1 but decreases rapidly in region 2, then the transport resistance is greater in region 2. This corresponds to efficient wind eddy transport above the surface

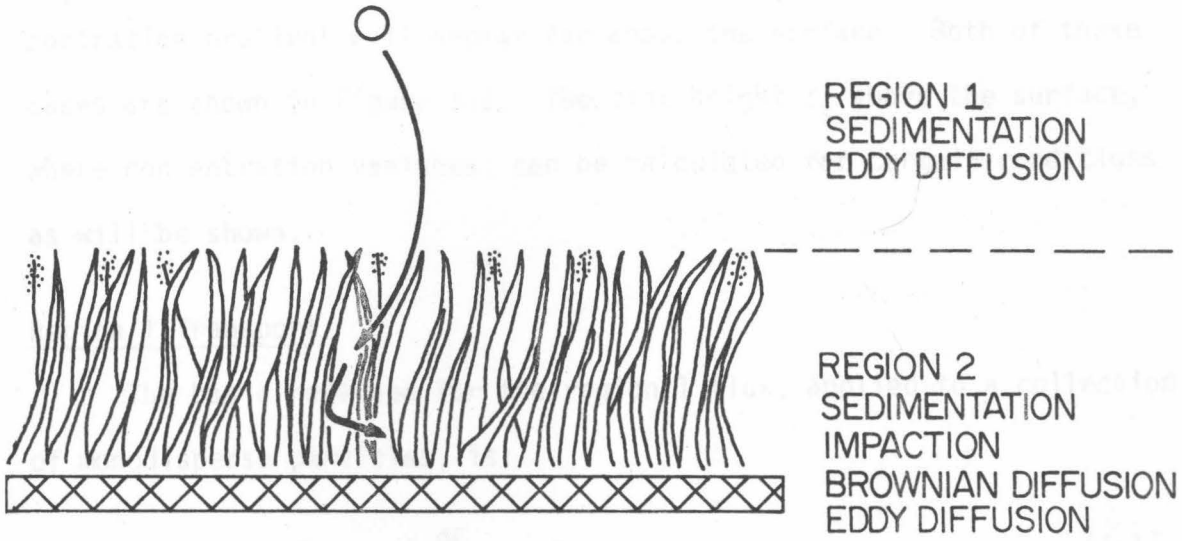

Figure I-1 Deposition may be considered a two-step process. First, the particles are brought down from the lowest layers of the atmosphere (region 1) into the canopy. Then the particles are transported onto the roughness elements of the vegetation (region 2).

yet poor filtration efficiencies inside the vegetation. On the other hand, if the resistance is significant in region 1, much of the concentration gradient will appear far above the surface. Both of these cases are shown in Figure I-2. The sink height z_s above the surface, where concentration vanishes, can be calculated for certain conditions as will be shown.

Region 1 Transport

The basic relation for the region 1 flux, applied to a collection of monodisperse particles, is:

$$J = - (D + \varepsilon_p) \frac{dC}{dz} - v_s C \qquad \text{(I-1)}$$

where J = flux in ng/cm^2 sec

D = Brownian diffusivity in cm^2/sec

ε_p = particle eddy diffusivity in cm^2/sec

C = airborne mass concentration of particles of a single discrete size, in ng/cm^3

z = height above the surface in cm corrected by the zero place displacement, if any

v_s = sedimentation velocity, cm/sec

The boundary condition for Equation I-1 is that the flux J in region 1 must be matched with the total deposition in region 2. Both D and v_s are functions of particle size. The eddy diffusion coefficient of the particles is assumed to be equal to that of the gas. In reality, the particles do not entirely follow the air eddies, so this must be viewed as an approximation (Friedlander, 1977). For

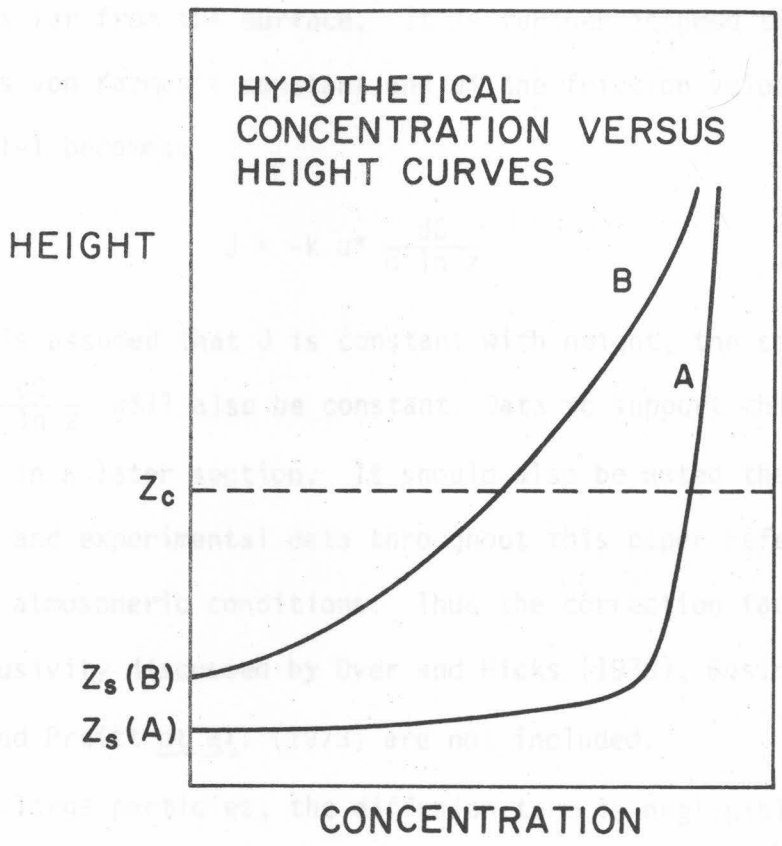

Figure I-2 Hypothetical curves of concentration versus height. The overall rate-limiting transport step can occur in either region 1 or region 2. Curve A corresponds to the latter case, where filtration is poor. Curve B illustrates the profile for efficient filtration, where there is appreciable atmospheric transport resistance. The canopy height is z_c, while height above ground where the concentration falls to zero, i.e., the sink height, is z_s. Note that the sink height is a function of the relative rates of transport through regions 1 and 2.

either very small particles or very large particles, the equation simplifies.

For small particles, v_s is negligible and $D \ll \varepsilon_p$ for ambient wind conditions far from the surface. It is further assumed that $\varepsilon_p = ku^*z$, where k is von Karman's constant and u* the friction velocity. Thus Equation I-1 becomes:

$$J = -k\, u^* \frac{dC}{d \ln z} \qquad \text{(I-2)}$$

Since it is assumed that J is constant with height, the concentration profile $\frac{dC}{d \ln z}$ will also be constant. Data to support this will be presented in a later section. It should also be noted that the equations and experimental data throughout this paper refer to normal adiabatic atmospheric conditions. Thus the correction factors for eddy diffusivity discussed by Dyer and Hicks (1970), Businger et al. (1971), and Pruitt et al. (1973) are not included.

For large particles, the diffusion term is negligible. Hence the flux becomes:

$$J = - v_s C \qquad \text{(I-3)}$$

The usual definition of deposition velocity is now incorporated:

$$V_g = - \frac{J}{C} \qquad \text{(I-4)}$$

Equations I-3 and I-4 show that the deposition velocity is equal to the sedimentation velocity for sufficiently large particles. Additional experimental data will be used to verify Equation I-3 in a later section.

Region 2 Transport

Inside the canopy, it is necessary to consider the filtration efficiency of the vegetative elements. This paper is concerned with aerosol deposition on Avena fatua (Appendix). As a model for determination of the collection efficiency, it is convenient to choose the single cylinder, normal to aerosol flow.

For the diffusion range, the flux J_f on a cylinder fiber of diameter d_f is given by (Friedlander, 1977):

$$J_f = - \frac{Sh\ D\ C}{d_f} \qquad \text{(I-5)}$$

where Sh = Sherwood number = $.683\ Re^{.466}\ Sc^{1/3}$ for $40 < Re < 4000$

Re = Reynolds number = $\frac{u\ d_f}{\nu}$, u = windspeed in cm/sec

ν = kinematic viscosity of air in cm^2/sec

Sc = Schmidt number = $\frac{\nu}{D}$

The equation for the Sherwood number has been obtained by analogy with heat transfer (Holman, 1972). Since the Sherwood number and concentration are functions of height inside the canopy, it is necessary to integrate Equation I-5 between the height where the concentration vanishes, $z = z_s$, and the cylinder height z_c:

$$J_f = - \frac{1}{z_c - z_s} \int_{z_s}^{z_c} \frac{Sh(z)\ D\ C(z)}{d_f}\ dz \qquad \text{(I-6)}$$

For N cylinders per unit area of ground, the total flux based on ground area becomes:

$$J = N\pi d_f (z_c - z_s) J_f = -N\pi D \int_{z_s}^{z_c} Sh(z)\, C(z)\, dz \qquad (I\text{-}7)$$

In the case of large particles in the impaction range, the expression for the efficiency η of a single cylinder is:

$$\eta = \frac{\text{particles/sec depositing on the cylinder}}{\text{particles/sec passing through area } [d_f (z_c - z_s)]} \qquad (I\text{-}8)$$

Then the deposition velocity of filtration by a single cylinder is:

$$v_g \text{ (for filtration)} = v_f = \frac{\eta u}{\pi} \qquad (I\text{-}9)$$

The efficiency η is a function of the Stokes number:

$$St = \frac{d_p^2\, u\, (\rho_p - \rho_a) K}{9\mu\, d_f} \qquad (I\text{-}10)$$

where d_p = particle diameter in cm

ρ_p = bulk density of the particle in g/cm^3

ρ_a = bulk density of the air in g/cm^3

μ = viscosity of the air, equal to $\nu\rho_a$, in g/cm sec

K = Cunningham slip correction factor

The efficiency has been computed numerically from potential flow theory by Brun et al. (1955) and measured over a range of Reynolds numbers by Wong and Johnstone (1953). A comparison of theory and experiment over the Reynolds number range of the present study is given by Friedlander (1977). An empirical expression for η, based on a least-squares fit of the data of Wong and Johnstone and following

the form suggested by Landahl and Herrmann (1949), is given by:

$$\eta = \frac{St^3}{St^3 + 0.753\ St^2 + 2.796\ St - 0.202} \qquad \text{(I-11)}$$

Combining Equations I-4 and I-9 and noting that the efficiency, windspeed, and concentration are functions of height, the impaction flux becomes:

$$J_f = -\frac{1}{z_c - z_s} \int_{z_s}^{z_c} \frac{\eta(z)\ u(z)\ C(z)}{\pi}\, dz \qquad \text{(I-12)}$$

or

$$J = -N\ d_f \int_{z_s}^{z_c} \eta(z)\ u(z)\ C(z)\ dz \qquad \text{(I-13)}$$

Steady-State Transport

The flux of particles toward the surface is assumed constant with height in region 1. In the steady-state, the flux through region 1 must equal the deposition of particles on the surfaces in region 2. It is thus possible to solve the flux equations for the two regions simultaneously to obtain the concentration profile and the deposition flux.

For the diffusion range, the applicable equations are:

$$J = -k\ u^* \frac{dC}{d\ \ln z} \quad \text{for region 1} \qquad \text{(I-2)}$$

$$\text{and } J = -N\pi D \int^{z_c} Sh(z)\ C(z)\ dz \quad \text{for region 2} \qquad \text{(I-7)}$$

For all except very great filtration efficiencies, the particle sink z_s is much smaller than the momentum sink z_o. But $u = 0$ for $z < z_o$, hence $Sh = 0$ and Equation I-7 becomes:

$$J = -N\pi D \int_{z_o}^{z_c} Sh(z)\, C(z)\, dz \qquad \text{(I-14)}$$

Although z_s is no longer explicit in Equation I-14, the particle sink is nevertheless important in the function $C(z)$. Hence z_s is a part of both Equations I-2 and I-14.

The concentration profile in region 2 could, in principle, be calculated from a solution to the equation of convective diffusion within the vegetation with a sink term for deposition on the vegetation elements and an expression for ε_p in the vegetation. The applicable form of this equation is:

$$u \frac{\partial C}{\partial x} = \frac{\partial\, \varepsilon_p \frac{\partial C}{\partial z}}{\partial z} - v_s \frac{\partial C}{\partial z} - v_f CA \qquad \text{(I-15)}$$

where A = area of vegetation elements per unit volume of the canopy in cm^{-1}

B.C. $\left(\varepsilon_p \frac{\partial C}{\partial z}\right)_{z=z_c}$, bottom of region 1

$= \left(\varepsilon_p \frac{\partial C}{\partial z}\right)_{z=z_c}$, top of region 2

$C(z=z_c)_{\text{bottom of region 1}}$

$= C(z=z_c)_{\text{top of region 2}}$

A numerical solution to this equation was beyond the scope of this study. Instead it was assumed that the concentration distribution was given by Equation I-2 with J constant within region 2 as well as in region 1. This would be expected to hold best for low filtration efficiencies. As shown later, the experimental results for very small particles supported this assumption.

Equations I-2 and I-14 may be solved simultaneously for z_s and J. The necessary input data to the model are the diameter and height of the cylinders and number of cylinders per unit area of ground, the wind profile above and within the canopy, and the size distribution of particles at one height, preferably above the canopy.

For the impaction range, a similar model may be set up. The applicable equations are:

$$J = - k u^* \frac{dC}{d \ln z} - v_s C, \text{ in region 1} \qquad \text{(I-16)}$$

$$\text{and} \quad J = - N d_f \int_{z_s}^{z_c} \eta (z) u(z) C(z) dz, \text{ in region 2} \qquad \text{(I-17)}$$

Impaction efficiencies for large particles may be quite high. Thus the particle sink z_s may be as great as or greater than z_o for these particles. Because of the sensitivity of Equation I-17 to z_s, measurements of the size distributions below as well as above the canopy height z_c are advisable. These measurements would allow a more accurate determination of z_s as an input to the model, rather than merely calculating z_s from Equations I-16 and I-17. However, for this study involving the trace metals, the size distributions have

been measured at only one height and the model has been applied to predict approximate values for z_s and J.

Sedimentation dominates deposition in region 2 in two cases: 1) very large particles which may sediment through the canopy faster than filtration can remove them, and 2) particles smaller than the critical impaction diameter $d_{p_{crit}}$ whose sedimentation velocities are larger than the corresponding diffusion filtration velocities. The first case does not occur for typical deposition conditions on a field of 50 cm high Avena except for d_p greater than 100 microns, which will not be treated here. The second case is important for d_p between 1.0 and 7.0 microns for these deposition conditions. Because the impaction efficiency is such a strongly increasing function of particle size for $d_p > d_{p_{crit}}$, the d_p range where both impaction and sedimentation play a role in the canopy will be small. Hence the interaction between sedimentation and impaction in region 2 will not be considered.

EXPERIMENTAL MEASUREMENTS

To test the models of the previous section, a number of experiments were performed. These involved measuring the deposition of Pb, Zn, and Cd on artificial surfaces exposed to the free atmosphere, and also studying condensation nuclei transport over a grassy field. The trace metal measurements were for the purpose of studying sedimentation and inertial impaction, while the condensation nuclei experiments yielded information on diffusional deposition.

Flat Plate Experiments

Deposition on flat surfaces may result from convective diffusion, turbulent (inertial) deposition, sedimentation, or any one of the minor mechanisms such as thermophoresis and electrostatics. The purpose of these experiments was to determine which mechanisms control the ambient deposition of Pb, Zn, and Cd on smooth, flat surfaces. It was expected that the data would also be useful as a lower limit for deposition on rough, natural surfaces.

Many experiments were performed during the spring and summer of 1975 on the roof of W.M. Keck Laboratories, Caltech. This site is more than 300 meters from the nearest well-traveled street, but less than one kilometer from several such streets.

The experiments involved measuring the deposition fluxes of the three trace metals on flat teflon plates, simultaneously with measuring the airborne size distributions of the trace metals isokinetically (Chapter II). Reasonable agreement was obtained when comparing the measured deposition fluxes with fluxes calculated from the size distribution data. Basically, the experiments showed that sedimentation of the small fraction of large airborne particles (d_p > 10 microns, aerodynamic diameter) controlled about 70% of the mass deposition of these species on the flat plates.

The importance of obtaining accurate isokinetic data was also illustrated by this study. Most previously published trace metal size distribution data in the literature were obtained nonisokinetically. These data show very little mass in particles greater than 10 microns. By comparison, Figures II-1 and II-2 show data from the

isokinetic size distribution experiments. There is considerable mass in large particles. Since the largest particles are the most important to overall mass deposition, isokinetic sampling is essential for this type of study.

Cylinder Experiments

Although sedimentation controls the deposition of Pb, Zn, and Cd on flat surfaces, this is not in general true for vegetated surfaces. Impaction may be important if there is sufficient mass in large particles, while convective diffusion may dominate if the particles are small. The deposition of trace metals on vertical teflon cylinders exposed to the free atmosphere was measured in a model study of deposition by impaction. Three similar experiments were run, during September 18-22, October 3-16, and October 25-November 4, 1976.

The cylinders were set up at the same site as the flat plate experiments. Simultaneously with the cylinder exposures, the flat teflon plates were also set up and the windspeed was recorded with a hot-wire anemometer. Due to the difficulty of sampling isokinetically, the size distributions were not measured again. Instead, it was assumed that the shape of the distributions was identical to the previously measured spectra of Figure II-2. These distributions were then normalized by comparing the flat plate data for each cylinder experiment with the July 1975 plate data. The deposition on the cylinders was principally from impaction of particles greater than 10 microns, and normalization on the basis of plate deposition was most accurate for these large particles. Further, there were no significant

differences among the size distribution measurements of the previous section. It was felt that these reasons provided justification for using the simple normalization procedure to estimate the size distributions during the cylinder experiments.

As in the sedimentation experiments, the idea here was to compare the measured depositions with calculated values. It is convenient to apply Equation I-12 to the trace metal size distributions by integrating over all d_p. Since the windspeed u is a function of time, it was thought perhaps necessary to integrate over the probability density function f(u), given in Appendix II. However, a numerical integration of f(u) for the first cylinder experiment showed that wind gusts were not important, but rather the mean windspeed characterized the impaction process. It was also verified that the windspeed was approximately constant with height over the cylinder length L. Thus the following form of Equation I-12 has been used:

$$J_f = \frac{-1}{\pi} \int_{dp} \eta(\bar{u}, d_p)\, \bar{u}\, c(d_p)\, d\, d_p \qquad \text{(I-18)}$$

where $\bar{u}$ = mean windspeed, and $c(d_p)$ = mass concentration distribution function

Table I-1 compares measured depositions with values calculated using Equation I-18. This equation was numerically integrated using the trapezoidal approximation. It might be mentioned that no significant difference was observed when the geometric mean particle diameter for each impactor size range, $\overline{dp_i} = \sqrt{dp_i dp_{i+1}}$, was used rather than the numerical integration. This is because the d_p ranges for the size cuts of Figure II-2 are sufficiently small.

TABLE I-1

Calculated and measured trace metal fluxes on vertically oriented cylinders. All values are in ng/cm^2 day.

	Date of Experiment	$J_{impaction}$ (calculated)	J_{total}^{*} (measured)	Surface Conditions
Cylinder Diameter = .104 cm				
Pb	Sept 18, 1976	125 ± 31	106 ± 9	wet
	Oct 3, 1976	229 ± 31	100 ± 3	dry
	Oct 25, 1976	202 ± 27	53 ± 3	dry
Zn	Sept 18, 1976	22.2 ± 6.2	27.6 ± 2.7	wet
	Oct 3, 1976	32.7 ± 5.0	32.6 ± 3.9	dry
	Oct 25, 1976	14.8 ± 3.8	5.2 ± 2.7	dry
Cylinder Diameter = .262 cm				
Pb	Oct 25, 1976	103 ± 19	31 ± 3	dry
	Oct 25, 1976	8.0 ± 2.5	4.5 ± 0.4	dry

*Diffusional flux is negligible for these trace metals, hence it is probable that impaction is the main deposition mechanism.

Reasonable agreement is seen for the first experiment. In this case the weather was foggy and small drops of water on the cylinder minimized particle bounceoff. The later experiments, which occurred during hot, dry weather, show smaller measured than calculated values. Chamberlain (1966b) and Chamberlain and Chadwick (1972) have shown that bounceoff may be a problem under these conditions.

Grassy Field Experiments: Condensation Nuclei Profiles

The trace metal experiments described in the previous sections were useful in studying the sedimentation and impaction ranges of particle deposition. Figure II-2 shows that there is appreciable Pb, Zn, and Cd mass in particles greater than 10 microns, so these species may be readily used to study large particle deposition mechanisms. However, it is difficult to experiment with trace metals in the diffusion range. This is because the much greater deposition velocities of the large particles tend to "swamp" diffusional deposition by the submicron material.

To study deposition by convective diffusion under ambient conditions, concentration profiles were measured with condensation nuclei counters (CNC). These instruments detect all particles larger than about 25 Angstroms (Environment One Corp, 1971). Since the number distribution usually peaks at a very small particle size (<0.1 micron), CNC's can be used to observe the behavior of small particles.

Two CNC's were used to measure profiles of condensation nuclei versus height above a field of Avena fatua, 65 cm tall. One CNC was positioned 4 meters above the ground, while the other unit sampled at

various heights below 4 meters. In this way the profile shown in Figure I-3 was obtained. (Actually these points are the average of several runs described in Appendix III, the standard deviation of which is given by the error bars.) Note that points both above and within the canopy were obtained.

According to Equation I-2, these points should lie on a straight line when plotted against the logarithm of height. This is verified by Figure I-4. It is now possible to use the slope of this line to calculate the flux. Using Equation I-2, a value of -42,600 particles/cm^2 sec is obtained, and Equation I-4 yields a deposition velocity of 0.94 cm/sec at a height of 4 meters.

The above calculations use the profile method applied to region 1. This method has been previously applied to measure the deposition of SO_2 (Fowler and Unsworth, 1974; Unsworth, 1974; Unsworth and Fowler, 1976; Garland et al., 1974; Garland, 1976; Shepherd, 1974) and O_3 (Aldaz, 1969; Turner et al., 1974). Hudson (1975) has measured the concentration of condensation nuclei at two heights and has estimated the flux from these data. A discussion of the application of the profile method to both gas and particle deposition is given by Droppo and Hales (1976).

It is possible to apply Equation I-14 to the data of Figure I-4 to calculate the expected deposition by filtration. The additional data necessary are the wind profile (Appendix V), the plant stem diameter and spacing (Appendix of this chapter) and the particle size distribution. For simplicity, and considering the approximate nature of this calculation, it was assumed that all of the particles

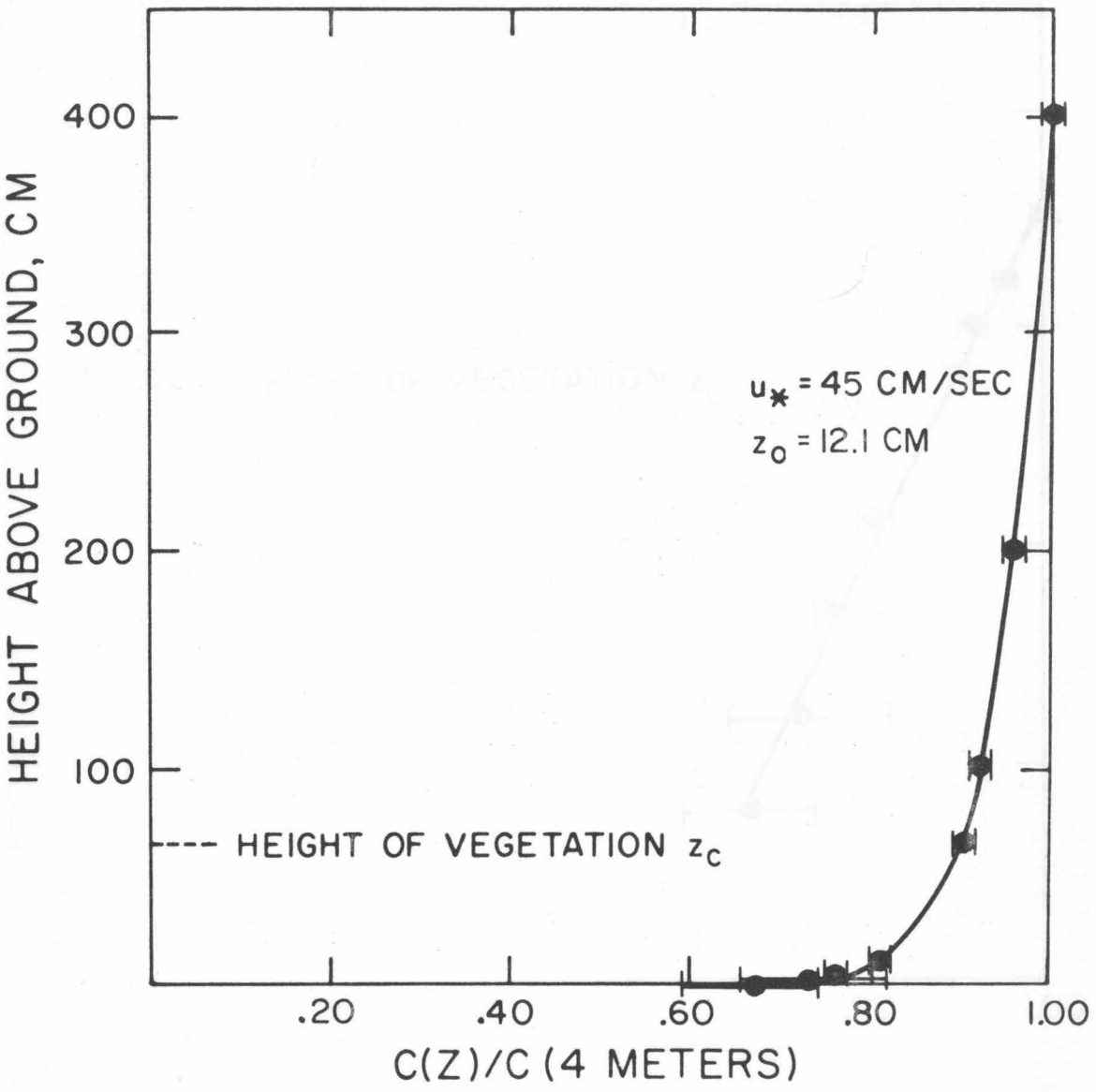

Figure I-3 Airborne concentration of condensation nuclei as a function of height above the ground in a residential area of Los Angeles near Occidental College, June, 1974. C(4 meters) = 45,200 particles/cm^3. Two condensation nuclei counters were used to make these measurements (General Electric CNC, and Environment One Model Rich 100).

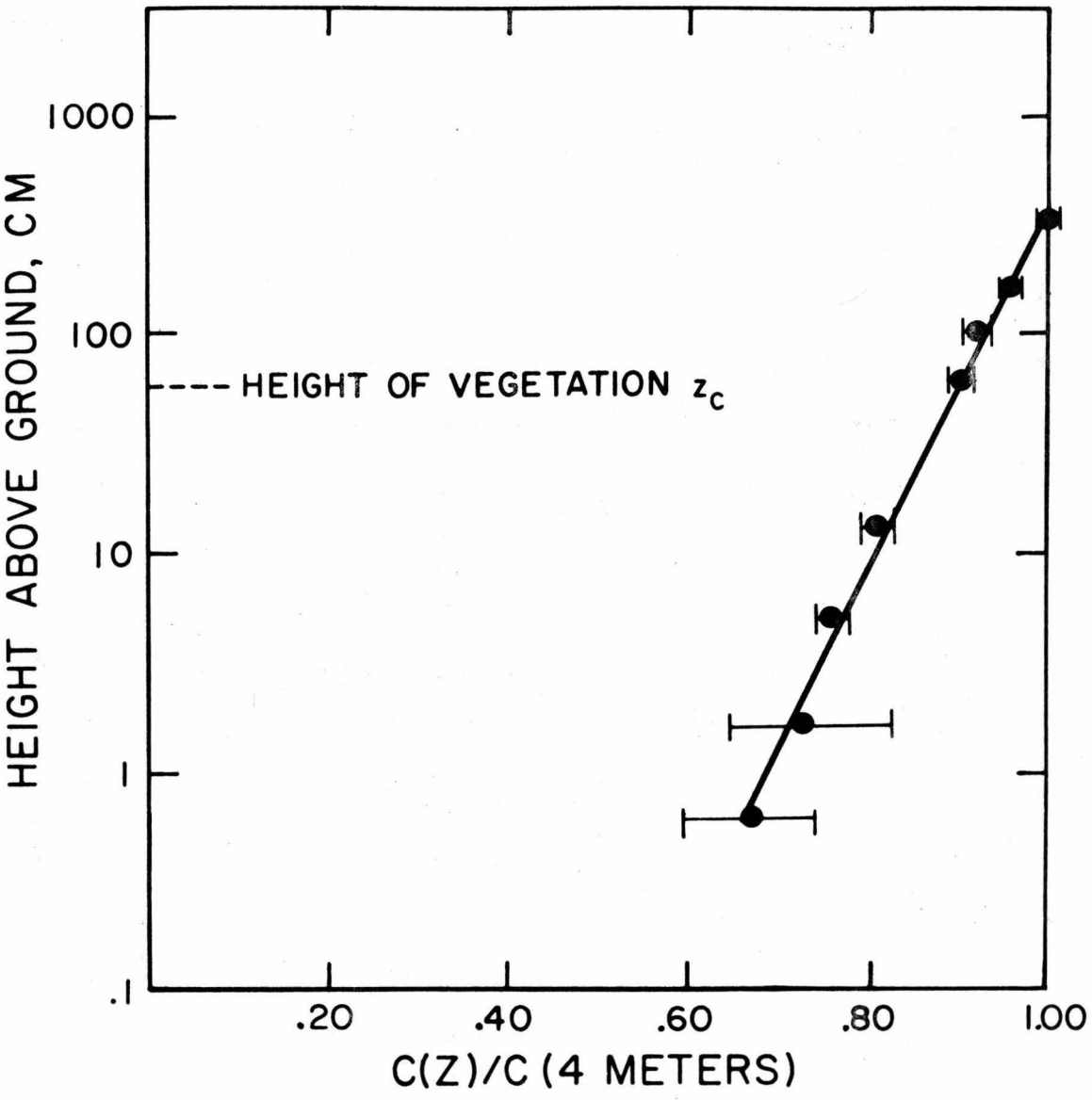

Figure I-4 The points of Figure I-3 plotted on a logarithmic scale. The resulting straight line can be used to calculate flux and deposition velocity.

measured by the CNC were of geometric diameter 0.03 microns. Later experiments using an Electrical Aerosol Analyzer, Thermo Systems model 3030, showed that a sharp peak in the number distribution typically occurs at about this diameter.

The flux calculated by filtration assuming d_p = 0.03 microns is -38,200 particles/cm^2 sec, compared with the profile calculation of -42,600. Considering the uncertainty in the particle diameter and the weakness in modeling Avena as cylinders, the agreement is reasonable.

It is not necessary to measure the concentration profile to use the filtration model although this was done above for verification. Only one concentration measurement at a known height is needed. Solving Equations I-2 and I-14 simultaneously for z_s and J will yield the flux. The assumption here is that the concentration profile is undisturbed by the vegetation down to z_o. This assumption was shown to be reasonable by Figure I-4.

The two equations may be solved by an iterative technique, illustrated here for the CNC experiments (Table I-2). Beginning with a concentration measurement at one height, 45,200 particles/cm^3 at z=400 cm, the flux on the Avena is calculated by assuming this concentration is invariant with height. The resulting flux, 37,200 particles/cm^2 sec, is used in Equation I-2 to calculate z_s. Since the concentration profile is now completely determined, Equation I-14 may be used to recalculate J. This procedure is continued until the desired accuracy is reached. Convergence is fairly rapid, as shown in Table I-2.

TABLE I-2

Result of simultaneous solutions of Equations I-2 and I-14 by an iterative technique for the flux J and concentration sink z_s.

Iteration	Mathematical Concentration Sink, z_s, cm	Flux J, particles/cm^2 sec
0	0	37,200
1	1.3×10^{-7}	33,300
2	9.8×10^{-9}	33,703
3	1.289×10^{-8}	33,658
∞	1.293×10^{-8}	33,663
Measured profile, filtration calculation in Region 2	2.09×10^{-6}	38,200
Measured profile, eddy diffusion calculation in Region 1	2.09×10^{-6}	42,600

Note that the iteration yields only an approximate value for the flux (33,663), compared with the other two calculations which actually use the measured profile. The true flux is probably close to 42,600.

DEPOSITION VELOCITY CURVES

The dependence of deposition velocity on particle diameter has been calculated for a typical field of Avena, 50 cm high, in Figure I-5. The plot shows v_g at heights of 150 cm and 400 cm above the ground, assuming u* = 21.2 cm/sec, z_o = 4 cm, and zero plane displacement d = 25 cm, which is based on the yearly average wind in the Los Angeles Basin (U.S. Weather Bureau) and wind profile measurements (Appendix V). The curve for the diffusion range was obtained by solving Equations I-2 and I-7 simultaneously, while the impaction curve values were obtained using Equations I-16 and I-17. Particle bounceoff was neglected.

Although it is straightforward to use the iterative method for the CNC data, it may be more difficult to use iteration for all situations. For example, when the iterative method was applied to impaction for 50 cm Avena, the calculated concentration sink z_s was larger than the canopy height z_c on the first iteration. In such cases, especially when the fiber efficiencies are high, trial and error must be used.

It is interesting to examine Figure I-5 in some detail. The deposition of particles smaller than about one micron is controlled by diffusion. The deposition velocity increases with decreasing particle size because the Brownian diffusivity increases. However, the curves level off for very small d_p, asymptotically approaching 5.3 cm/sec (150 cm) and 3.1 cm/sec (400 cm). These values represent the limiting

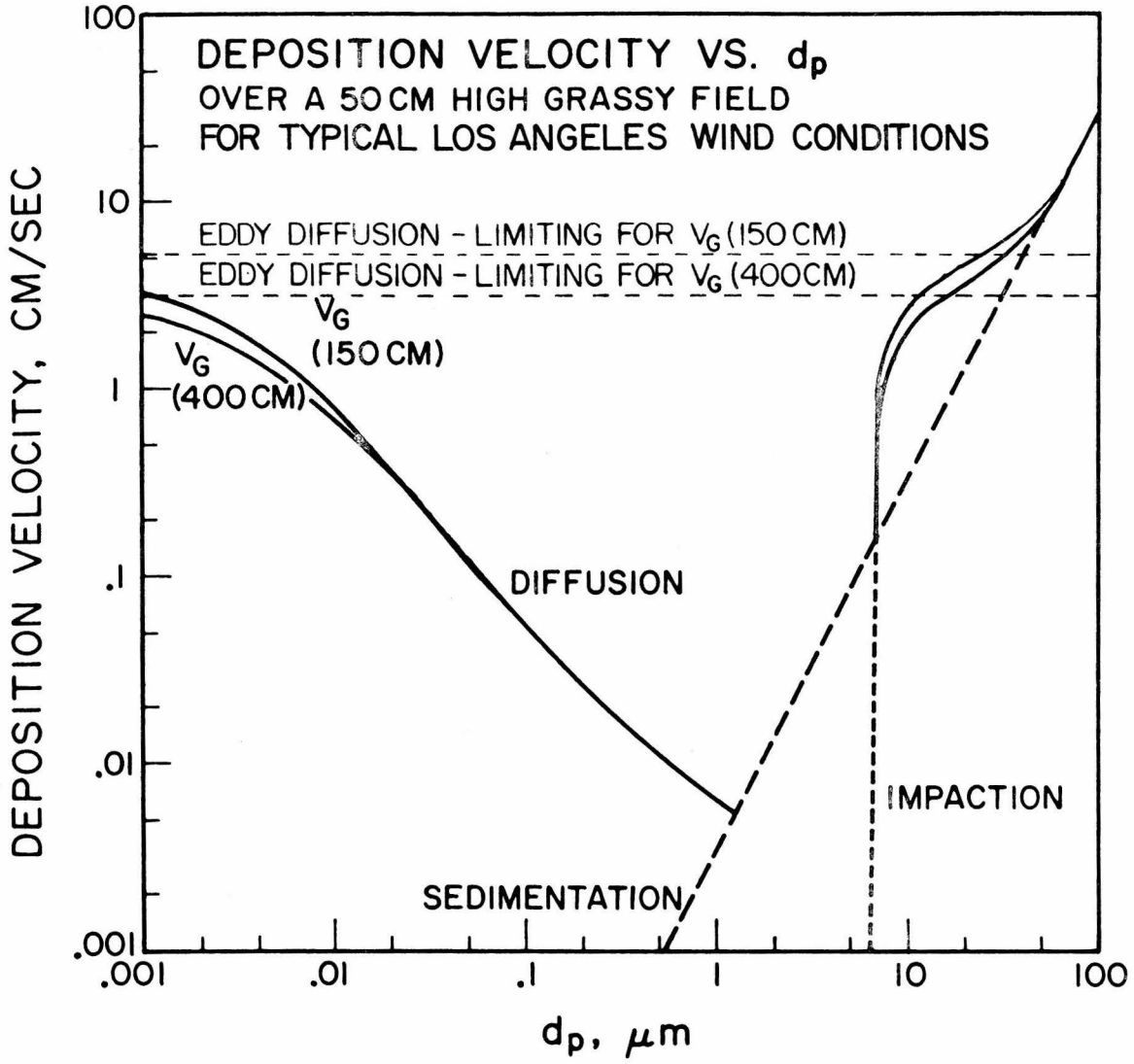

Figure I-5 Calculated values of deposition velocity as a function of particle size for heights of 150 cm and 400 cm above the ground, for a field of Avena fatua, wild oat grass. Particle density is assumed to be 1 g/cm^3. The field was assumed to be composed of a collection of uniform cylinders with the following properties:

Canopy height z_c = 50 cm
Fiber diameter d_f = 0.2 cm
Fiber spacing N = 8600/m^2
Windfield: u* = 21.2 cm/sec
z_o = 4.0 cm
d = 25.0 cm

Note that since the variable z in the text refers to the height above the zero-plane displacement d, the deposition velocity curves apply for values of z = 125 cm and 375 cm, respectively.

rates at which particles are delivered to the grass by eddy diffusion through region 1. The limiting value is approached for particles smaller than 0.001 microns (10 Å) for which the filtration efficiency is very high.

The critical impaction diameter for these conditions, where St = 1/8 (Fuchs, 1964), is 6.5 microns. In the size range between 1 and 7 microns, both diffusion and impaction are negligible, and sedimentation controls. The impaction curve rises steeply, but then begins to level off at about 10 microns when the overall process again becomes rate-limited by wind eddies. For larger particle diameters, however, v_g continues to increase because of transport by sedimentation in region 1. For $d_p \gtrsim 10$ microns, as for $d_p \lesssim 0.001$ microns, the deposition velocity is rate-limited by atmospheric transport.

Comparison of the theoretical curves of Figure I-5 with the experimental data of Chamberlain (1966b) for a grassy surface shows good qualitative agreement; quantitative comparisons were not made because the properties of the vegetation were quite different. Trends in the curves of Figure I-5 are also similar to trends in the curves of Sehmel and Hodgson (1976), which are based on experimental data.

DEPOSITION IN FIELDS OF AVENA FATUA: COMPARISON WITH EXPERIMENT

The deposition model can be used to predict trace metal fluxes on a grassy field. The procedure is to obtain effective deposition velocities from Figure I-5 for each of the fifteen size ranges in Figure II-2. Then the total flux may be calculated by summation:

$$J = - \sum_{i=1}^{15} v_{g_i} (\overline{d_{p_i}}) C_i \qquad (I\text{-}19)$$

The value of $\overline{d_{p_i}}$ for each size range i is assumed to be the geometric mean value defined earlier. This method was shown to be satisfactory for the teflon cylinder experiments.

The calculation has been performed for Pb, yielding 94 ng/cm^{2}day (Table I-3). This value may be compared to the measurements of the Pb content of Avena in the Los Angeles area, by Rabinowitz (1972). The average for the LA Basin is 168 μg Pb/g of plant. Huntzicker et al. (1975) have shown that the Pb deposition in Pasadena, at the same site as the Figure II-1 and II-2 measurements, is approximately equal to the average Pb deposition throughout the LA area. Thus the value of 168 ppm is assumed to apply to Pasadena. It is also assumed that the deposition on the Avena occurred over a 9-month period, based on information supplied by Rabinowitz (personal communication). Combining these data with measurements of the leaf and stem weights and the spacing of the plants (Appendix of this chapter), the deposition rate can be determined:

$$\frac{168 \times 10^3 \text{ ng Pb}}{\text{g of plant}} \times \frac{0.122 \text{ g of plant}}{\text{cm}^2 \text{ ground area}} \times \frac{1}{270 \text{ days}} = 76 \text{ ng/cm}^2\text{day}$$

It is seen that the measured value is about 80% of the calculated result. This agreement is good considering the approximations involved. A number of factors may be responsible for the low measured value. For example, particle bounceoff would tend to decrease the lead content. Another factor might be washoff by rain, although other investigators have shown that this is probably not important (Rains and Thornton,

1970). About 90% of the deposited lead comes from impaction of particles larger than 10 μm. Zinc and cadmium have greater fractions of airborne mass in d_p > 10 μm than lead, hence these trace metals are also controlled by impaction.

The effect of surface roughness in increasing the deposition velocity can be seen in these data. The measured lead deposition on Avena was 76 ng/cm^2 day, while the flat surface measurements yielded 31.7 ng/cm^2 day (Table II-2). Comparisons in the literature of deposition on flat and rough surfaces show similar increases.

Figures I-6 through I-9 show optical microscope photographs of particles depositied on samples of Avena fatua. The plants were picked in January 1977; they were assumed to have collected particles over the previous nine months. Figures I-6, I-7, and I-9 were obtained using 100 X magnification. Figure I-8 was obtained using 25 X magnification.

TABLE I-3

Calculated deposition fluxes of Pb on a field of Avena fatua. The calculation uses deposition velocities from Figure I-5 and the airborne Pb size distribution of Figure II-2.

Mechanism	Deposition	Approximate d_p Range
Diffusion	1 ng/cm^2 day	< 1 μm
Sedimentation	25	> 1 μm
Impaction	68	> 7 μm
Total	94 ng/cm^2 day	

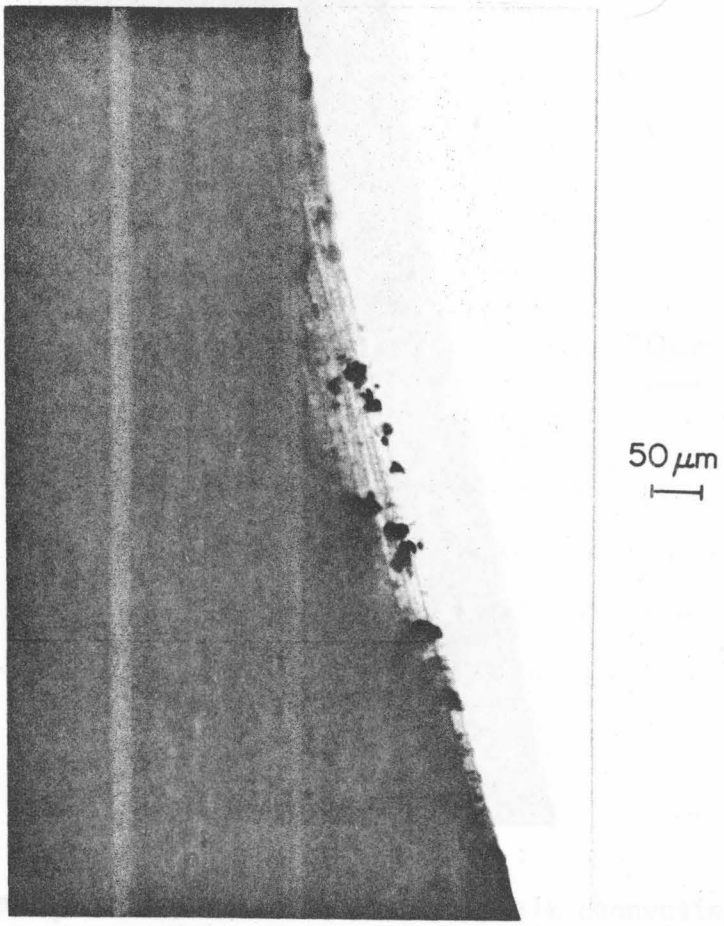

Figure I-6 Particles deposited on a 0.2 cm diameter stem of Avena fatua, at about 40 cm above the ground. The plant was picked near a busy street corner in Pasadena (Del Mar Blvd. and Lake Avenue). This photograph shows a particularly dirty area on the stem.

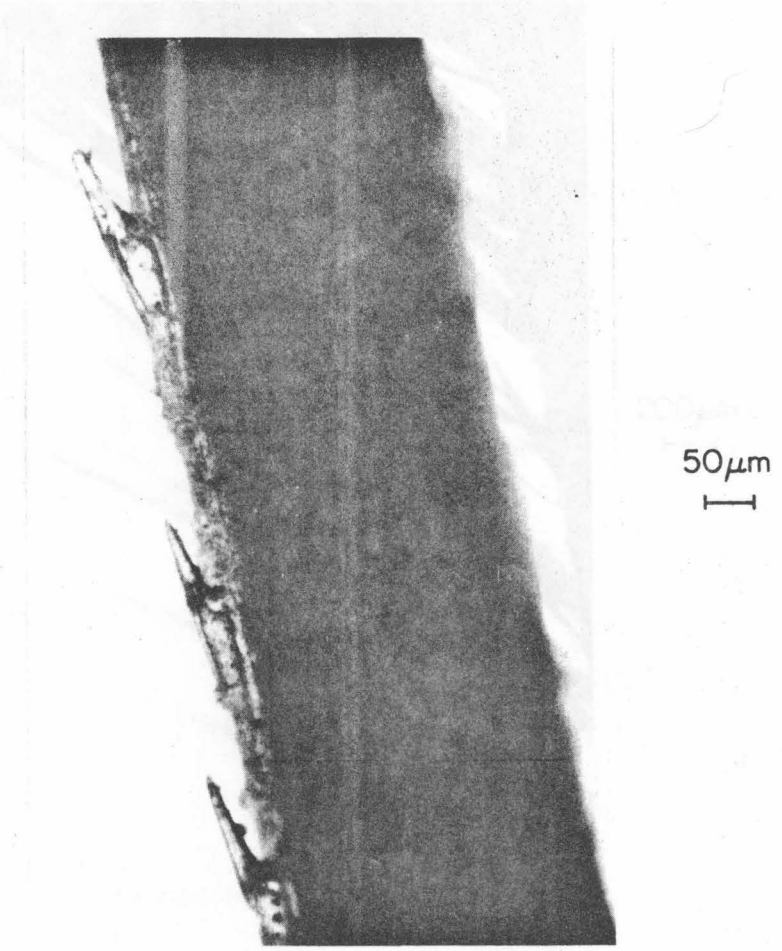

Figure I-7 Particles deposited on a small stalk connecting seed pods with the main stem. The sharp protrusions have greater Stokes numbers associated with them, hence higher collection efficiencies. However, there are too few protrusions to influence the total deposition on the plant. This sample of Avena was obtained in Ernest Debs Park, Los Angeles.

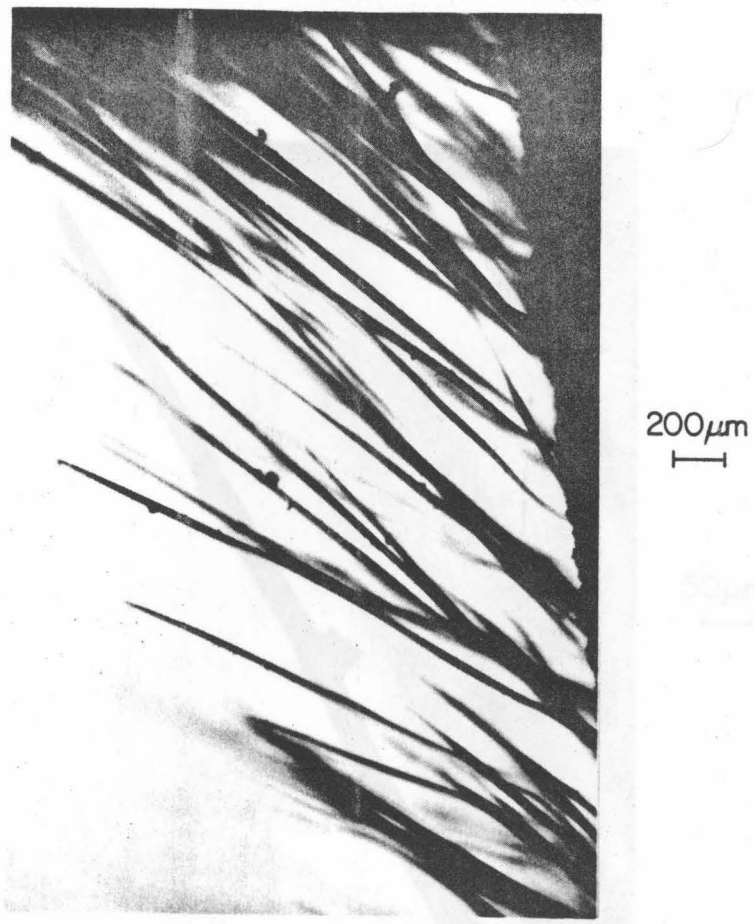

Figure I-8 Fine hairs on the seed pods, which are efficient particle collectors. However, the surface area of the stems and leaves is far greater than that of the hairs, so only a small fraction of the total deposition occurs on the seed pods. This plant is the same as in Figure I-7.

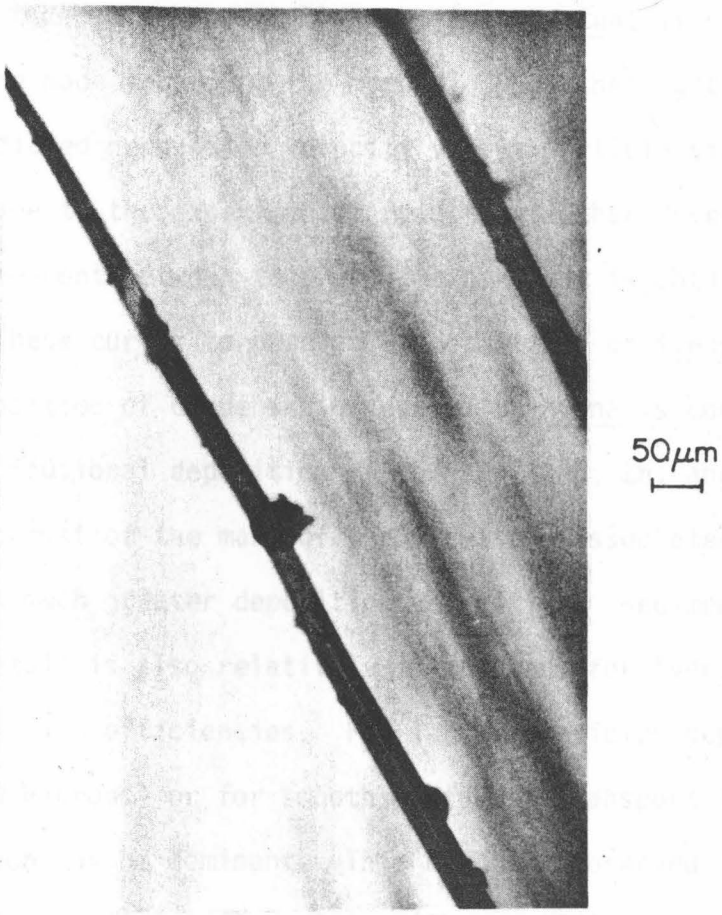

Figure I-9 Close-up view of the seed pod hairs of Figure I-8. This photograph shows deposited small particles. Although not important for Avena, the presence of small hairs on vegetation may significantly alter the particle collection efficiency of the canopy.

CONCLUSIONS

Filtration is an important deposition mechanism for particle removal over certain types of vegetation. Convective diffusion and inertial impaction are the primary filtration processes.

Results of controlled laboratory experiments (by others) for deposition on cylinders can be applied to *Avena fatua*, if simplifying assumptions are made regarding the morphology of the vegetation. Curves of predicted deposition velocity versus particle size are similar in shape to the experimental results of other investigators. Reasonable agreement between theory and experiment is obtained when using one of these curves to predict Pb deposition on *Avena*.

The deposition of condensation nuclei on *Avena* is controlled by diffusion. Diffusional deposition of the small Pb, Zn, and Cd particles is negligible; most of the mass of the metals is associated with large particles with much greater deposition velocities. Sedimentation of these trace metals is also relatively unimportant for *Avena* because of the large impaction efficiencies. For larger particles depositing on *Avena* ($d_p \gtrsim 50$ microns) or for smooth surfaces, transport to the surface by sedimentation may be dominant. This has been observed for trace metal deposition on flat teflon plates (Chapter II).

The filtration concept cannot be readily applied to predict the deposition on many natural surfaces. In addition to the difficulty of adequately describing the detailed geometries and windflow patterns associated with natural vegetation, a sound physical understanding of turbulent inertial mechanisms is lacking. Also, reentrainment has not been considered in the development of this model.

A major problem in the application of the method is the determination of an accurate particle size distribution. This is particularly difficult for urban and industrial sources where the concentration of large particles is high and isokinetic sampling is required. However, the model described in this study can be used to predict approximately the particle deposition on relatively uniform, vegetated fields where the filtration efficiency of the vegetation and the particle size distribution are known.

APPENDIX:

Description of *Avena fatua*

Wild oat grass, *Avena fatua*, is one of the most common weed grasses on the west coast (Hitchcock, 1935). Several fields of *Avena* in the Los Angeles area were examined, and measurements were made of typical heights, weights, spacing, and morphology of these plants. A drawing of a typical plant is shown in Figure I-10.

Avena consists of a stem (approximately 0.1-0.2 cm diameter), a few leaves (approximately 0.2 cm width or slightly greater), and seed pods (2-3 cm long and several mm wide). A typical plant has a 50 cm stem and a total length of about 85 cm of leaves and seed pods. There are about 3200 plants/m^2 ground area.

In this analysis, each plant is assumed to consist of 135 cm of cylinders of diameter 0.2 cm. Since the total plant height is 50 cm, the following calculation may be made:

$$3200 \frac{\text{plants}}{m^2} \times \frac{135}{50} \frac{\text{cylinders of 50 cm height}}{\text{plant}} = 8600 \frac{\text{50-cm cylinders}}{m^2}$$

The weight of a typical 50 cm stem is 260 mg, while the 85 cm of leaves and empty seed pods weighs 120 mg. These values are used to convert trace metal content of the plants (in ppm by weight) into deposition rate.

Figure I-10 A typical specimen of Avena fatua, wild oat grass. Plant height = 50 cm, total length of leaves and seed pods = 85 cm, and diameter of stem, leaves and seed pods ≈ 0.2 cm.

CHAPTER II

THE DEPOSITION OF TRACE METAL-CONTAINING PARTICLES ON FLAT, SMOOTH SURFACES IN THE LOS ANGELES AREA

ABSTRACT

Measurements were made of deposition from the free atmosphere of lead, zinc, and cadmium on flat teflon plates. To determine the mechanisms of deposition, simultaneous measurements were made of the airborne size distributions of these metals by isokinetic sampling with a cascade impactor. Measurements of the airborne mass of lead, zinc, and cadmium indicated 17%, 32%, and 37% in the size range greater than 10 μm (aerodynamic diameter), respectively. Calculations based on these data showed about 70% of the total mass deposition for each metal was due to sedimentation of these large particles. The bulk of the airborne mass of these metals, in particles much smaller than 10 μm, played only a minor role in the deposition process.

INTRODUCTION

Airborne concentrations of trace metals in urban areas have been measured by several investigators, and it is generally known that urban air contains significantly higher trace metal levels than air from non-urban regions. For example, relatively high airborne concentrations of lead have been measured near roadways by Bullock and Lewis (1968), Cahill and Feeney (1973), and Daines et al. (1970). Studies by Cardina (1974) and by Pierson and Brachaczek (1974) have shown elevated levels of tire dust containing zinc near roadways. Metallurgical emissions also contribute to urban levels of zinc and other trace metals (Huntzicker and Davidson, 1975).

In addition to airborne concentrations, deposition rates of trace metals have been measured. Atkins (1969), Peirson et al. (1973), Patterson and Settle (1974), Servant (1976), and Huntzicker et al. (1975) examined the deposition of lead and other trace metals onto artificial surfaces. A summary of similar studies involving lead has been compiled by Chamberlain (1974b). Many investigators have examined lead deposition onto soil and vegetation near roadways (Rabinowitz, 1972; Kloke and Riebartsch, 1964; Heichel and Hankin, 1972; Rolfe and Haney, 1975). Rapid decreases in the lead content of soil and vegetation with increasing distances from roadways have been noted by several experimenters, while others have attempted to determine the origin of lead in roadside vegetation, whether deposited airborne material or translocated from the soil.

In spite of the wealth of trace metal data available, little research has been done to investigate the deposition mechanisms

involved. Several investigators have measured the deposition of monodisperse particles in the laboratory and under controlled field conditions, but these results have not previously been applied to ambient trace metal deposition.

A thorough understanding of these deposition mechanisms has many applications. Information on particle residence time in the atmosphere, the effects of sources on downwind regions, and background information for tracer studies are closely related to deposition rates.

The purpose of this study was to determine the chief deposition mechanisms for airborne lead, zinc, and cadmium-containing particles on flat surfaces. Isokinetic measurements of the airborne size distributions for these species combined with deposition data from the literature provide a means of calculating the expected deposition. The calculated values are compared to deposition measurements made simultaneously with the size distribution experiments. In this way the mechanisms of deposition are revealed.

It is expected that these calculated and measured depositions for smooth, flat surfaces will be lower limits to the deposition on rough, natural surfaces.

THEORY

It is convenient to begin by defining the deposition velocity v_g:

$$v_g = - \frac{J}{C} \qquad \text{(II-1)}$$

where v_g has units of cm/sec, J is the flux of material to a surface in ng/cm^2 sec, and C is the airborne mass concentration in ng/cm^3.

The flux is assumed to be constant with height above the surface, although C and v_g are functions of height.

The relationship between flux and concentration can be written:

$$J = - (D + \varepsilon_p) \frac{dC}{dz} - v_s C \qquad \text{(II-2)}$$

where D and ε_p are the Brownian and eddy diffusivities, respectively, in cm^2/sec, z is the height above the surface in cm, and v_s is the sedimentation velocity in cm/sec. The minus signs are necessary since the flux downward to a surface is a negative quantity, yet the deposition velocity is defined as positive.

Equation II-2 applies to both small and large particles. This general case has been examined by Chamberlain (1966b) and Sehmel (1970), who have assumed various forms for ε_p in the region near the surface.

For very small or very large particles, the analysis of deposition simplifies. For small particles, eddy diffusion and Brownian diffusion are the principal deposition mechanisms. In the case of large particles, inertial mechanisms and sedimentation are most important.

Sehmel (1973) has shown that sedimentation is the controlling deposition mechanism for a smooth surface and a small windspeed (2.2 m/sec), for particles larger than 0.3 μm aerodynamic diameter. For the light winds encountered in the present trace metal study, sedimentation would, therefore, be applicable for the upper portions of the size distributions. The proper form of Equation II-2 is thus:

$$J = - v_s C \qquad \text{(II-3)}$$

SOURCE SIZE DISTRIBUTIONS: A LITERATURE SURVEY

Lead

Many researchers have measured lead size distributions at the source, the automobile tailpipe. Hirschler et al. (1957, 1964), Ninomiya et al. (1971), Ter Haar et al. (1972), and Habibi (1973) operated vehicles using leaded gasoline under conditions designed to simulate a variety of driving patterns. They each found a wide range of diameters in the emitted lead-containing particles, including substantial fractions of large particles (greater than 5 μm aerodynamic diameter). Lee et al. (1971) conducted a similar study but found 95% of the lead in particles smaller than 0.5 μm. Mueller et al. (1964) operated his vehicles under steady cruising conditions and found 20-38% of the lead smaller than 2 μm aerodynamic diameter.

Difficulties in performing these tailpipe experiments as well as variations in automobiles, fuel, and driving cycles account for the differences among the results of the above investigators. Habibi (1970) discusses some of these difficulties. In general, however, the results indicate that relatively new, steadily cruising automobiles emit predominantly submicron lead. Older autos and rapidly accelerating or decelerating autos emit both supermicron and submicron lead. It is therefore likely that ambient urban atmospheres, receiving emissions from wide varieties of vehicles and driving patterns, contain a broad spectrum of sizes of lead-containing particles.

Zinc and Cadmium

There are at least two major types of zinc sources, namely emissions from metallurgical plants and combustors, and also the

abrasion of automobile tires, according to Huntzicker and Davidson (1975). The stationary source emissions are generally submicron, while the tire dust is supermicron (Cardina, 1974; Pierson and Brachaczek, 1974; Dannis, 1974). It is thus likely that the measured ambient zinc size distribution would be bimodal. The cadmium distribution may resemble the zinc spectrum. Substances which contain zinc generally contain trace amounts of cadmium, since the two elements are found together in nature (Friberg et al., 1974). In some regions, additional sources of cadmium may be present (Huntzicker and Davidson, 1975).

AMBIENT SIZE DISTRIBUTIONS: A LITERATURE SURVEY

Lead

Size distributions of lead were measured near heavily travelled streets by Tufts (1959), Lininger et al. (1966), Cholak et al. (1968), Daines et al. (1970), and Lundgren (1970). These investigators found most of the lead in submicron particles. A study by Robinson and Ludwig (1967) found little difference between lead size distributions in urban and remote areas, with most of the lead submicron. Although the above studies show considerable variation in the shapes of the size distributions, most of the results indicate about one-third of the total lead mass in supermicron particles.

Zinc and Cadmium

Harrison et al. (1971) measured ambient lead and cadmium size distributions, while Lee et al. (1968, 1972) examined lead, zinc, and cadmium distributions in urban areas. Their results show that zinc and cadmium are found in considerably larger particles than lead. For

example, Lee et al. (1972) found 32% of the lead, 60% of the zinc, and 72% of the cadmium in supermicron particles.

AMBIENT SIZE DISTRIBUTIONS: ISOKINETIC EXPERIMENTS

Measurements of the ambient trace metal size distributions above have been concerned with the respirable range near and below one micron. These studies were generally nonisokinetic and, therefore, underestimated the amount of material in large particles. Watson (1954) has shown that sampling with an air inlet oriented 90^{o} to the wind, such as an upright impactor, results in collecting less than 45% of the 12 μm particles and less than 10% of the 37 μm particles present (aerodynamic diameters).

To obtain accurate measurements of the size distributions, isokinetic impactor runs were conducted using a modified Andersen model 20-000 Sampler. The modifications involved construction of a new orifice and two top stages for better fractionation of large particles. Sticky teflon Temp-R-Tape (Connecticut Hard Rubber Company) was used as an impactor substrate. It was found that the adhesive and the particles completely dissolved in a hot solution of 1 part concentrated HF and 20 parts concentrated HNO_3. After evaporation and redissolving, the resulting solution was analyzed for lead and zinc with flame atomic absorption spectroscopy, and for cadmium with flameless atomic absorption (carbon rod atomization). The complete analytical procedure is described by Huntzicker et al. (1975).

Measurements were made on the roof of W.M. Keck Laboratories at the California Institute of Technology, more than 300 meters from the nearest well-travelled street but less than one kilometer from several

such streets. The impactor was positioned horizontally facing into the wind, 150 cm above the roof surface. Previous measurements had shown that resuspended roof dust was not a problem at this height (Figure A III-1). The wind direction was checked frequently during the runs, and if the direction was found to have changed by more than 20^{o}, the impactor direction was also changed. It was found that the wind direction changed little during the experiments, although brief gusts of $\pm 45^{o}$ occurred occasionally. A flow rate of 13.2 liters per minute was used, since at this flow the orifice airspeed was approximately equal to the average windspeed. The errors in the data due to deviations from isokinetic sampling, as well as other errors, are discussed in Appendix VI.

The isokinetic impactor experiments took place during May 13-18, 1975, and during July 16-20, 1975. Sampling was from 8:00 AM to 8:00 PM daily. The modified Andersen impactor and Millipore after-filter were used, in addition to a total filter run in parallel with the impactor.

The lower impactor stages (3 through 6) were calibrated using monodisperse polystyrene latex and polyvinyltoluene particles (Dow Chemical Company). The resulting $d_{p_{50}}$ values at 13.2 liters per minute agreed with the Andersen specifications when adjusted for the flow rate difference (Figure A I-1). The top stages were calibrated by running the impactor isokinetically at the same site as the trace metal experiments, and the collected atmospheric particles were sized geometrically under the optical microscope. Details of the impactor calibration are described in Appendix I.

It is interesting to compare these isokinetic measurements with nonisokinetic results obtained at the same site in 1972 and 1974. Table II-1 shows that the amount of mass detected in particles larger than 10 μm aerodynamic diameter is considerably greater during the isokinetic experiments.

It is possible that the one to three-year period between nonisokinetic and isokinetic runs may be partly responsible for the differences in Table II-1. Lee and Goranson (1975) have shown that the total mass distribution has been shifting toward slightly larger particle sizes in recent years. Seasonal differences among the runs may also be significant.

It may be asked whether particles as large as 10 μm or greater can remain airborne for appreciable periods of time. Lundgren and Paulus (1973) have measured a significant number of large airborne particles (up to 100 μm) in an area with no strong local sources. Further they found that 90% of the mass deposited on a dustfall plate was associated with particles in the range 25-120 μm. They estimated that such large particles can be transported up to several kilometers from their source. In addition, Johnson (1976) has detected particles as large as 55 μm in diameter at a height of 300 m above St. Louis. Evidence of large airborne lead particles has been shown by Gillette and Winchester (1972), Tufts (1959), and Lundgren (1970).

Normalized distributions for lead, zinc, and cadmium based on aerodynamic diameters are shown in Figure II-1 for the May 1975 experiment and in Figure II-2 for the July 1975 experiment. For the July run, the total airborne concentrations of lead, zinc, and cadmium

TABLE II-1

Percentage of mass greater than 10 μm aerodynamic diameter for non-isokinetic runs (1972, 1974) and isokinetic runs (1975). Details of the nonisokinetic runs are given by Huntzicker et al. (1975). Impactor cutoffs are based on effective mass mean diameters (Appendix I). If standard $d_{p_{50}}$ values had been used, the percentages would have been slightly smaller.

	Pb	Zn	Cd
November 1972	5%	11%	-%
February 1974	11	15	-
May 1975	17	38	28
July 1975	17	32	37

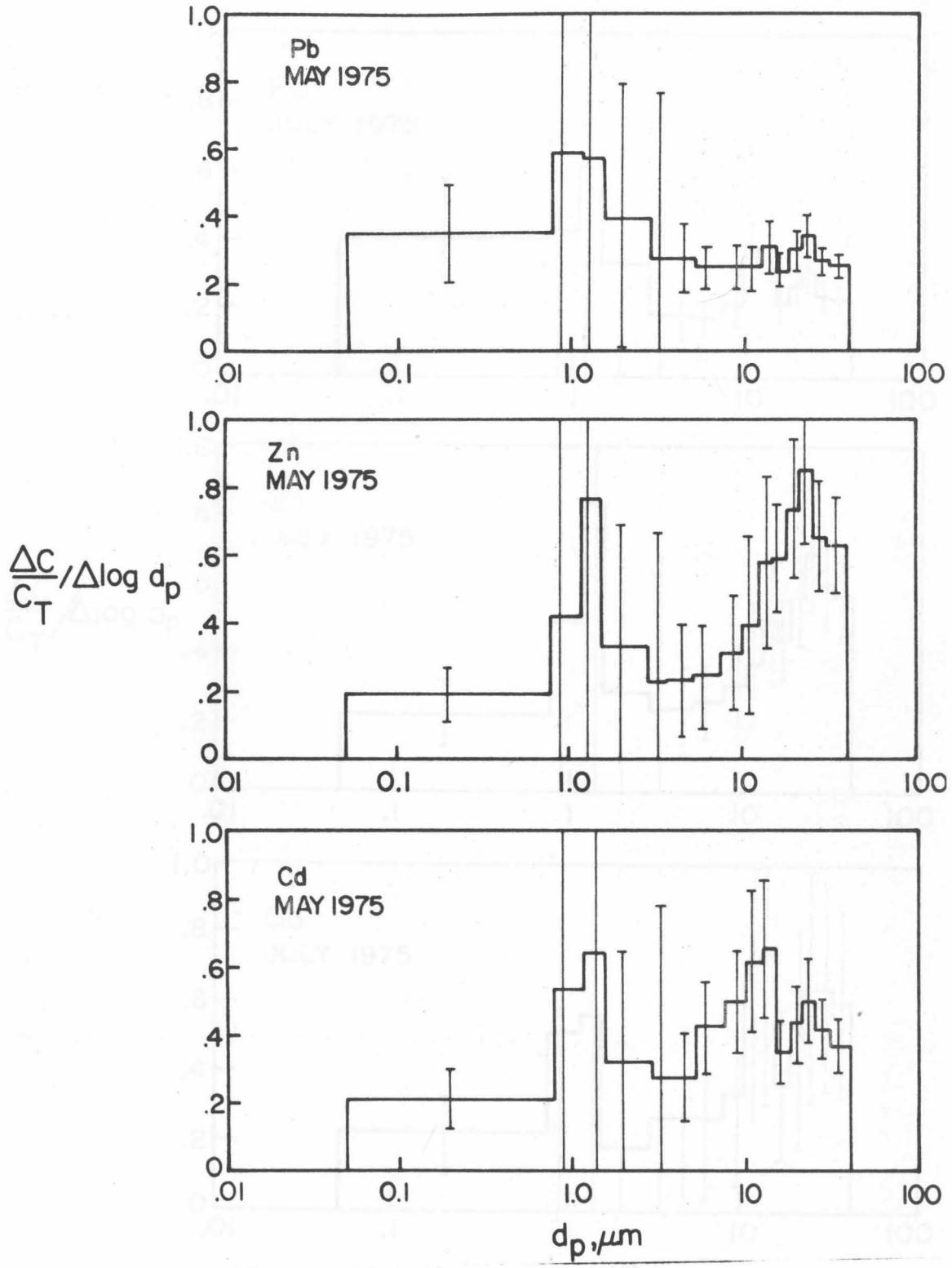

Figure II-1 Normalized size distributions for lead, zinc, and cadmium for the May 1975 experiment. ΔC represents the airborne mass concentration while C_T represents the sum of the ΔC's from all size ranges for each trace metal.

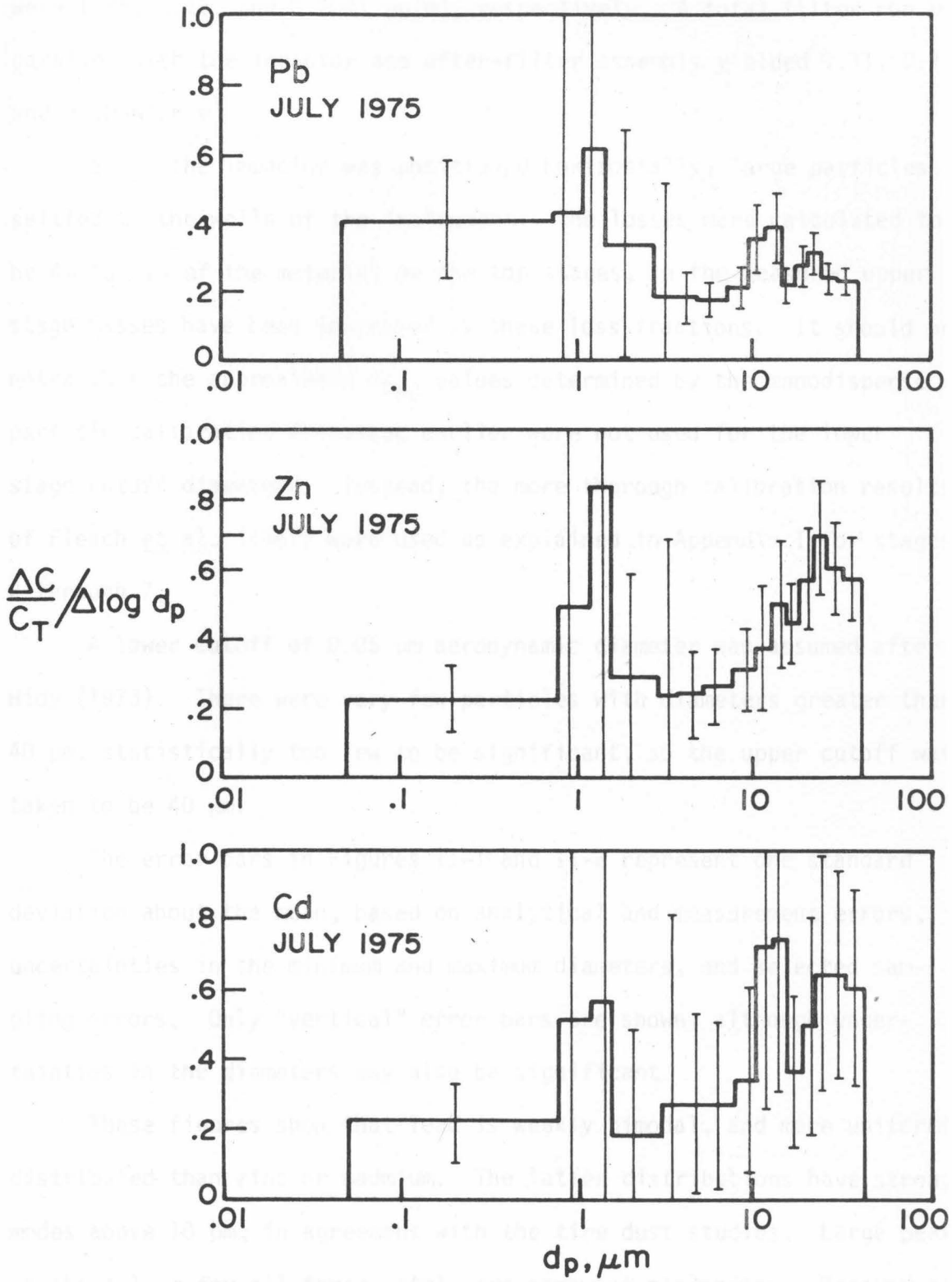

Figure II-2 Normalized size distributions for lead, zinc, and cadmium for the July 1975 experiment.

were 1.25, 0.13, and 0.0041 $\mu g/m^3$, respectively. A total filter run in parallel with the impactor and after-filter assembly yielded 1.11, 0.13, and 0.0036 $\mu g/m^3$.

Since the impactor was positioned horizontally, large particles settled to the walls of the instrument. The losses were calculated to be 4% to 11% of the material on the top stages, so the measured upper stage masses have been increased by these loss fractions. It should be noted that the approximate $d_{p_{50}}$ values determined by the monodisperse particle calibration discussed earlier were not used for the lower stage cutoff diameters. Instead, the more thorough calibration results of Flesch et al. (1967) were used as explained in Appendix I for stages 2 through 7.

A lower cutoff of 0.05 μm aerodynamic diameter was assumed after Hidy (1973). There were very few particles with diameters greater than 40 μm, statistically too few to be significant, so the upper cutoff was taken to be 40 μm.

The error bars in Figures II-1 and II-2 represent one standard deviation about the mean, based on analytical and measurement errors, uncertainties in the minimum and maximum diameters, and selected sampling errors. Only "vertical" error bars are shown, although uncertainties in the diameters may also be significant.

These figures show that lead is weakly bimodal, and more uniformly distributed than zinc or cadmium. The latter distributions have strong modes above 10 μm, in agreement with the tire dust studies. Large peaks at about 1 μm for all three metals are somewhat misleading. Because of

the nonideal shapes of the impactor efficiency curves, the actual peaks may occur at a smaller diameter, as discussed in Appendix I.

DEPOSITION OF TRACE METALS

Several measurements of deposition velocities of lead in urban and rural areas have been made. Chamberlain (1974b) has summarized the results of several investigations. These and other data are presented in Table II-2.

The data of Table II-2 are best understood by considering a lead particle source emitting a known size distribution. As this lead is transported away from the source, depositional loss to the ground as well as other processes will affect the shape of the size distribution. Large lead particles with high deposition velocities will be lost first. Far from the source, most of the large particles will have deposited out, so a smaller deposition velocity would be expected. (It is assumed that particle growth is unimportant in the size range of interest.) This trend may be observed in Table II-2. The highest deposition velocity, 1.8 cm/sec, has been measured closest to the source, and the smallest value, 0.07 cm/sec, has been measured in a remote area. The value of 1.8 cm/sec may be an upper limit due to nonisokinetic sampling.

The value of 0.29 cm/sec was obtained by dividing the measured lead flux onto a flat teflon plate by the total airborne concentration measured by the impactor and after-filter. It should be possible to calculate this lead flux, and also the zinc and cadmium fluxes, using the size distributions of Figure II-2 and proper deposition velocities for each size range.

TABLE II-2

Dry deposition velocities for lead from several investigations.

Location	Deposition Surface	cm/sec v_g	Investigator
Wilderness area, Northern California	Teflon plate	0.07	Patterson, 1975
San Nicolas Island	Filter paper	0.093	Peirson, 1973
Average, rural and industrial sites, Great Britain	Filter paper	0.27	Peirson, 1973
Pasadena, California	Teflon plate	0.29	Present study
Average, measurements near highways	Many different surfaces	0.32	Chamberlain, 1974
Freeway shoulder, Los Angeles	Teflon plate	1.8	Huntzicker and Davidson, 1975

Many researchers (Chamberlain, 1966b; Islitzer and Dumbauld, 1963; Sehmel, 1972; Sehmel et al., 1973) have shown that deposition velocities over rough surfaces are generally greater than sedimentation velocities for similarly sized particles. This effect is especially evident at high windspeeds. For a smooth surface and low windspeeds, however, Sehmel (1973) has shown that sedimentation governs deposition. Thus Equation II-3 presented earlier is applicable.

Sehmel's data show that the deposition velocities for small particles are greater than sedimentation. However, when the submicron trace metal fluxes were calculated using Sehmel's deposition velocity data, the results were negligible compared to the sedimentation of larger particles. Thus, in the calculations which follow, sedimentation is applied to small as well as large particles with no loss of accuracy.

Equation II-3 as written applies only to a collection of monodisperse particles. For a mass concentration distribution $c(d_p)$, the total flux is:

$$J = \int v_s\ (d_p)\ c(d_p)\ d(d_p) \qquad \text{(II-4)}$$

where

$$\int c(d_p)\ d(d_p) = C, \text{ total mass concentration} \qquad \text{(II-5)}$$

In order to apply Equation II-4 to the distributions of Figure II-2 it is assumed that the mass concentration distribution $c_i(d_p)$ is a separate known function in each of the fifteen size ranges. Each size range i covers the interval $d_{p_i} < d_p < d_{p_{i+1}}$. The flux resulting

from the material in each size range is summed to obtain the total flux:

$$J = \sum_{i=1}^{15} J_i = \sum_{i=1}^{15} \int_{d_{p_i}}^{d_{p_{i+1}}} v_s\,(d_p)\; c_i\,(d_p)\; d(d_p) \qquad \text{(II-6)}$$

Since it is assumed that $c_i(d_p)$ is uniformly distributed with respect to log d_p, the proper expression for c_i is:

$$c_i(\log d_p) = \frac{C_i}{\log d_{p_{i+1}} - \log d_{p_i}} \qquad \text{(II-7)}$$

where C_i is the total mass concentration in size range i. The equation for $v_s(d_p)$ for these sizes is obtained from Fuchs (1964):

$$v_s(d_p) = \frac{(\rho_p - \rho_a)\; g\; K}{18\;\mu}\; d_p^{\,2} \qquad \text{(II-8)}$$

where ρ_p = bulk density of the sedimenting particle, ρ_a = bulk density of the air, g is the acceleration due to gravity, K is the Cunningham slip correction factor, and μ is the kinematic viscosity of the air.

When Equations II-7 and II-8 are substituted into Equation II-6, the resulting integrated expression for total flux is:

$$J = \sum_{i=1}^{15} \frac{(\rho_p - \rho_a)\; g\; K}{18\;\mu} \left[\frac{1}{2\ln 10}\; \frac{d_{p_{i+1}}^{\,2} - d_{p_i}^{\,2}}{\log d_{p_{i+1}} - \log d_{p_i}} \right] C_i \qquad \text{(II-9)}$$

The fluxes calculated from Figure II-2 and Equation II-9 are presented in Table II-3. The fluxes may be compared with the measured deposition onto flat teflon plates, exposed simultaneously with the

TABLE II-3

Calculated and measured fluxes to flat surfaces on the roof of W.M. Keck Laboratory at Caltech. All values are in ng/cm^2 day.

	Measured Fluxes for July 1975 Experiment			Calculated Fluxes	
	J_{top}	J_{bottom}	$J_{sedimentation}$	$J_{sedimentation}$ July 1975	$J_{sedimentation}$ May 1975
Pb	31.7	7.0	24.7 ± 9%	29.2 ± 9%	28.9 ± 6%
Zn	12.0	3.82	8.18 ± 12%	6.5 ± 11%	7.7 ± 10%
Cd	0.238	0.085	0.153 ± 58%	0.224 ± 25%	0.448 ± 10%

July 1975 impactor run. Fluxes calculated from the May 1975 impactor experiment are also listed. Care must be taken when comparing the calculated May 1975 fluxes with the July 1975 measured values. As shown in Table II-4, airborne concentrations of the trace metals were different during the two experiments.

Table II-3 shows measured depostion on both upward-facing (top) and downward-facing (bottom) plates. The bottom plate fluxes are considerably smaller than the top plate fluxes. This agrees with the results of Gregory (1961) who found a greater deposition of 32 μm diameter Lycopodium spores on the top of a glass microslide than on the bottom, for small windspeeds.

In a separate experiment at the same site, the number of large particles with geometric diameters greater than 10 μm which had deposited on these flat plates was determined using an optical microscope. The ratio of large particles on the bottom plate to large particles on the top plate was 0.044. Thus it is likely that the trace metal deposition on the bottom plate was primarily due to small particles.

There are data in the literature which compare small particle deposition on upward and downward-facing flat surfaces. Bullas (1953) has measured the deposition of fission product activity from nuclear test explosions, on the top and bottom of a flat surface. This activity is generally attached to condensation nuclei with diameters of less than 0.1 microns (Chamberlain, 1960). He measured a value of 0.7 for a ratio of bottom surface deposition to top surface deposition. Megaw and Chadwick (1957) produced a uranium fume and measured the deposition on top and bottom flat surfaces. The fume consisted of 83% by mass small

TABLE II-4

Airborne concentrations during the two isokinetic impactor experiments. All values are in ng/m^3.

	July 1975	May 1975
Pb	1254 ± 3%	1160 ± 2%
Zn	127 ± 6%	131 ± 9%
Cd	4.1 ± 15%	11.6 ± 5%

particles with diameters less than about 0.2 μm, but with some supermicron material. Their value of the ratio was 0.6.

These values are somewhat less than unity, which is consistent with the data and observations of Sehmel (1971). He has found that gravity assists the turbulent transport of small particles on horizontal upward-facing surfaces by forcing the particles downward into regions of smaller eddies. This results in slightly greater fluxes on top surfaces than on bottom surfaces.

As an approximation, it is assumed in this analysis that the deposition of small trace metal particles is equal on top and bottom surfaces. Thus the net sedimentation flux $J_{sedimentation}$ is equal to the top plate flux minus the bottom plate flux. These values are also shown in Table II-3.

Comparing the calculated and measured sedimentation fluxes shows that reasonable agreement has been obtained. Since the sedimentation flux is about 70% of the total top plate flux, it is concluded that sedimentation is the dominating deposition mechanism for these trace metals at this site.

CONCLUSIONS

The airborne size distributions of lead, zinc, and cadmium at Caltech in Pasadena, California, are bimodal. The upper mode, located above 10 μm aerodynamic diameter, is considerably stronger for zinc and cadmium than for lead.

The size distributions can be used to predict the mass deposition of these trace metals on a flat surface under ambient conditions.

Using sedimentation as the mechanism for deposition, it is calculated that over 95% of the deposition mass is due to the fraction of particles greater than 10 μm aerodynamic diameter. The deposition mass from sedimentation is about 70% of the deposition mass from all mechanisms on an upward-facing flat plate, for each trace metal.

The percentages of particles of greater than 10 μm aerodynamic diameter are 17%, 32%, and 37% for lead, zinc, and cadmium, respectively. On the basis of the deposition data and the size distribution measurements, it is concluded that small particles play only a minor role in the deposition process.

The deposition velocity of a species may decrease as the species moves away from its source, if the depositional loss of particles from the atmosphere is faster than particle growth. The deposition velocity of lead, for example, decreases from 1.8 cm/sec near a freeway to 0.07 cm/sec in a remote area.

Although sedimentation of large particles may dominate mass deposition near the source, this may not be the case far from sources. Once the large particles have deposited out, the smaller material may remain airborne for considerable periods of time. These particles may eventually deposit by diffusional deposition or other mechanisms.

In some cases, attachment of small particles to larger particles may be important. For example, the lead size distribution near long stretches of rural highways may be dominated by the very small particles produced by steadily cruising automobiles. Far from the roadway, attachment to large dust particles may increase the lead mass median aerodynamic diameter.

The above analysis applies only for deposition on smooth surfaces. Deposition velocities on rough, natural surfaces are likely to be greater than sedimentation velocities, even for large particles.

Parts of this chapter were presented at the Third International Conference on Environmental Sensing and Assessment (Davidson et al., 1975), and have been published in the Journal of Powder Technology (Davidson, 1977).

APPENDIX I:

CALIBRATION OF THE MODIFIED ANDERSEN IMPACTOR

In order to sample isokinetically and to fractionate larger particle sizes, an Andersen model 20-000 Sampler was modified. The modifications involved construction of a new orifice and two additional stages. The new orifice was similar in design to the original model, but the diameter was one-half inch rather than one inch. The new stages were similar to the regular Andersen stages, but used larger jet diameters. The uppermost stage (stage A) had 222 jets of 1/8 inch diameter, while stage B had 110 jets of the same diameter.

Calibration of the impactor was accomplished in two series of runs. The first runs used monodisperse polystyrene latex and polyvinyltoluene particles (Dow Chemical Company) which were used to calibrate the lower stages. Then the top three stages (A, B, and the regular stage 1) were calibrated by sizing ambient particles under an optical microscope (American Optical Spencer Microstar binocular microscope, 100x magnification using a No. 426 10x micrometer eyepiece and 10x objective lens). A flow rate of 13.2 liters per minute (LPM) was used for all calibration runs.

The monodisperse particle runs used 0.794, 1.01, 2.02, and 5.7 μm particles. One particle size was used at a time. The mass of particles depositing on each of the eight regular Andersen stages (0 through 7) during each of the four runs was measured. There were too few 5.7 μm particles to obtain accurate weights, so these particles were counted under the optical microscope. Using these data, the curves of Figure A I-1 were obtained.

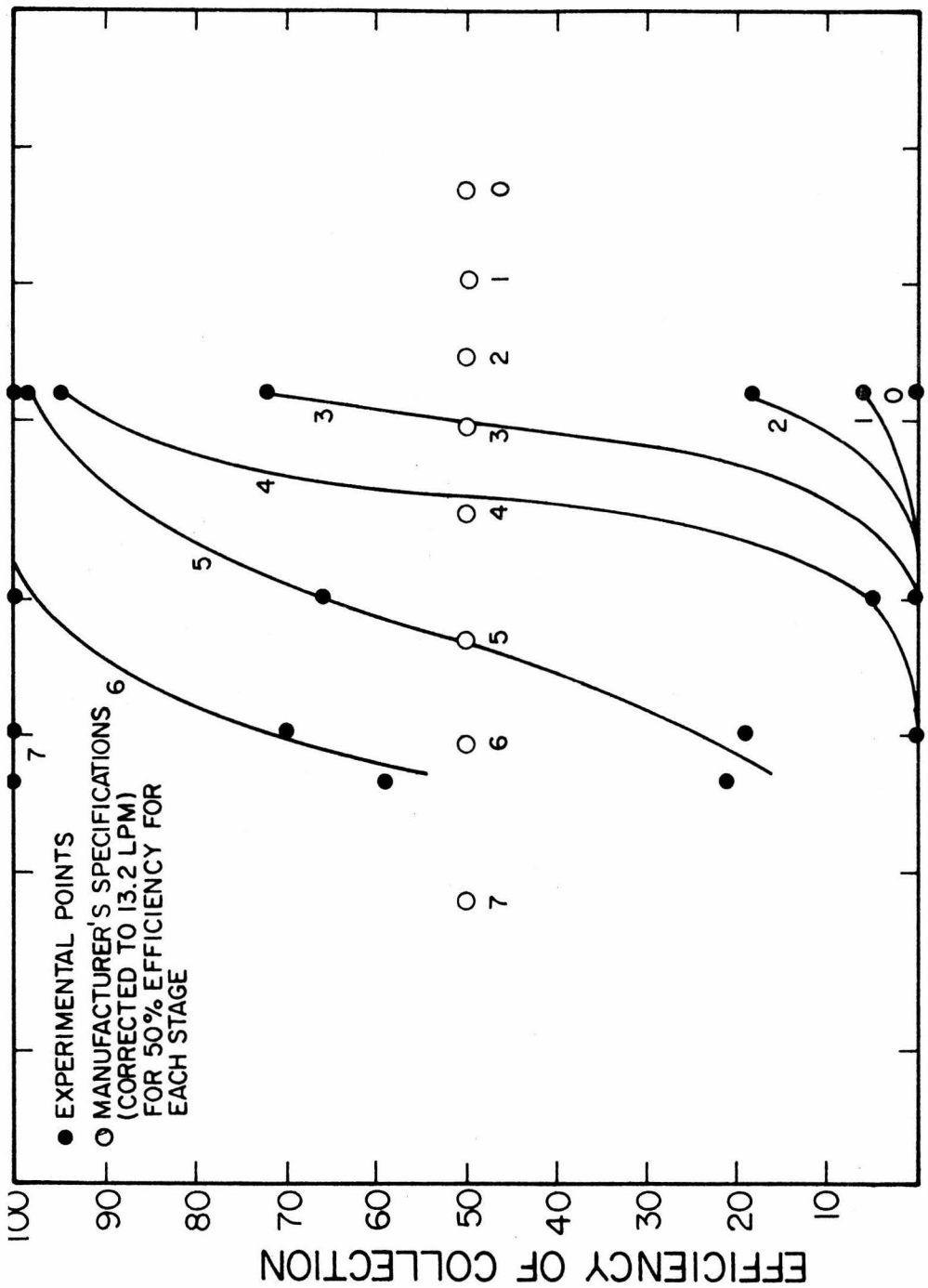

Figure A I-1 Efficiency of collection versus particle diameter for the Anderson impactor, stages 0 through 7. The reasonable agreement between experimental curves and Andersen specifications implies that the impactor may be operated satisfactorily at 13.2 liters per minute.

Reasonable agreement is seen to exist for those stages with sufficient data. Thus it was deemed acceptable to use the more thorough calibration results of Flesch et al. (1967) corrected from 28.3 to 13.2 LPM.

The size distributions of Figures II-1 and II-2 assume a uniform mass distribution with respect to log d_p on each impactor stage. This yields only a stairstep approximation to the true distribution, but there is no physical basis for interpolating values between the cutoffs. To be consistent with the uniform mass assumption, it is assumed that a uniform mass distribution impinges upon an impactor stage with a known efficiency curve, such as one of the curves of Figure A I-1.

All particles greater than $d_{p_{max}}$ will be captured by the stage, while all particles smaller than $d_{p_{min}}$ will pass the stage. Particles between $d_{p_{min}}$ and $d_{p_{max}}$ will have various collection efficiencies depending on the shape of the curve. The effective "mass mean diameter" cutoff for this stage, d_{p_m}, can be defined as:

$$\log d_{p_m} = \frac{\int_{\log d_{p\,min}}^{\log d_{p\,max}} \log d_p \, m(\log d_p)\, \eta\,(\log d_p)\, d \log d_p}{\int_{\log d_{p\,min}}^{\log d_{p\,max}} m(\log d_p)\, \eta\,(\log d_p)\, d \log d_p} \qquad \text{(A I-1)}$$

Since the distribution is assumed to be uniform in mass with respect to $\log d_p$, $m(\log d_p)$ is a constant and can be cancelled out of the above equation:

$$\log d_{p_m} = \frac{\int_{\log d_{p_{min}}}^{\log d_{p_{max}}} \log d_p \, \eta \, (\log d_p) \, d \log d_p}{\int_{\log d_{p_{min}}}^{\log d_{p_{max}}} \eta \, (\log d_p) \, d \log d_p} \qquad \text{(A I-2)}$$

The standard deviation of d_{p_m} can also be obtained:

$$\sigma^2 \log d_{p_m} = \frac{\int_{\log d_{p_{min}}}^{\log d_{p_{max}}} (\log d_p - \log d_{p_m})^2 \, \eta \, (\log d_p) \, d \log d_p}{\int_{\log d_{p_{min}}}^{\log d_{p_{max}}} \eta \, (\log d_p) \, d \log d_p} \qquad \text{(A I-3)}$$

The curves of Flesch, et al. (1967) have been used to determine the d_{p_m} cutoffs and $\sigma_{d_{p_m}}$ for the lower impactor stages. Values are shown in Table A I-1. For the size distributions of Figures II-1 and II-2, the d_{p_m} and $\sigma_{d_{p_m}}$ values were recalculated for a flow rate of 13.2 liters per minute.

Inspecting the standard deviations, it is clear that the efficiency curves are highly nonideal. The large particle stages are in fact more nonideal than the lower stages. This is because the Reynolds numbers in the jets decrease in the upper stages, hence the air velocity profiles across the jets are more nonuniform (Marple and Liu, 1974; Marple, et al. 1974). Thus a particle being carried through the center

TABLE A I-1

Values of mass mean cutoff diameters d_{p_m} and the standard deviations, for the Andersen impactor efficiency curves. The curves are from Flesch et al. (1967) for the calibration flow rate of 28.3 liters per minute. The values for stage 7 (not studied by Flesch et al.) were obtained by assuming the same shape efficiency curve as stage 6 but with a stage 7 $d_{p_{50}}$ value according to Andersen specifications.

Impactor Stage	d_{p_m} µm	$\sigma_{d_{p_m}}$ µm
2	6.63	2.25
3	3.78	1.51
4	1.98	0.74
5	1.06	0.50
6	0.80	0.43
7	0.53	0.29

of a jet has a different velocity than a particle near the jet wall and hence a different impaction efficiency. Stages A, B, and 1 have the lowest Reynolds numbers and the greatest standard deviations, necessitating the calibration with atmospheric particles.

Bounceoff and wall losses also affect the nonideality of an impactor (Hidy, 1973; May, 1964; Rao, 1975), but these problems have not been examined in detail in this study.

The standard deviations for stages 6 and 7 are greater than 50% of the d_{p_m} values, according to Table A I-1. If there is a submicron peak between 0.1 and 0.5 μm equivalent diameter, as measured by Hering (1977), then a sizable fraction of these small particles may deposit on stages 6 and 7. Thus the large peaks at 1 μm may be influenced by submicron material.

The upper three stages of the impactor were calibrated by running the impactor isokinetically at the same site as the trace metal experiments, a few weeks later. The atmospheric particles were sized geometrically under the optical microscope. Many of the particles were observed to be spores, insect parts, and other organic material when compared to photographs by McCrone and Delly (1973). Thus a density of 1 g/cm^3 was assumed, after Lundgren and Paulus (1974) who measured a density of 1.1 g/cm^3 for such particles.

The number and mass distributions for each of the top three stages are shown in Figures A I-2, A I-3, and A I-4. In order to obtain satisfactory statistics, a total of 1236 particles were sized for stage A, 1186 for stage B, and 1104 for stage 1. The upper cutoff of 40 μm was

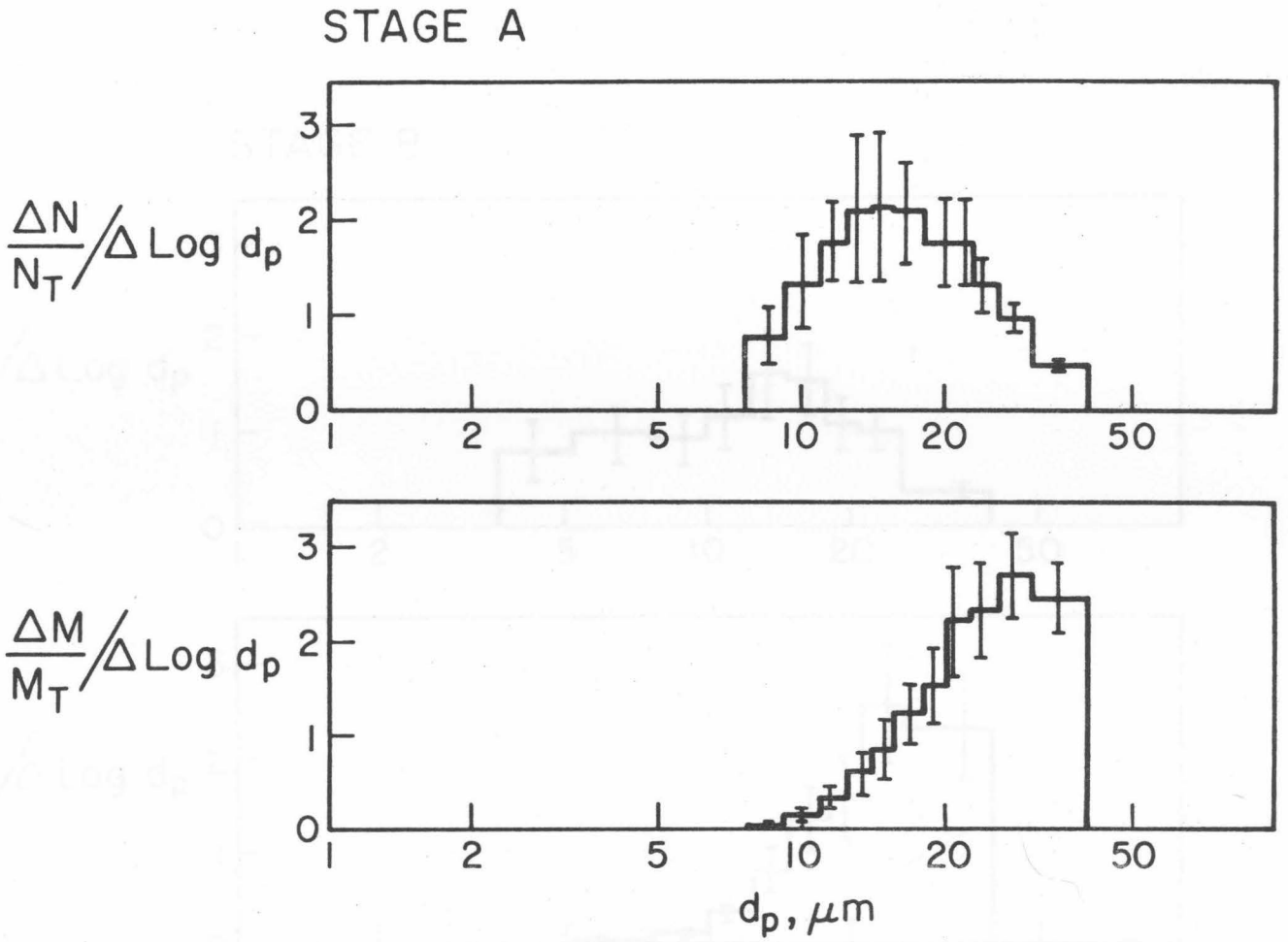

Figure A I-2 Number and mass distributions for stage A of the modified Andersen impactor. ΔN is the number concentration in each size range in particles/cm^3, while N_T is the total number concentration in all size ranges. M represents the mass concentration based on unit density spherical particles and the values of N.

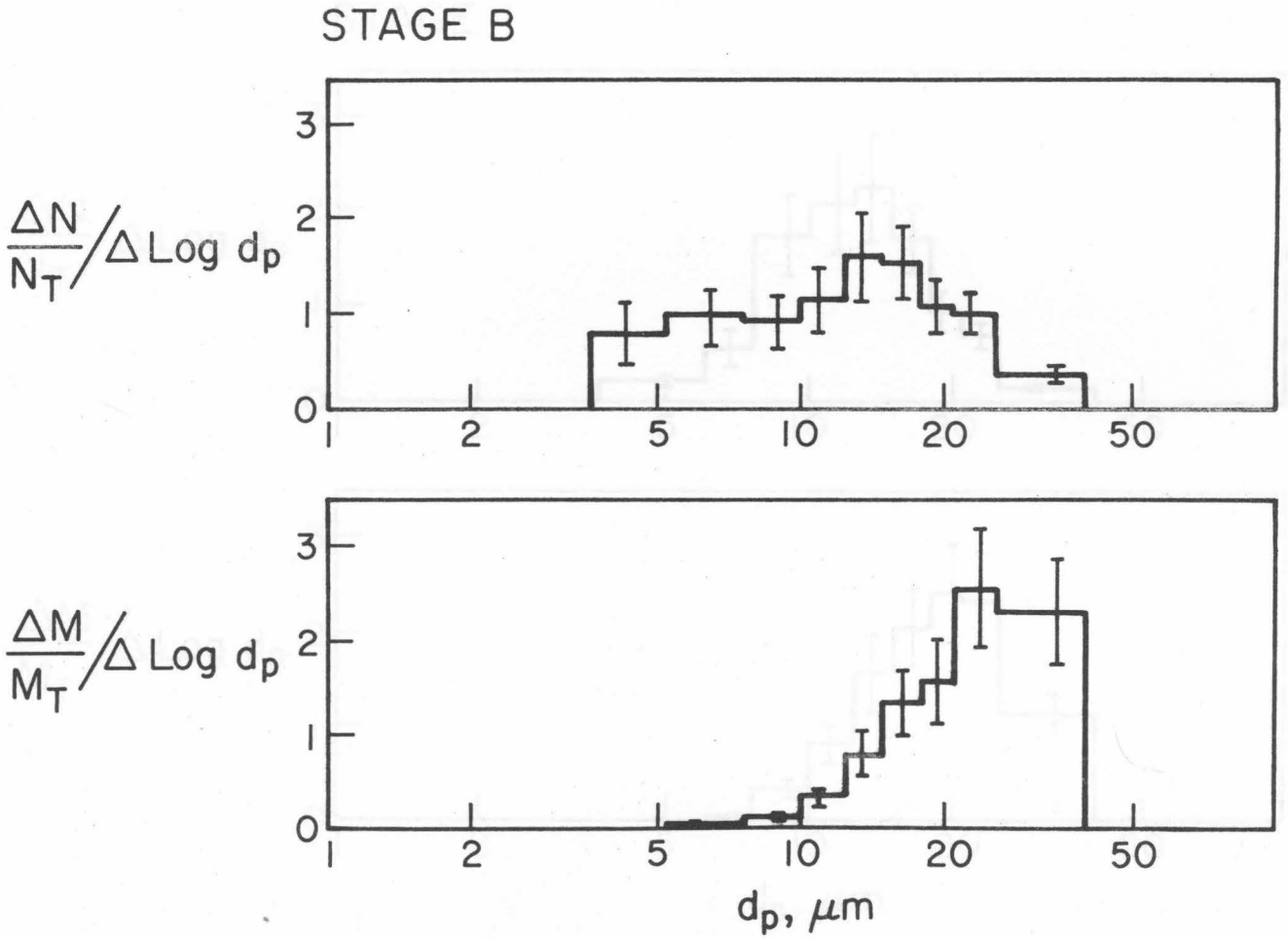

Figure A I-3 Number and mass distributions for stage B of the modified Andersen impactor.

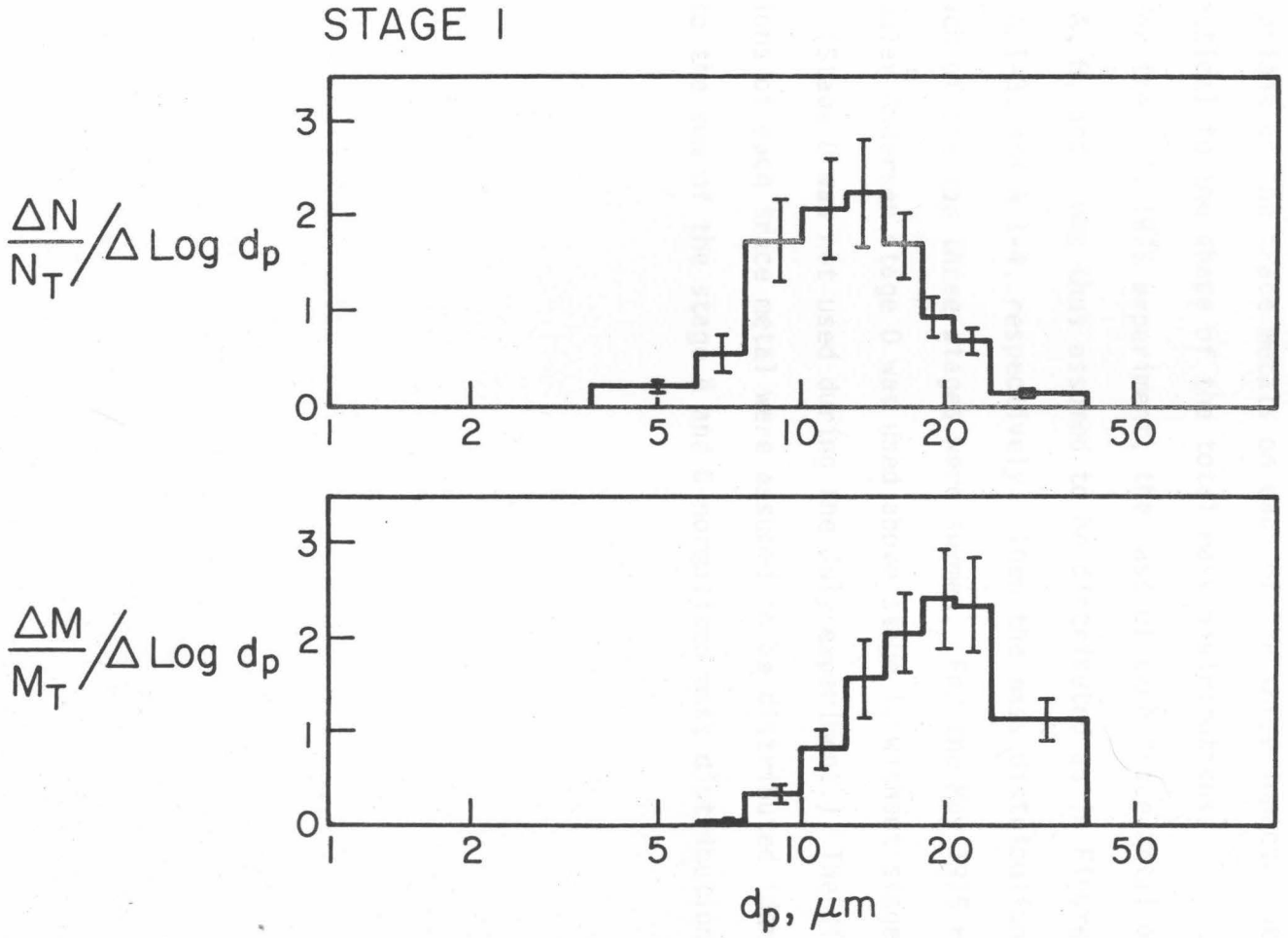

Figure A I-4 Number and mass distributions for stage 1 of the regular Andersen impactor.

assumed since there were statistically too few particles measured above this size. These data were used by assuming that the shape of the size distributions of the trace metals on each of the three impactor stages was identical to the shape of the total mass distributions.

For the July 1975 experiment, the mass of each trace metal on stages A, B, and 1 was thus assumed to be distributed as in Figures A I-2, A I-3, and A I-4, respectively. Then the mass distributions from each of the top three stages were summed. For the May 1975 run, the regular Andersen stage 0 was used above stage 1, without stages A and B. (Stage 0 was not used during the July experiment.) The distributions of each trace metal were assumed to be distributed identically to the sum of the stage A and B normalized mass distributions.

APPENDIX II:

THE DEPOSITION OF SULFATES

INTRODUCTION

The studies involving trace metal deposition showed that the large particles with diameters greater than 10 microns aerodynamic diameter dominated deposition on both a smooth, flat surface and a rough vegetated surface. It was thus convenient to study large particle transport mechanisms such as sedimentation and impaction. However, it was not possible to study the diffusional deposition of small particles using trace metals because only a tiny fraction of the total flux was due to diffusion.

In order to study diffusional deposition, profiles of condensation nuclei concentration were measured above a grassy field. These data enabled estimates of deposition by diffusion which were useful in verifying the filtration model. But because the size distributions of the condensation nuclei were not known, these measurements were of limited value.

The deposition of sulfates was studied in order to examine diffusional deposition from the free atmosphere. Size distributions of sulfates could be measured, there were sufficiently high concentrations of atmospheric sulfates to make analysis easy, and sulfate deposition was believed to be important in its own right. The analysis technique was only semi-quantitative, however, and thus the results were of an approximate nature.

The procedure followed in the sulfate experiments was similar to that of the trace metal experiments. First, a model was developed for calculating the expected sulfate deposition onto flat surfaces. Then the airborne size distributions were measured. The size distribution data were used in the predictive model to calculate expected fluxes. Next, these calculated fluxes were compared to measured sulfate fluxes.

The agreement between calculated and measured fluxes is not as close as in the trace metal experiments. However, order-of-magnitude agreement suggests that the model may be useful for promoting a better understanding of small particle deposition from the atmosphere. It is believed that the main weaknesses in these experiments involved the analytical measurement techniques, rather than defects in the predictive models.

THEORY

The physical problem of diffusional deposition of particles onto a smooth, horizontal flat plate from a horizontal wind has been discussed by Friedlander (1977). This situation is illustrated in Figure A II-1. The local flux J(x) in ng/cm^2 sec for this case is given by Friedlander:

$$J(x) = .339 \frac{D}{x} Re_x^{1/2} Sc^{1/3} C_\infty \qquad \text{(A II-1)}$$

where D = Brownian diffusivity in cm^2/sec

x = distance along the plate from the upstream edge, in cm

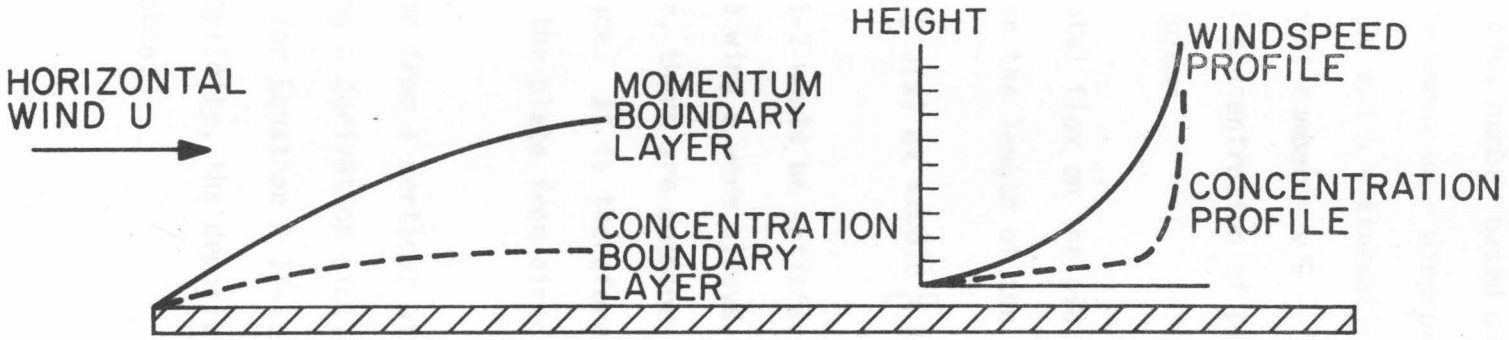

Figure A II-1 Deposition of particles on a smooth, horizontal plate from a horizontal wind. The deposition flux decreases with downstream distance along the plate due to increasing thicknesses of the boundary layers. The concentration boundary layer is relatively thin because most of the resistance to mass transport is close to the plate.

Re_x = Reynolds number based on distance along the plate

= $u_\infty x/\nu$ where u_∞ = windspeed far from the plate in cm/sec and ν = kinematic viscosity of air in cm^2/sec.

Sc = Schmidt number = ν/D

C_∞ = mass concentration of particles far from the plate, in ng/cm^3

To determine the total flux on the plate, one merely integrates Equation A II-1 over the length of the plate L:

$$J = \frac{1}{L} \int_0^L J(x)\, dx = 0.678 \frac{D}{L} Re_L^{1/2}\, Sc^{1/3}\, C_\infty \qquad \text{(A II-2)}$$

Equation A II-2 would be satisfactory for predicting fluxes onto a flat plate if the wind u were always parallel to the plate. In the atmosphere, however, there are components of wind in all directions due to natural turbulence. It is therefore necessary to consider windflow in the vicinity of the plate from directions other than parallel to the plate.

The deposition from a vertical wind, perpendicular to the plate, can be modeled using a derivation similar to that discussed by Friedlander (1977) for Equation A II-1. Figure A II-2 illustrates this case. For simplicity, the deposition surface is assumed to be an infinitely long ribbon.

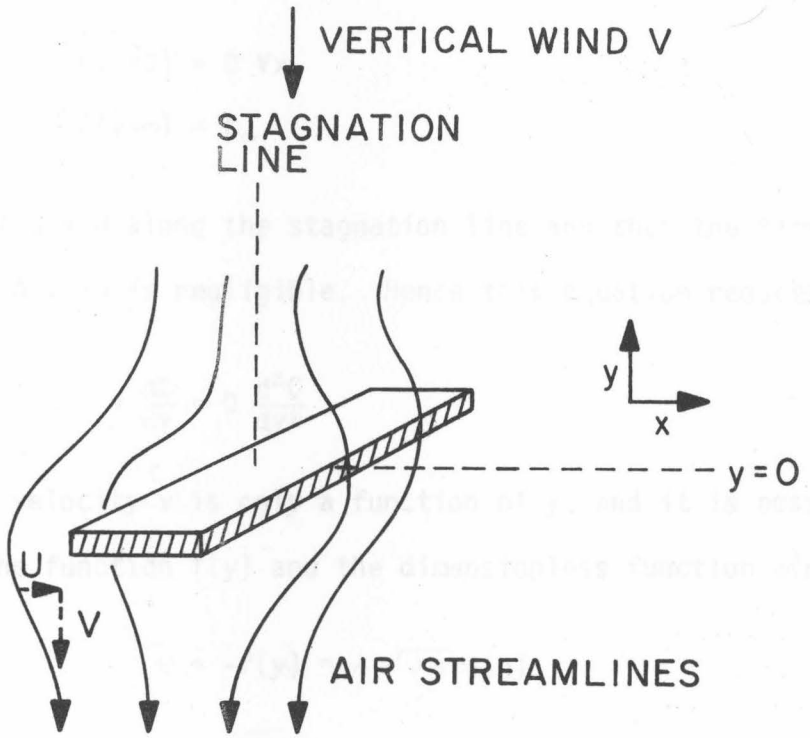

Figure A II-2 Deposition of particles on a smooth, horizontal plate from a vertical wind. The plate in this case is a uniformly accessible surface. That is, particle deposition on the plate is not a function of position.

The convective diffusion equation applicable to this problem is:

$$u \frac{\partial C}{\partial x} + v \frac{\partial C}{\partial y} = D \frac{\partial^2 C}{\partial y^2} \qquad \text{(A II-3)}$$

with boundary conditions

$$C(y=0) = 0 \quad \forall x$$

$$C(y \to \infty) = C_\infty$$

Note that $u = 0$ along the stagnation line and that the first term in Equation A II-3 is negligible. Hence this equation reduces to:

$$v \frac{dC}{dy} = D \frac{d^2 C}{dy^2} \qquad \text{(A II-4)}$$

Thus the velocity v is only a function of y, and it is possible to define the function $f(y)$ and the dimensionless function $\phi(\eta)$:

$$v = -f(y) = -\sqrt{\nu a}\, \phi(\eta) \qquad \text{(A II-5)}$$

$$\text{where } \eta = \sqrt{\frac{a}{\nu}}\, y, \text{ dimensionless} \qquad \text{(A II-6)}$$

$$\text{and } a = v_\infty / L, \text{ in } \sec^{-1} \qquad \text{(A II-7)}$$

Next it is convenient to expand $v(y)$ and $\phi(\eta)$ in Taylor series about $y=0$ and $\eta=0$:

$$v(y) = v(0) + \left(\frac{dv}{dy}\right)_{y=0} y + \left(\frac{d^2 v}{dy^2}\right)_{y=0} \frac{y^2}{2!} + \ldots \qquad \text{(A II-8)}$$

and

$$\phi(\eta) = \phi(0) + \left(\frac{d\phi}{d\eta}\right)_{\eta=0} \eta + \left(\frac{d^2 \phi}{d\eta^2}\right)_{\eta=0} \frac{\eta^2}{2!} + \ldots \qquad \text{(A II-9)}$$

But $v(0) = 0$, and it is also known that $\left(\frac{d\phi}{d\eta}\right)_{\eta=0} = 0$ hence $\left(\frac{dv}{dy}\right)_{y=0} = 0$. Thus Equation A II-8 becomes:

$$v(y) \approx \left(\frac{d^2v}{dy^2}\right)_{y=0} \frac{y^2}{2!} = -\frac{a^{3/2}}{\nu^{1/2}} \left(\frac{d^2\phi}{d\eta^2}\right)_{\eta=0} \frac{y^2}{2!} \qquad \text{(A II-10)}$$

Denoting $\left(\frac{d^2\phi}{d\eta^2}\right)_{\eta=0}$ by $\phi''(0)$, Equation A II-4 can be rearranged and combined with Equation A II-10:

$$\frac{d^2C}{dy^2} + \frac{v_\infty^{3/2}}{DL^{3/2}\nu^{1/2}} \frac{\phi''(0)}{2} y^2 \frac{dC}{dy} = 0 \qquad \text{(A II-11)}$$

Next, note that $\frac{v_\infty^{3/2}}{DL^{3/2}\nu^{1/2}} = \frac{Sc\ Re_L}{L^3}$ so that Equation A II-11 becomes:

$$\frac{d^2C}{dy^2} + \frac{Sc\ Re_L^{3/2}}{L^3} \frac{\phi''(0)}{2} y^2 \frac{dC}{dy} = 0 \qquad \text{(A II-12)}$$

Equation A II-13 can be solved by letting $G = dC/dy$ and rewriting the equation as:

$$\frac{dG}{dy} + \frac{Sc\ Re_L^{3/2}}{L^3} \frac{\phi''(0)}{2} y^2 G = 0 \qquad \text{(A II-13)}$$

The solution of Equation A II-13 is:

$$G(y) = C_1 \exp\left(-\frac{Sc\ Re_L^{3/2}}{L^3} \frac{\phi''(0)}{2} \frac{y^3}{3}\right) \qquad \text{(A II-14)}$$

$$\Rightarrow C(y) = \int_0^y G(y')\,dy' = \int_0^y C_1 \exp\left(-\frac{Sc\ Re_L^{3/2}}{L^3} \frac{\phi''(0)}{2} \frac{y'^3}{3}\right) dy' \qquad \text{(A II-15)}$$

where C_1 is an arbitrary constant.

Applying the boundary conditions of Equation A II-3 yields:

$$C(y) = \frac{Sc^{1/3}\, Re_L^{1/2}}{L} \frac{\phi''(0)^{1/3}}{6^{1/3}} \frac{C_\infty}{\Gamma(4/3)}$$

$$\int_0^y \exp\left(-\frac{Sc\, Re_L^{3/2}}{L^3} \frac{\phi''(0)}{2} \frac{y'^3}{3}\right) dy' \qquad \text{(A II-16)}$$

It is now straight-forward to determine the flux:

$$J = -D\left(\frac{dC}{dy}\right)_{y=0} = \frac{D\phi''(0)^{1/3}}{6^{1/3}\Gamma(4/3)} \frac{Re_L^{1/2} Sc^{1/3}}{L} C_\infty \qquad \text{(A II-17)}$$

The value of $\phi''(0)$ is given by Schlicting (1960) as 1.2326, hence the final expression for flux becomes:

$$J = 0.661 \frac{D}{L} Re_L^{1/2}\, Sc^{1/3}\, C_\infty \qquad \text{(A II-18)}$$

Note that since the situation pictured in Figure A II-2 and mathematically described by Equation A II-18 represents deposition on a uniformly accessible surface, the integrated flux will equal the local flux. That is, the flux J in Equation A II-18 is not a function of x.

Comparing Equations A II-2 and A II-18 shows that very little difference in deposition is expected whether the plate is parallel or perpendicular to the airflow. The general form of the flux equation is thus:

$$J = K(\theta) \frac{D}{L} \left(\frac{u_\infty L}{\nu}\right)^{1/2} \left(\frac{\nu}{D}\right)^{1/3} C_\infty \qquad \text{(A II-19)}$$

where $K(0^o) = 0.678$

and $K(90^o) = 0.661$

If $f(u)$ and $f(\theta)$ are the probability density functions of the wind velocity (in any direction) and wind angle relative to the plate, respectively, then application of Equation A II-19 to the atmosphere, denoting the windspeed far from the plate by u, yields:

$$J = \int_{\theta} \int_{u} K(\theta) \frac{D}{L} \left(\frac{uL}{\nu}\right)^{1/2} \left(\frac{\nu}{D}\right)^{1/3} C_{\infty} f(u) f(\theta) \, du \, d\theta \qquad \text{(A II-20)}$$

Since $K(\theta)$ is nearly independent of θ, Equation A II-20 can be written:

$$J = \int_{u} K \frac{D}{L} \left(\frac{uL}{\nu}\right)^{1/2} \left(\frac{\nu}{D}\right)^{1/3} C_{\infty} f(u) \, du \qquad \text{(A II-21)}$$

A further approximation can be made with regard to $f(u)$. It is assumed that the probability density function for the horizontal wind determined by Best (1935) and later confirmed by Pasquill (1974) applies in this case. The expression for $f(u)$ is:

$$f(u) = \frac{1}{\sqrt{2\pi}\, \bar{u}/\sqrt{26}} \exp\left[-\frac{1}{2} \frac{(u-\bar{u})^2}{(\bar{u}/\sqrt{26})^2}\right] \qquad \text{(A II-22)}$$

This function may be substituted into Equation A II-21 and integrated numerically. However, $f(u)$ has a small standard deviation ($\bar{u}/\sqrt{26}$), and it is believed that the influence of brief wind gusts is negligible. This was shown to be true for impaction on cylinders by performing the numerical integration; the integrated results agreed with calculations incorporating $\bar{u}$ to within 1%. Thus Equation A II-19 will be used directly, with K = 0.678 and a mean windspeed $\bar{u}$.

Experiments were also performed using pipes. The deposition of ambient sulfate aerosols on the walls of the pipes was measured. These experiments, while not directly applicable to deposition on natural surfaces, had the advantage of better control over the experiment parameters. For example, the airspeed through the pipes could be controlled (unlike ambient windspeeds). Also, impactors and filters could be used to selectively prevent various sizes of particles from entering the pipes.

The equations for pipe deposition by convective diffusion are similar to the flat plate expressions. According to Friedlander (1977), the flux to the pipe walls at a sufficient distance from the entrance for turbulent flow, Re $\gtrsim$ 2100, is:

$$J = 0.042 \frac{D}{d} F^{1/2} \, Re \, Sc^{1/3} \qquad \text{(A II-23)}$$

where d = pipe diameter in cm

and F = Fanning friction factor, dimensionless

This equation will be used to predict sulfate deposition in the pipe deposition experiments.

Convective diffusion is not the only mechanism influencing sulfate deposition. The turbulent inertial mechanism first studied by Friedlander (1957) applies to particle sizes larger than about 1 μm. Calculations based on the sulfate size distributions, however, showed that this mechanism was of negligible importance compared to convective diffusional deposition of the much larger airborne mass of submicron particles.

EXPERIMENTS: PRESENTATION OF DATA

The three types of experimental data include deposition on flat surfaces, deposition on the inside walls of pipes, and size distribution measurements. All experiments were performed on the roof of Keck Laboratories.

Flat Surface Experiments

The sulfate aerosols were collected on stainless steel strips, mounted on glass microslides or plywood. The mounting scheme is shown in Figure A II-3. Analysis was performed using the method of Roberts (1975). This method involves discharging capacitors through a strip, which heats and thereby vaporizes the sulfates. The gaseous sulfur is then pulled into a Meloy model SA 160-2 Total Sulfur Analyzer.

For calibration purposes, standard solutions of $(NH_4)_2SO_4$ and $CaSO_4$ were made up. The solutions contained 15 ng of sulfur per microliter. A Hamilton model 7001-NCH Microliter Syringe was used to place one microliter of standard solution on a cleaned stainless steel strip. Then the strip was flashed, and the linear output signal of the Meloy sulfur analyzer was integrated. This yielded a value corresponding to 15 ng of sulfur. The assumption here is that all of the sulfur in the drop of solution is vaporized by the capacitor discharge.

The vaporization temperature of $(NH_4)_2SO_4$ is less than 500^{o} C, while $CaSO_4$ vaporizes at 1149^{o} C (Roberts, 1975). By varying the charging voltage on the capacitors, it was possible to control when these and other sulfur compounds were vaporized.

Figure A II-4 shows the relative recovery of $(NH_4)_2SO_4$ and $CaSO_4$ as functions of capacitor voltage. Note that $CaSO_4$ recovery drops off

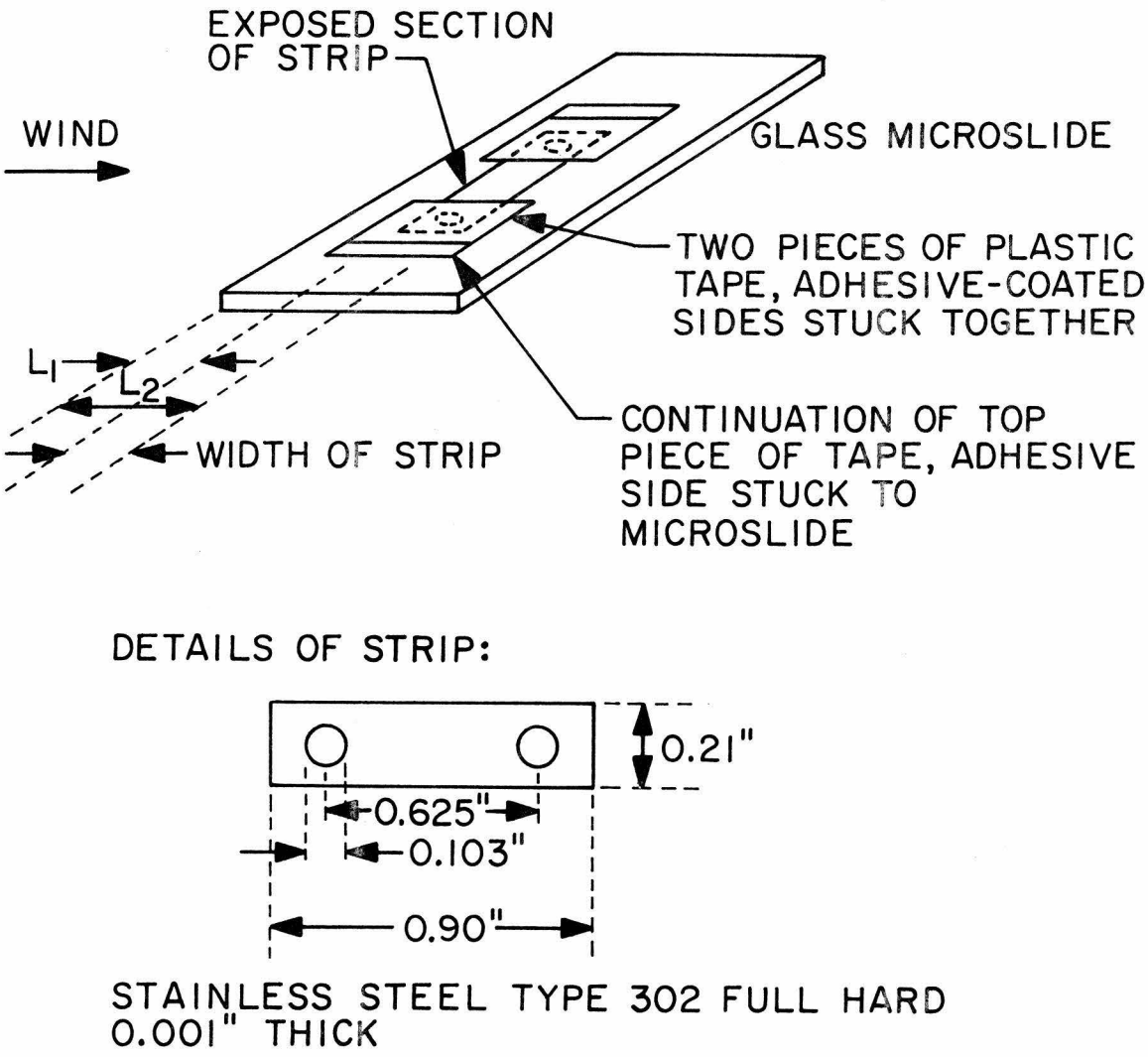

Figure A II-3 Mounting scheme for stainless steel strips for measuring sulfate deposition. The glass microslides were taped to small pieces of plywood. The plywood was in turn supported by "C"-clamps on a wooden post 350 cm tall, mounted to the surface of the Keck Laboratory penthouse roof. This location was the same site as that used for the trace metal experiments.

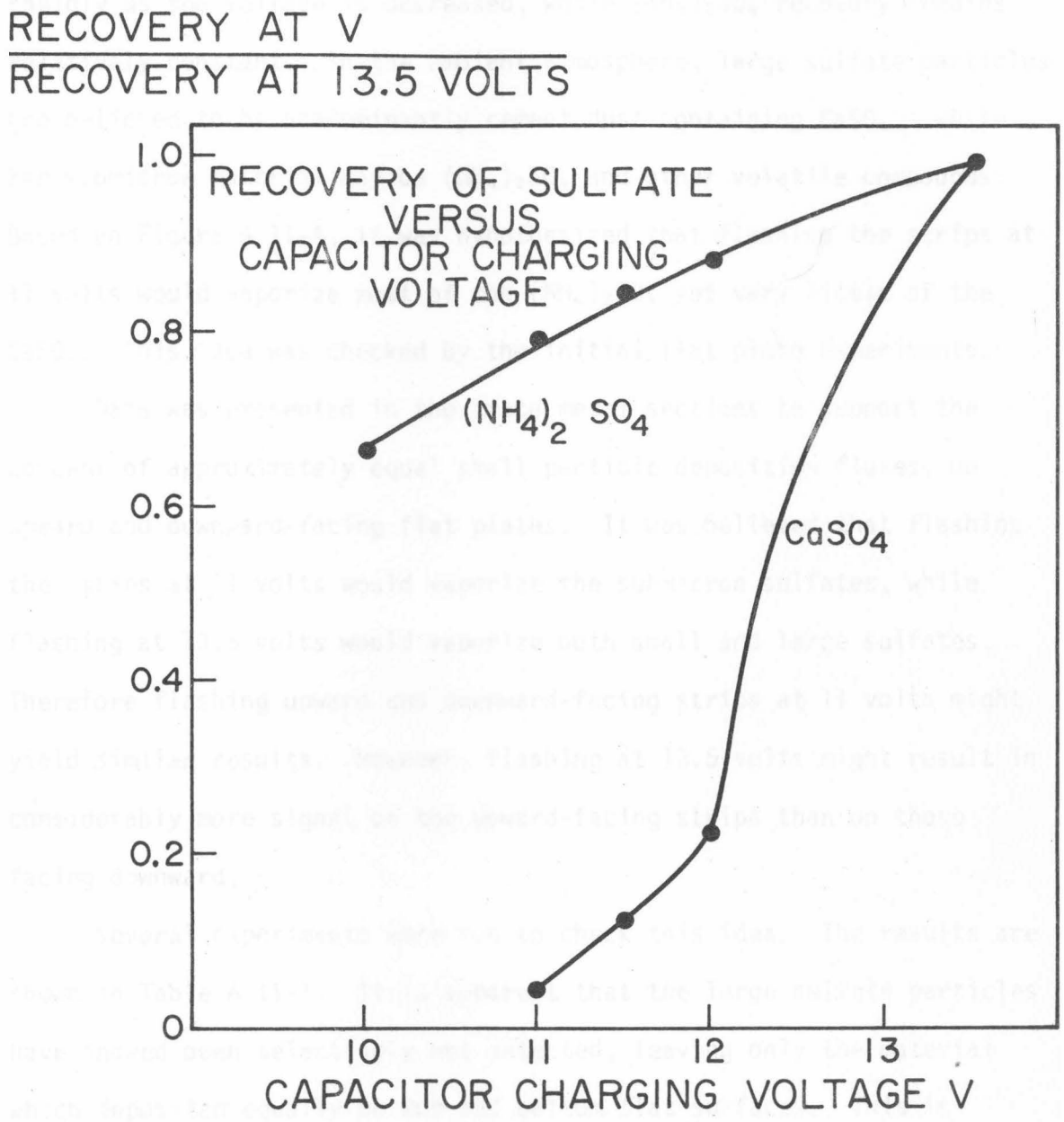

Figure A II-4 The recovery of two standard solutions of sulfate as a function of capacitor charging voltage. The solutions were 15 ng/microliter $(NH_4)_2\ SO_4$ and 15 ng/microliter $CaSO_4$. Note that the $(NH_4)_2SO_4$ is barely affected by a decrease in capacitor voltage, while $CaSO_4$ decreases markedly. On the basis of these data, the flashing voltage of 11 volts was chosen.

rapidly as the voltage is decreased, while $(NH_4)_2SO_4$ recovery remains relatively constant. In the ambient atmosphere, large sulfate particles are believed to be predominantly cement dust containing $CaSO_4$, while the submicron material may be $(NH_4)_2SO_4$ and other volatile compounds. Based on Figure A II-4, it was hypothesized that flashing the strips at 11 volts would vaporize most of the $(NH_4)_2SO_4$ yet very little of the $CaSO_4$. This idea was checked by the initial flat plate experiments.

Data was presented in the trace metal sections to support the concept of approximately equal small particle deposition fluxes, on upward and downward-facing flat plates. It was believed that flashing the strips at 11 volts would vaporize the submicron sulfates, while flashing at 13.5 volts would vaporize both small and large sulfates. Therefore flashing upward and downward-facing strips at 11 volts might yield similar results. However, flashing at 13.5 volts might result in considerably more signal on the upward-facing strips than on those facing downward.

Several experiments were run to check this idea. The results are shown in Table A II-1. It is apparent that the large sulfate particles have indeed been selectively not detected, leaving only the material which deposited equally on top and bottom flat surfaces. This is presumably submicron aerosol material. In all subsequent experiments, the capacitor was charged to 11 volts.

Three additional flat plate experiments were performed. The first of these runs was designed to detect differences in daytime versus nighttime deposition. Day strips were exposed from 7 AM to 5 PM, while the

TABLE A II-1

Deposition of sulfates on flat surfaces facing upward and downward, as a function of capacitor charging voltage. Number of samples is shown in parentheses.

1975 Date	Deposition of Sulfates in ng S/cm^2 day		Capacitor Voltage*	Ratio of: Top surface deposition / Bottom surface deposition
	Top surface	Bottom surface		
Oct. 23-27	13.03 ± 0.61 (2)	3.96 ± 0.18 (2)	13.5 volts	0.304 ± 0.020
Oct. 23-30	20.61 ± 3.03 (3)	7.37 ± 0.73 (3)	13.5	0.357 ± 0.063
Dec. 2-10	10.62 ± 3.41 (4)	11.65 ± 2.46 (4)	11.5	1.097 ± 0.042
Dec. 17-23	56.19 ± 6.04 (8)	24.81 ± 3.38 (8)	13.5	0.442 ± 0.077
	32.27 ± 4.90 (7)	22.46 ± 3.21 (7)	11.5	0.696 ± 0.145
	25.80 ± 8.76 (5)	30.72 ± 5.22 (5)	11.0	1.191 ± 0.452
Dec. 24-30	25.33 ± 3.49 (5)	10.52 ± 0.99 (5)	13.5	0.415 ± 0.069
	9.07 ± 1.34 (9)	8.50 ± 0.93 (9)	11.0	0.937 ± 0.172
Summary of above experiments			13.5	0.333 ± 0.018
			11.5	0.738 ± 0.137
			11.0	0.969 ± 0.161

*The total energy released during capacitor discharge is given by $E = \frac{1}{2}\,\mathrm{Cap}\,V^2$ where Cap is the capacitance and V is the voltage. The October 23-27 and October 23-30 experiments used 11.3 volts with 285 μF capacitance. All subsequent experiments used 200 μF capacitance. The capacitor voltages for the first two experiments have therefore been normalized to $V = \sqrt{\frac{285}{200}}\ 11.3 = 13.5$ volts, in order that the effective voltage may be compared with later experiments.

night strips were exposed from 5 PM to 7 AM. The next two experiments compared deposition on grounded and ungrounded strips, both mounted on phosphor bronze sheets.

Results of these experiments are shown in Table A II-2. The data suggest that daytime and nighttime deposition are about equal, and that electrical charge effects are not of prime importance.

It is interesting to note that sulfate deposition undergoes considerable variation from day to day. Comparing the data of Tables A II-1 and A II-2 shows that submicron (11 volt flashing) deposition ranged from about 3 to 30 ng S/cm^2 day. In the discussion section, attempts will be made to calculate the expected sulfate deposition and compare the calculated value to the above measured data.

Pipe Experiments

To obtain better control over the experiments, vertical pipes were set up on the roof of Keck Laboratory, and sulfate deposition on the inner pipe walls was measured. PVC, glass, and brass pipes were used.

For the PVC pipes, strips were mounted on 20 mil thick FEP teflon sheets which were then rolled into a cylinder and slipped inside the pipes. In the glass pipe experiments, double-sided Scotch tape was used to affix the strips directly to the glass. For the brass pipes, small windows were cut out of the pipe walls. These windows, which were also made of brass, were grooved so that the strips could be slipped into a notch without the use of tape or glue. The strips were mounted 24 pipe diameters downstream from the entrance in the PVC pipes, 38 diameters

TABLE A II-2

Deposition of sulfates during day and night, and on electrically grounded and ungrounded strips. All samples flashed at 11.0 volts. Number of samples is shown in parentheses.

1976 Date		Sulfate deposition, ng S/cm^2 day	
		Top surface	Bottom surface
Jan. 23-30	Day	7.31 ± 0.68 (11)	
	Night	7.51 ± 0.87 (13)	
June 18-28	Ungrounded		3.25 ± 0.49 (6)
	Grounded		5.82 ± 0.92 (8)
June 29-July 6	Ungrounded		2.98 ± 0.57 (7)
	Grounded		3.39 ± 0.43 (5)

downstream in the glass pipes, and 63 diameters downstream in the brass pipes. During some of the pipe experiments, flat surface deposition was measured simultaneously. A summary of the pipe experimental data is shown in Table A II-3.

Size Distributions

A low pressure modified Battelle impactor (Hering et al., 1977) was used to measure sulfate size distributions on April 5, 1976 (1 run), April 21 (1 run), April 23 (3 runs), and July 27 (3 runs). The April measurements used strips not coated with sticky material, and hence bounce-off rendered the data inaccurate. The July 27 runs used strips coated with 2 μl of a solution containing 1.5% silicon oil in hexane. Later experiments by Hering et al. (1977) showed that data obtained with this coating were still subject to some inaccuracy, but the error in the measurements is believed correct to within a factor of two (Hering, 1977). The size distribution data are shown in Figure A II-5 and Table A II-4.

EXPERIMENTS: DISCUSSION OF DATA

Since reliable size distribution data were not obtained during the flat plate experiments, it is impossible to accurately calculate the expected sulfate deposition. Estimates of the theoretical flux can be made, however, by assuming reasonable airborne concentrations and particle sizes based on the July distribution data.

Referring to Figure A II-3, the proper form of Equation A II-2, integrated from L_1 to L_2 is:

Description and results of sulfate pipe deposition experiments. Number of samples is shown in parentheses.

Experiment Number	1976 Date	Pipe material, Pipe diameter	Air Velocity in pipe	Re	Misc. Information	Deposition, ng S/cm^2 day
1	Mar. 15-24	PVC, 2.4 cm	184 cm/sec	2820	Pipe 1, open entrance	7.41 ± 1.41 (9)
					Pipe 2, total filter on pipe entrance	0.64 ± 0.25 (9)
					Flat surface deposition (Continuous experiment, day and night)	9.45 ± 2.77 (5)
2	Apr. 5-7	Glass, 3.7 cm	217 cm/sec	5120	Open entrance	10.44 ± 0.96 (9)
					Flat surface deposition	12.13 ± 2.16 (4)
					(Daytime experiment, 8 AM - 5 PM, daily)	
3	Apr. 21-30		217 cm/sec	5120	Open entrance (Identical to experiment 2, except Po^{210} source was used to decharge the double-sided Scotch tape. All subsequent experiments with glass pipes were subjected to decharging.)	6.61 ± 0.79 (3)

TABLE A II-3 Continued

Experiment Number	1976 Date	Pipe material, Pipe diameter	Air Velocity in pipe	Re	Misc. Information	Deposition ng S/cm^2 day
4	May 11-16	Glass, 3.7 cm	93 cm/sec	2200	Pipe 1, open entrance	5.88 ± 0.90 (6)
					Pipe 2, Andersen impactor stage 6 on entrance, d_p <0.45 μm (Continuous experiment, day and night)	7.12 ± 0.98 (9)
5	May 27-31		116 cm/sec	2740	Pipe 1, Andersen impactor stage 6 on entrance, d_p <0.45 μm	
					Daytime 8 AM - 6 PM	5.74 ± 0.62 (7)
					Pipe 2, Andersen impactor stage 6 on entrance, d_p <0.40 μm	
					Nighttime 10 PM - 4 AM	5.49 ± 0.56 (7)
6	June 11-16		98 cm/sec	2300	Pipe 1, Andersen impactor stage 6 on entrance, d_p <0.44 μm	2.57 ± 0.31 (8)
					Pipe 2, total filter on pipe entrance (Continuous experiment, day and night)	1.35 ± 0.16 (6)

TABLE A II-3 Continued

Experiment Number	1976 Date	Pipe material, Pipe diameter	Air Velocity in pipe	Re	Misc. Information	Deposition ng S/cm^2 day
7	July 23-Aug 2	Brass, 1.9 cm	322 cm/sec	3910	Pipe 1, Andersen impactor stage 7 on entrance, d_p <0.31 μm	1.61 ± 0.20 (3)
					Pipe 2, total filter on pipe entrance (Continuous experiment, day and night)	0.90 ± 0.08 (3)

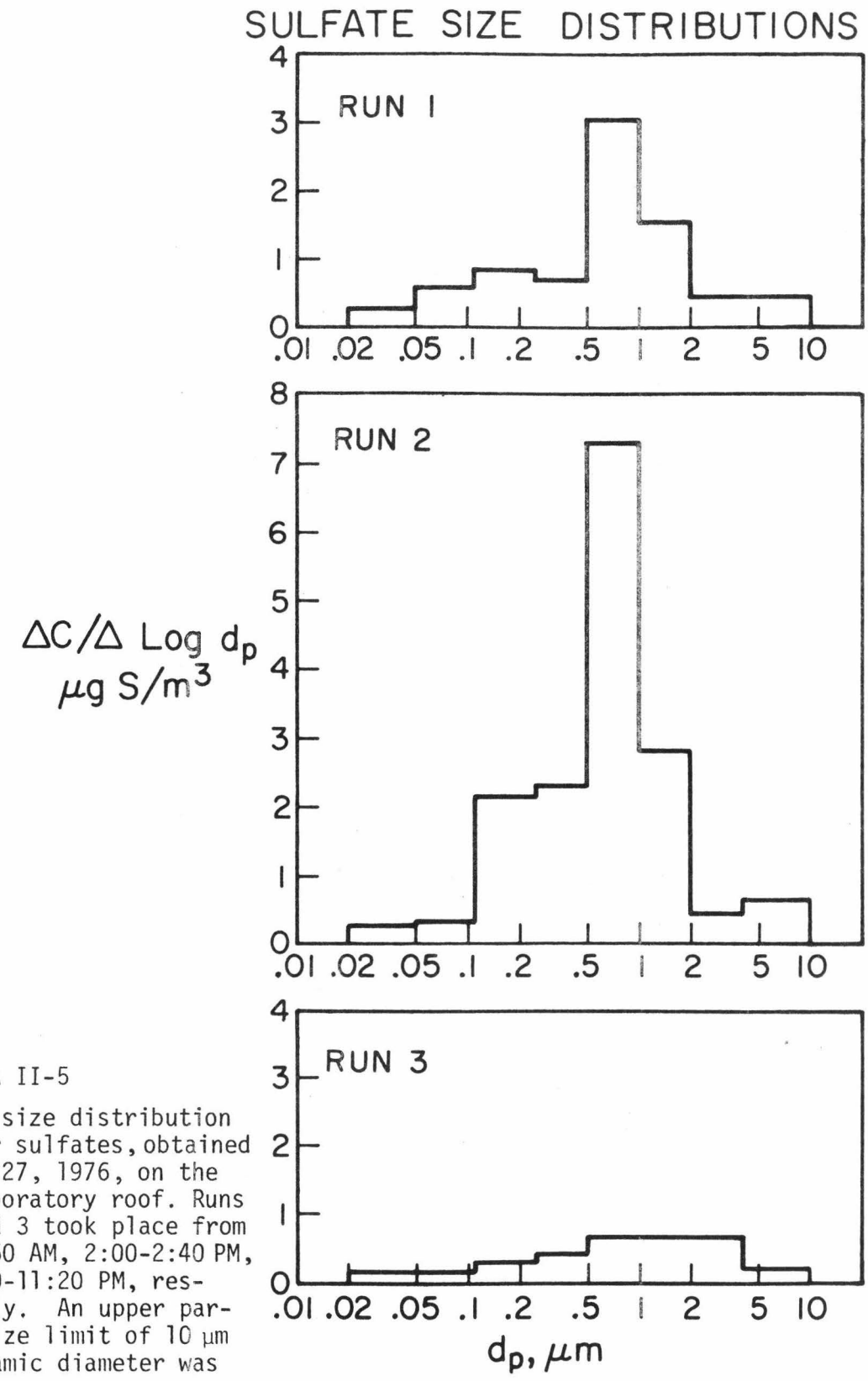

Figure A II-5

Ambient size distribution data for sulfates, obtained on July 27, 1976, on the Keck Laboratory roof. Runs 1, 2, and 3 took place from 8:20-9:50 AM, 2:00-2:40 PM, and 9:50-11:20 PM, respectively. An upper particle size limit of 10 μm aerodynamic diameter was assumed.

TABLE A II-4

Sulfate size distribution data for July 27, 1976.

Impactor Stage	Lower dp	Run 1, 8:20-9:50 AM Concentration ng S/m³	Run 1, 8:20-9:50 AM ΔC/Δlog dp ng S/m³	Run 2, 2:00-2:40 PM Concentration ng S/m³	Run 2, 2:00-2:40 PM ΔC/Δlog dp ng S/m³	Run 3, 9:50-11:30 PM Concentration ng S/m³	Run 3, 9:50-11:30 PM ΔC/Δlog dp ng S/m³
1	4 μm	161	405	261	657	85	215
2	2	125	414	128	427		
3	1	467	1551	849	2819	617	683
4	0.5	917	3048	2196	7294		
5	0.25	210	696	690	2294	123	408
6	0.11	304	853	767	2152	107	301
7	0.05	201	586	117	343	56	162
8	0.02	109	275	105	265	64	160
TOTAL CONCENTRATIONS		2494		5114		1052	

$$J = 0.678 \frac{D}{L_2 - L_1} \frac{(L_2^{1/2} - L_1^{1/2})\, u^{1/2}}{\nu^{1/2}} \left(\frac{\nu}{D}\right)^{1/3} C_\infty \qquad \text{(A II-24)}$$

where L_1 = 3.48 cm

and L_2 = 4.01 cm

Examining the size distribution data of Figure A II-5 and Table A II-4, it is probable that not much sulfate mass is found in particles smaller than 0.02 μm aerodynamic diameter. An upper limit to the flux can be calculated by assuming that the greatest airborne sulfate concentration measured, 5 μg S/m^3 during a run on July 27, is found in particles of 0.02 μm. Particles larger than this size have smaller Brownian diffusivities and hence smaller expected fluxes. (The mechanism of turbulent inertial deposition is not important for submicron particles.) It is unlikely that airborne sulfate levels were greater than 5 μg S/m^3 during the flat plate experiments, since July 27 was characterized by fairly heavy smog.

Using C = 5 μg S/m^3, d_p = 0.02 microns, and a reasonable windspeed, u = 200 cm/sec, the flux calculated by Equation A II-24 is 3.82 ng S/cm^2 day. This value may be compared to measured submicron fluxes of 2.98 to 30.72 ng S/cm^2 day (using 11 volt data). The calculated value is seen to agree with the measured fluxes only for the smallest measured values. This is surprising, since the calculation is based on a maximum airborne concentration and a maximum particle diffusivity.

It is possible that SO_2 gas molecules, with very high diffusivities, were becoming adsorbed onto the strips. It is also possible that particles smaller than 0.02 microns or larger than 1 micron were present in sufficient concentrations to contribute significantly to the flux. Of course, applying Equation A II-24 to the free atmosphere is in itself an approximation to the true, complicated deposition mechanisms. This equation only accounts for convective diffusional transport through a well-developed boundary layer.

The pipe deposition fluxes may also be calculated, using Equation A II-23. Since the size distributions of Figure A II-5 were obtained during the final pipe experiment, it is reasonable to use the distributions to calculate the flux for comparison with this experiment. This calculation is shown in Table A II-5. Here d = 1.9 cm, Re = 3910, and F = 0.01 (Perry, 1973). Using equations for turbulent inertial pipe deposition developed by Friedlander and Johnstone (1957) yielded negligible results compared to the convective diffusion calculation.

As with the flat surface calculation, these results show somewhat smaller theoretical than experimental fluxes. It is possible that errors in the size distribution measurements are partially responsible. Since July 27 was a day of considerable smog, the measured values of 2.5, 5.1 and 1.1 $\mu g\ S/m^3$ seem somewhat low. According to Hering (1977), obtaining complete recovery of sulfate by flashing the strips is difficult.

In spite of discrepancies between calculated and measured values, a number of interesting conclusions can be drawn. For example, flat surface and pipe deposition are of comparable values, usually 5-10 ng

TABLE A II-5

Calculated and measured deposition fluxes for the July 1976 sulfate pipe experiment.

Impactor Stage i	$(D_i)_{eff}=\sqrt{D_i D_{i+1}}$ Effective diffusion coefficient	Run 1 8:20-9:50 AM ΔC, $\frac{ng\ S}{m^3}$	Run 1 J, $\frac{ng\ S}{cm^2\ day}$	Run 2 2:00-2:40 PM ΔC, $\frac{ng\ S}{m^3}$	Run 2 J, $\frac{ng\ S}{cm^2\ day}$	Run 3 9:50-11:20 PM ΔC, $\frac{ng\ S}{m^3}$	Run 3 J, $\frac{ng\ S}{cm^2\ day}$
1	-						
2	-						
3	-						
4	4.18×10^{-7}	917	0.0206	2196	0.0493	-	-
5	1.01×10^{-6}	210	0.0085	690	0.0279	123	0.0050
6	3.04×10^{-6}	304	0.0256	767	0.0647	107	0.0091
7	1.17×10^{-5}	201	0.0416	117	0.0243	56	0.0115
8	5.61×10^{-5}	109	0.0644	105	0.0620	64	0.0376
	Total calculated flux, $d_p < 0.5$ μm (Stages 5-8)		0.1401		0.1789		0.0631

Measured flux, July 23-Aug. 2, $d_p < 0.31$ μm

1.61 ± 0.20 ng S/ cm^2 day (SO_2 + Sulfates)

-0.90 ± 0.08 ng S/ cm^2 day (SO_2)

0.71 ± 0.22 ng S/ cm^2 day Sulfates

S/cm^2 day, although a few higher values were measured. If airborne sulfate concentrations are assumed to be 1-5 ng S/m^3, then the deposition velocity for sulfate would be about 0.01 to 0.10 cm/sec.

Adsorption of SO_2 on the strips does not appear to be a serious problem. This is evident by comparing deposition fluxes in pipes with total aerosol filters to fluxes in pipes without the filters. Such comparisons may be made in experiments 1, 6, and 7 of Table A II-3. The measured depositions of SO_2 were 0.64, 1.35, and 0.90 ng S/cm^2 day, while pipe deposition of sulfate plus SO_2 ranged from 1.61 to 10.44 ng S/Cm^2 day.

It is interesting to note that in experiments 6 and 7, the measured sulfur levels were considerably smaller than in the previous two pipe experiments. This may have been due in part to a change in ambient concentrations, and in part to different impactor stage cutoff diameters. The smallest cutoff, d_p = 0.31 μm, also yielded the lowest sulfur deposition of the four runs.

The nighttime concentration of sulfates was seen to decrease considerably from daytime levels during the size distribution runs. However, the smallest particles detected, 0.02-0.05 μm, did not undergo as severe a decrease as the larger sulfates. This fact, in addition to the deposition data showing similar daytime and nighttime values, supports the concept of deposition controlled by very small particles.

Since the flat surface and pipe depositions were of comparable values in experiments 1 and 2, it is likely that the same deposition mechanisms were important in both cases. Thus pipe experiments are seen to be a potentially valuable aid in studying ambient deposition. The

chief advantages of pipe experiments over flat surface measurements involve control over the windspeed and the option of selectively eliminating certain particle sizes from the ambient distribution.

CONCLUSIONS

Sulfate deposition velocities over flat, smooth surfaces are estimated to be 0.01 to 0.1 cm/sec. The fluxes over rough natural surfaces are expected to be somewhat larger. Sulfate size distributions have a peak at about 0.5 microns, although some material exists at 0.02 microns. The overall data suggest convective diffusion as an important deposition mechanism. However, lack of accurate size distribution data prevents reaching a definite conclusion.

APPENDIX III

TRACE METAL AND CONDENSATION NUCLEI DEPOSITION DATA

Chapters I and II present summaries of the deposition data for lead, zinc, cadmium, and condensation nuclei. This appendix lists the individual data points for each experiment. First, lead, zinc, and cadmium flat plate deposition data for the experiments on Keck Laboratory roof are presented. Then size distribution and flat plate data are presented for nickel and vanadium. Approximate data were obtained for these species during the rooftop experiments. Next, the deposition of trace metals at several sites in Southern California is discussed and additional data are presented. Finally the individual data points of the condensation nuclei experiments are given.

Deposition of Lead, Zinc, and Cadmium on the Keck Laboratory Roof

Deposition of trace metals was measured as part of the sedimentation and cylinder impaction experiments, and also to test for resuspension of roof dust. Flat teflon plates were placed at various heights above the roof surface during several runs in 1975 and 1976. The data are presented in Table A III-1. The average values and corresponding standard deviations are plotted in Figure A III-1.

The data of Table A III-1 show that surface stickiness does not significantly affect the deposition of these trace metals. Hence, the sticky and nonsticky values were averaged to obtain the points plotted in Figure A III-1. The cadmium data are characterized by large uncertainies and considerable scatter, so only the lead and zinc profiles

Deposition of Pb, Zn, and Cd on flat teflon plates during several experiments on the Keck Laboratory Roof.

Experiment Number	Date	Height Above Roof	Position of teflon plate: Upward-Facing (U) or Downward-Facing (D)	Type of teflon: Sticky (S) Nonsticky (N)	Deposition fluxes, ng/cm^2 day		
					Pb	Zn	Cd
Sedimentation Experiment 1	Apr.17-27, 1975	58 cm	U	N	25.4 ± 1.40	7.49 ± 0.513	0.152 ± 0.126
		"	D	N	6.64 ± 1.40	2.18 ± 0.513	0 ± 0.126
		"	D	S	19.1 ± 1.40	4.04 ± 0.513	0.002 ± 0.126
Sedimentation Experiment 2	May 12-18	"	U	N	28.9 ± 1.65	8.25 ± 1.40	0.150 ± 0.131
		"	D	N	15.1 ± 1.65	2.20 ± 1.40	0.018 ± 0.131
Resuspension Experiment 1	May 29-June 10	1	U	N	37.2 ± 0.428	11.6 ± 0.187	0.070 ± 0.029
		"	U	S	44.4 ± 0.735	21.5 ± 0.322	0.234 ± 0.050
		58	U	N	27.8 ± 0.428	6.68 ± 0.187	0.064 ± 0.029
		"	D	N	4.52 ± 0.428	0.435 ± 0.187	0 ± 0.029
Resuspension Experiment 2	July 3-8	11	U	N	36.4 ± 1.21	9.35 ± 0.346	0.129 ± 0.060
		"	U	S	32.8 ± 1.21	8.54 ± 0.346	0.056 ± 0.060
		149	U	N	19.1 ± 1.22	4.37 ± 0.347	0.078 ± 0.061
		"	U	S	23.1 ± 1.22	4.62 ± 0.347	0.004 ± 0.061
		350	U	N	22.5 ± 1.20	6.23 ± 0.343	0.093 ± 0.060
		"	U	S	24.3 ± 1.20	4.72 ± 0.344	0.049 ± 0.060
		149	D	N	5.13 ± 1.22	1.52 ± 0.347	0.128 ± 0.061
		"	D	S	7.01 ± 1.22	1.10 ± 0.347	0 ± 0.061
		350	D	N	3.45 ± 1.20	0.806 ± 0.343	0.015 ± 0.060
		"	D	S	5.53 ± 1.20	0.949 ± 0.344	0 ± 0.060

TABLE A III-1 (Continued)

Sedimentation Experiment 3	July 16-20	148	U	N	22.8 ± 1.15	6.04 ± 0.400	0.042 ± 0.036
		"	U	S	14.8 ± 1.15	6.79 ± 0.400	0.106 ± 0.036
		350	U	N	22.7 ± 1.14	8.85 ± 0.400	0.068 ± 0.035
		"	U	S	19.6 ± 1.14	4.58 ± 0.400	0.146 ± 0.035
		148	D	S	4.41 ± 1.15	1.07 ± 0.400	0.098 ± 0.036
		350	D	S	2.48 ± 1.14	0.437 ± 0.398	0.042 ± 0.035
		*157	U	N	32.8 ± 2.32	12.8 ± 0.808	0.122 ± 0.072
		*157	U	S	30.5 ± 2.32	11.2 ± 0.808	0.354 ± 0.072
		*157	D	S	7.01 ± 2.32	3.82 ± 0.808	0.085 ± 0.072
Cylinder Impaction Experiment 1	Sept. 18-22, 1976	350	U	N	18.3 ± 4.82	3.81 ± 1.39	-
		"	D	N	4.58 ± 4.82	0.113 ± 1.39	-
Cylinder Impaction Experiment 2	Oct. 3-16	350	U	N	30.9 ± 1.35	5.66 ± 0.270	0.043 ± 0.086
		"	D	N	5.45 ± 1.35	0.115 ± 0.270	0.024 ± 0.086
		*150	U	N	47.8 ± 3.24	11.0 ± 0.644	0.088 ± 0.206
		**150	U	N	31.3 ± 3.04	5.50 ± 0.606	0.028 ± 0.194
Cylinder Impaction Experiment 3	Oct. 25-Nov. 3	350	U	N	23.6 ± 1.46	3.27 ± 0.680	-
		"	D	N	5.89 ± 1.46	1.28 ± 0.680	-
		*150	U	N	41.9 ± 3.61	6.39 ± 1.68	-
		**150	U	N	32.4 ± 3.62	2.04 ± 1.68	-

*Plate exposed 8 AM - 8 PM daily.
**Plate exposed 8 PM - 8 AM daily.

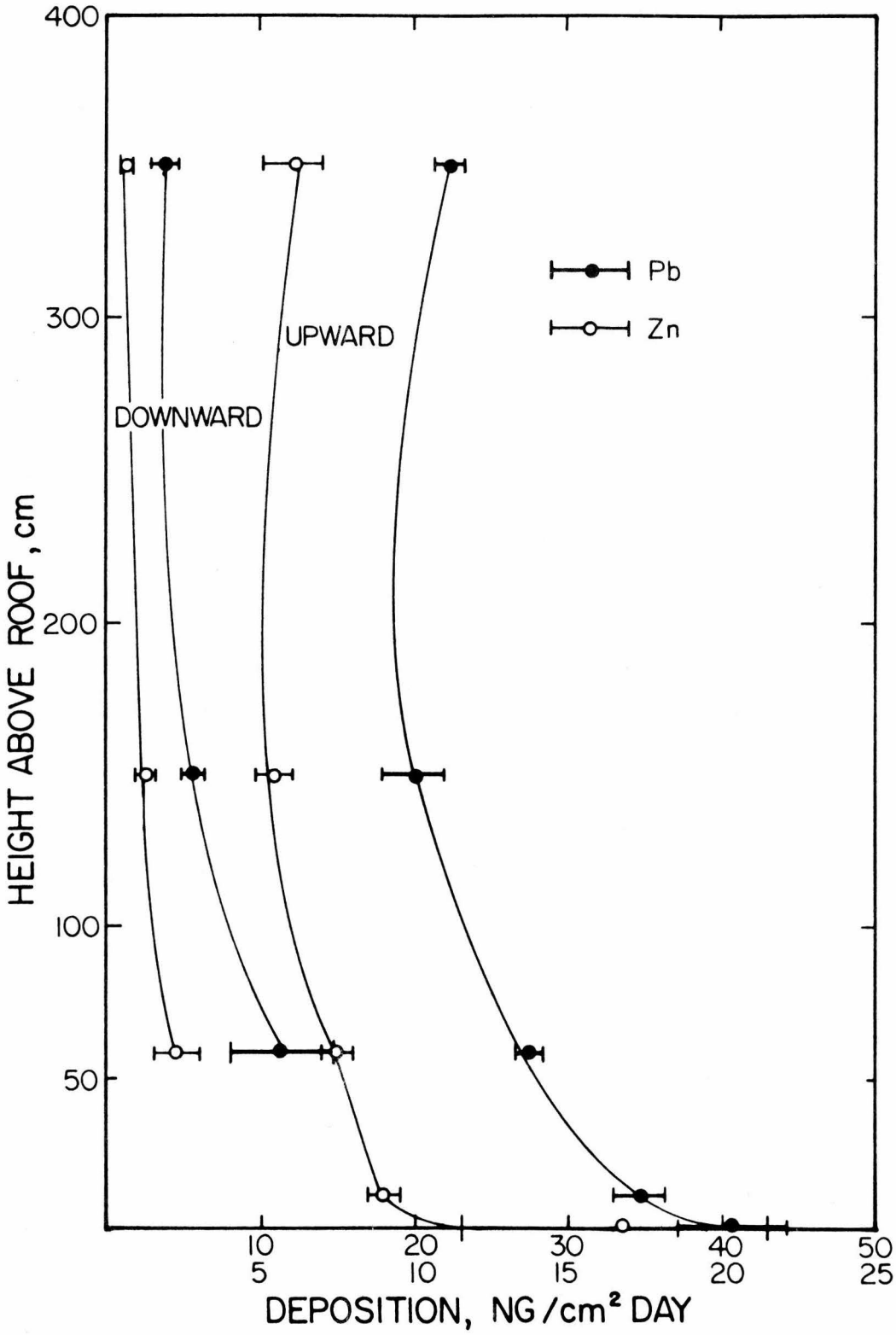

Figure A III-1 Deposition of lead and zinc on flat teflon plates as a function of height above the roof of Keck Laboratory.

are shown. Resuspended roof dust is seen to be a problem only below 150 cm.

Table A III-2 lists the size distribution data for Figures II-1 and II-2. The calculated flux data from Equation II-9 are also shown.

Deposition of Nickel and Vanadium on the Keck Laboratory Roof

The data for lead and zinc show relatively small standard deviations because of low blank levels for most of the experiments. Cadmium blank measurements in general yielded higher values than lead and zinc. The large error bars for $d_p > 4$ μm for cadmium in Figures II-1 and II-2 are mainly due to the high blanks. Because of this problem, the cadmium data must be regarded as approximate.

Nickel and vanadium data were not presented in Chapters I and II because many experiments were characterized by either very large blanks (on the order of the sample values) or by a lack of any blank measurement. The data for these two trace metals is presented here only to indicate general trends in the deposition and shapes of the size distributions. No standard deviations are given because the errors are expected to be greater than 100%.

The size distributions for nickel and vanadium for the July 1975 experiment are shown in Figure A III-2. The total airborne mass concentrations measured with the impactor and after-filter were 42.4 ng/m^3 for nickel and 30.0 ng/m^3 for vanadium, compared to total filter measurements of 12.2 and 13.5 ng/cm^3, respectively. These differences illustrate the difficulties of measuring the low ambient levels of nickel and vanadium.

TABLE A III-2

Size distribution information for the May 1975 and July 1975 sedimentation experiments.

Table (a) shows the size ranges, effective average diameters $\overline{d_p}$, and corresponding sedimentation velocities v_s $(\overline{d_p})$ using Equations II-8 and II-9. Tables (b), (c), and (d) list lead, zinc, and cadmium concentrations in each size range, respectively. Values of $(\Delta C/C_T)/\Delta \log d_p$ for Figures II-1 and II-2 are also given. In addition, the calculated sedimentation flux data are shown for each size range.

The standard deviations for total flux given in parantheses have been calculated by considering the lower impactor stages separately from the upper stages (those calibrated with atmospheric particles) when determining the fluxes. These errors are greater because a greater weighting factor is given to the impactor nonideality errors.

(a)

Andersen Impactor Size Ranges

Size Range i	Lower d_p, μm	$\overline{d_p}$, μm	$v_s(\overline{d_p})$, cm/sec
1	0.05	-	-
2	0.78 ± 0.42	0.973 ± 0.376	0.00336 ± 0.00259
3	1.18 ± 0.64	1.36 ± 0.486	0.00635 ± 0.00454
4	1.55 ± 0.74	2.19 ± 0.643	0.0156 ± 0.00919
5	2.90 ± 1.08	3.24 ± 0.604	0.0318 ± 0.0126
6	3.6 ± 0.4	4.38 ± 0.285	0.0579 ± 0.00754
7	5.2 ± 0.4	6.36 ± 0.285	0.122 ± 0.0110
8	7.6 ± 0.4	8.77 ± 0.284	0.233 ± 0.0151
9	10.0 ± 0.4	11.18 ± 0.284	0.378 ± 0.0192
10	12.4 ± 0.4	13.58 ± 0.283	0.558 ± 0.0233
11	14.8 ± 0.4	16.37 ± 0.283	0.811 ± 0.0281
12	18.0 ± 0.4	19.58 ± 0.283	1.159 ± 0.0336
13	21.2 ± 0.4	23.17 ± 0.283	1.624 ± 0.0397
14	25.2 ± 0.4	27.95 ± 0.283	2.363 ± 0.0479
15	30.8 ± 0.4	35.49 ± 0.284	3.810 ± 0.0610
	40.4 ± 0.4		

TABLE A III-2 (b)

Lead Data, Sedimentation Exp. 2, May 1975

Size Range i	ΔC, ng/m^3	$\frac{\Delta C/C_T}{\Delta \log d_p}$	J,(Eq. II-9) ng/cm^2 day
1	485.15 ± 19.39	0.350 ± 0.146	-
2	119.64 ± 7.654	0.583 ± 1.099	0.035 ± 0.027
3	80.17 ± 6.875	0.570 ± 1.474	0.044 ± 0.032
4	122.93 ± 7.728	0.391 ± 0.379	0.166 ± 0.098
5	29.68 ± 2.348	0.273 ± 0.491	0.082 ± 0.033
6	50.70 ± 3.998	0.274 ± 0.103	0.254 ± 0.039
7	46.68 ± 3.817	0.244 ± 0.0634	0.492 ± 0.060
8	33.85 ± 2.988	0.245 ± 0.0630	0.681 ± 0.075
9	26.61 ± 3.588	0.245 ± 0.0676	0.869 ± 0.125
10	27.09 ± 2.790	0.304 ± 0.0790	1.306 ± 0.145
11	23.34 ± 2.254	0.237 ± 0.0483	1.635 ± 0.168
12	24.29 ± 2.544	0.295 ± 0.0612	2.432 ± 0.264
13	29.61 ± 3.246	0.340 ± 0.0616	4.155 ± 0.467
14	26.40 ± 2.996	0.261 ± 0.0403	5.390 ± 0.621
15	34.34 ± 4.047	0.251 ± 0.0337	11.304 ± 1.344
Total	1160.47 ± 25.58		Total 28.9 ± 1.602 (± 1.799)

Lead Data, Sedimentation Exp. 3, July, 1975

1	611.36 ± 23.74	0.408 ± 0.170	-
2	95.49 ± 9.386	0.431 ± 0.812	0.028 ± 0.022
3	93.44 ± 9.357	0.615 ± 1.590	0.051 ± 0.037
4	114.09 ± 9.674	0.336 ± 0.326	0.154 ± 0.092
5	21.46 ± 3.009	0.182 ± 0.329	0.059 ± 0.025
6	36.67 ± 5.124	0.183 ± 0.0722	0.183 ± 0.035
7	36.13 ± 5.088	0.175 ± 0.0497	0.382 ± 0.064
8	31.43 ± 3.992	0.210 ± 0.0576	0.632 ± 0.090
9	41.29 ± 5.338	0.353 ± 0.0962	1.348 ± 0.187
10	36.86 ± 4.014	0.383 ± 0.101	1.777 ± 0.207
11	22.85 ± 2.900	0.214 ± 0.0473	1.601 ± 0.211
12	23.80 ± 3.139	0.269 ± 0.0599	2.384 ± 0.322
13	29.04 ± 4.090	0.309 ± 0.0624	4.075 ± 0.582
14	25.98 ± 4.008	0.238 ± 0.0444	5.304 ± 0.825
15	33.77 ± 5.314	0.229 ± 0.0390	11.118 ± 1.758
Total	1253.67 ± 32.16		Total 29.2 ± 2.088 (± 2.678)

TABLE A III-2 (c)

Zinc Data, Sedimentation Exp. 2, May 1975

Size Range i	ΔC, ng/m^3	$\Delta C/C_T$ $\Delta \log d_p$	J,(Eq. II-9) ng/cm^2 day
1	29.81 ± 1.486	0.191 ± 0.0812	-
2	9.662 ± 5.242	0.418 ± 0.819	0.0028 ± 0.0026
3	12.13 ± 5.250	0.765 ± 2.005	0.0067 ± 0.0056
4	11.82 ± 5.249	0.333 ± 0.356	0.0159 ± 0.0118
5	2.817 ± 1.751	0.230 ± 0.438	0.0077 ± 0.0057
6	4.841 ± 2.982	0.232 ± 0.167	0.0242 ± 0.0152
7	5.243 ± 2.995	0.243 ± 0.153	0.0553 ± 0.0320
8	4.866 ± 2.332	0.312 ± 0.170	0.0980 ± 0.0474
9	4.857 ± 2.924	0.397 ± 0.260	0.1586 ± 0.0958
10	5.844 ± 2.118	0.581 ± 0.257	0.2817 ± 0.1028
11	6.592 ± 1.244	0.593 ± 0.163	0.4619 ± 0.0886
12	6.860 ± 1.324	0.738 ± 0.205	0.6869 ± 0.1341
13	8.363 ± 1.636	0.851 ± 0.220	1.1734 ± 0.2313
14	7.457 ± 1.476	0.654 ± 0.157	1.5224 ± 0.3029
15	9.698 ± 1.944	0.629 ± 0.143	3.1924 ± 0.6420
Total	130.859 ± 11.667		Total 7.69 ± 0.7789 (± 0.8001)

Zinc Data, Sedimentation Exp. 3, July 1975

1	34.19 ± 2.491	0.226 ± 0.0957	-
2	10.92 ± 3.047	0.488 ± 0.928	0.0032 ± 0.0026
3	12.82 ± 3.058	0.835 ± 2.166	0.0070 ± 0.0053
4	9.980 ± 3.043	0.290 ± 0.295	0.0135 ± 0.0075
5	2.858 ± 1.015	0.240 ± 0.441	0.0079 ± 0.0042
6	4.894 ± 1.728	0.242 ± 0.124	0.0245 ± 0.0092
7	5.499 ± 1.736	0.263 ± 0.107	0.0582 ± 0.0190
8	4.735 ± 1.356	0.314 ± 0.119	0.0952 ± 0.0280
9	4.409 ± 1.795	0.372 ± 0.177	0.1440 ± 0.0591
10	4.845 ± 1.316	0.498 ± 0.182	0.2336 ± 0.0642
11	4.774 ± 0.847	0.443 ± 0.115	0.3345 ± 0.0605
12	5.133 ± 0.894	0.570 ± 0.146	0.5141 ± 0.0908
13	6.563 ± 1.184	0.690 ± 0.164	0.9208 ± 0.1676
14	6.604 ± 1.233	0.598 ± 0.132	1.3485 ± 0.2532
15	8.504 ± 1.623	0.570 ± 0.119	2.7994 ± 0.5361
Total	126.728 ± 7.416		Total 6.52 ± 0.6328 (± 0.7269)

TABLE A III-2 (d)

Cadmium Data, Sedimentation Exp. 2, May 1975

Size Range i	ΔC, ng/m³	$\Delta C/C_T$ / $\Delta \log d_p$	J,(Eq. II-9) ng/cm² day
1	2.960 ± 0.1168	0.213 ± 0.0893	-
2	1.100 ± 0.2728	0.536 ± 1.018	0.0003 ± 0.0003
3	0.9025± 0.2717	0.642 ± 1.668	0.0005 ± 0.0004
4	1.022 ± 0.2723	0.325 ± 0.326	0.0014 ± 0.0016
5	0.3016± 0.0908	0.277 ± 0.506	0.0008 ± 0.0004
6	0.5159± 0.1546	0.278 ± 0.133	0.0026 ± 0.0008
7	0.8143± 0.1567	0.426 ± 0.135	0.0086 ± 0.0018
8	0.6943± 0.1220	0.502 ± 0.152	0.0140 ± 0.0026
9	0.6699± 0.1521	0.618 ± 0.206	0.0219 ± 0.0051
10	0.5883± 0.1102	0.659 ± 0.203	0.0284 ± 0.0054
11	0.3456± 0.0648	0.350 ± 0.0926	0.0242 ± 0.0046
12	0.3597± 0.0690	0.436 ± 0.116	0.0360 ± 0.0070
13	0.4384± 0.0853	0.503 ± 0.124	0.0615 ± 0.0121
14	0.3909± 0.0769	0.419 ± 0.0896	0.0798 ± 0.0158
15	0.5084± 0.1014	0.372 ± 0.0798	0.1674 ± 0.0335
Total	11.6117± 0.6126		Total 0.448 ± 0.0407 (± 0.0462)

Cadmium Data, Sedimentation Exp. 3, July 1975

1	1.086 ± 0.129	0.221 ± 0.101	-
2	0.376 ± 0.268	0.518 ± 1.047	0.0001 ± 0.0001
3	0.282 ± 0.268	0.567 ± 1.563	0.0002 ± 0.0002
4	0.204 ± 0.268	0.183 ± 0.301	0.0003 ± 0.0004
5	0.105 ± 0.090	0.273 ± 0.546	0.0003 ± 0.0003
6	0.1808± 0.1526	0.276 ± 0.258	0.0009 ± 0.0005
7	0.184 ± 0.1534	0.272 ± 0.240	0.0020 ± 0.0016
8	0.1683± 0.1196	0.344 ± 0.264	0.0034 ± 0.0024
9	0.2793± 0.1588	0.728 ± 0.465	0.0091 ± 0.0052
10	0.2379± 0.1232	0.754 ± 0.447	0.0115 ± 0.0060
11	0.1291± 0.0686	0.370 ± 0.216	0.0090 ± 0.0048
12	0.1457± 0.0843	0.500 ± 0.313	0.0146 ± 0.0085
13	0.1998± 0.0933	0.649 ± 0.334	0.0280 ± 0.0131
14	0.2313± 0.0964	0.647 ± 0.297	0.0472 ± 0.0197
15	0.2950± 0.1255	0.610 ± 0.280	0.0971 ± 0.0413
Total	4.1045 ± 0.6226		Total 0.224 ± 0.0493 (± 0.0569)

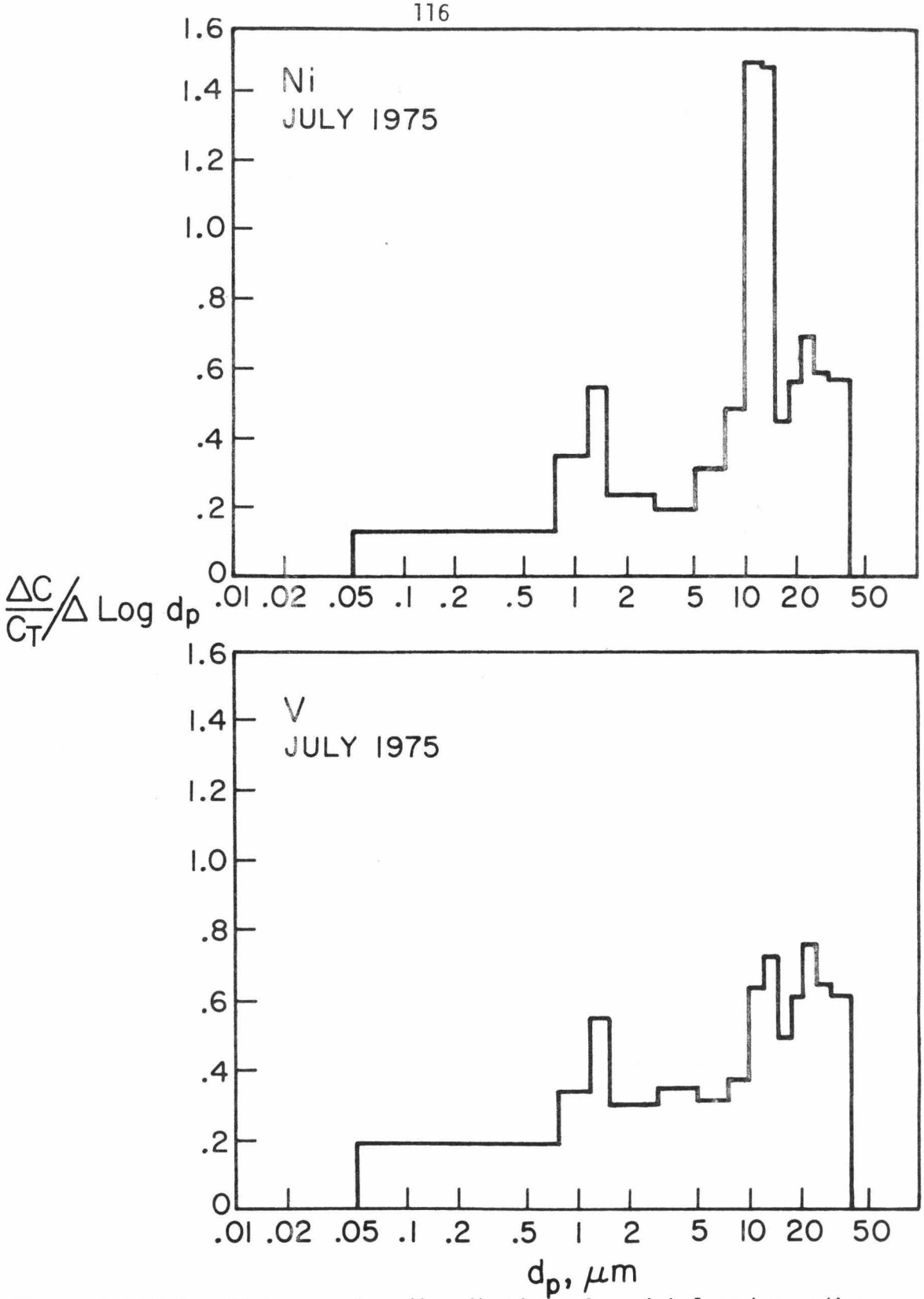

Figure A III-2. Airborne size distributions for nickel and vanadium.

The size distributions have been used to calculate deposition by sedimentation, using Equation II-9. Results which compare measured and calculated depositions are shown in Table A III-3. This is analogous to Table II-3 for lead, zinc, and cadmium. The measured fluxes are average values for sticky and nonsticky teflon. A listing of the individual data points for flat plate deposition is shown in Table A III-4, for the July 1975 experiment.

The results suggest that contamination is a serious problem. This is evident by noting that the airborne concentrations determined by summing impactor stage data are much greater than the total filter data. Further, the large values of bottom plate deposition in Table A III-4 indicate possible contamination, since lead, zinc, and cadmium (which had similar size distributions) had small J_{bottom} values.

Deposition of Trace Metals Throughout Southern California

During 1973 - 1975, flat teflon plates were placed at several sites in and surrounding the Los Angeles Basin. In the 1973 and 1974 experiments, upward-facing plates were located in central Los Angeles and the Eastern suburbs, in the Coachella Valley, in the Antelope Valley, on peaks in the San Gabriel Mountains, and in the coastal areas. Additional experiments were run in the spring of 1975 to estimate deposition on the ocean. Upward and downward-facing plates were mounted on three US Coast Guard buoys in the San Pedro Channel.

A map of the region is shown in Figure A III-3. Each experimental site is numbered, and the corresponding data are presented in Table

TABLE A III-3

Measured and calculated deposition fluxes for nickel and vanadium on flat teflon plates for the July 1975 experiment. All values are in ng/cm^2 day.

	Measured Fluxes			Calculated Fluxes
	J_{top}	J_{bottom}	$J_{sedimentation}$	$J_{sedimentation}$
Ni	2.36	1.71	0.65	2.47
V	1.03	0.800	0.23	1.71

TABLE A III-4

Deposition of Ni and V on flat teflon plates during the July 1975 experiment.

Height above roof	Position of Teflon plate: Upward-Facing (U) Downward-Facing (D)	Type of Teflon Sticky (S) or Nonsticky (N)	Deposition Fluxes ng/cm^2 day	
			Ni	V
148 cm	U	N	0.766	0.416
148	U	S	2.39	0.521
350	U	N	1.54	0.532
350	U	S	5.56	0.715
148	D	S	1.43	0.374
350	D	S	2.64	0.450
*157	U	N	2.55	0.975
*157	U	S	2.18	1.08
*157	D	S	1.71	0.800

*Plate exposed 8 AM - 8 PM daily

Legend for Figure A III-3. Locations of deposition measurement sites. All sites were at most 15 m above ground level.

Site Number	Location
1	Roof of Keck Laboratory, Caltech, Pasadena. Plate mounted 150 cm above roof surface.
2	Ground level, Caltech Hydraulics Laboratory, Azusa.
3	Roof of apartment building, Anaheim.
4	Roof of Rancho Los Amigos Hospital, Downey.
5	Roof of private residence, Beverly Hills.
6	Roof of apartment building, Sherman Oaks.
7a	Solano Avenue offramp of northbound Pasadena Freeway, 2 m from edge of right lane of freeway, 2 m above roadway.
7b	Roof of apartment building, 30 m from roadway.
7c	Roof of private residence, 150 m from freeway.
8	Roof of Millikan Physics Laboratory, Pomona College, Pomona.
9	Hill above south end of Sierra Avenue, Fontana.
10	Hill above corner of Beaumont Road and Bryn Mawr Road, Bryn Mawr.
11	Rock pile near West Garnet, 300 m south of Interstate 10, near junction with State Highway 62.
12	Rock pile 1 kilometer south of site 11.
13	Roof of water tank on Ramon Road in Hidden Springs.
14	A few meters above aqueduct on land owned by Coachella Valley Water District, near Indio.
15	Roof of shed owned by Coachella Velley Water District, near aqueduct at the end of Avenue 52.

Site Number	Location
16	Rock pile 200 m south of Fort Tejon Road near junction with State Highway 138, Pearblossom.
17	Clearing 1000 m south of Avenue G near junction with 120th Street East, Hi Vista.
18	Hill 350 m west of the small paved road through North Edwards, 3000 m north of junction with State Highway 58.
19	Rock pile 1000 m north of small park on 20 Mule Team Road, 10 kilometers east of California City.
20	Roof of USFS lookout tower atop Morton Peak (elev. 4624 feet).
21	Rock pile near intersection of Glendora Ridge Road with dirt road leading to Sunset Peak USFS lookout tower (elev. 4500 feet).
22	Roof of maintenance shed in Mount Wilson Skyline Park (elev. 5600 feet).
23	Rock pile near USFS lookout tower atop Warm Springs Mountain (elev. 4020 feet).
24	Roof of restroom facility on Zuma Beach.
25	Roof of lifeguard tower on Santa Monica Beach.
26	Roof of maintenance building at Marineland Amusement Park, Palos Verdes Peninsula.
27	Roof of Caltech Marine Laboratory, Corona del Mar.
28	On a cement structure on hill above USC Marine Laboratory, Catalina Island.
29	On an abandoned shed above east shore of San Clemente Island.
30	On beach near USC Marine Laboratory, Catalina Island.

Site Number	Location
31	On rock pile in Cottonwood Canyon, 1000 m south of the paved road connecting Avalon with the Isthmus, Catalina Island.
32	Near peak of Blackjack Mountain, Catalina Island.
33	Roof of private residence on 38th Street in San Pedro.
34	USCG Buoy, 1 kilometer south of Palos Verdes Peninsula.
35	USCG Buoy, 5 kilometers south of Palos Verdes Peninsula.
36	USCG Buoy, 15 kilometers south of Palos Verdes Peninsula.

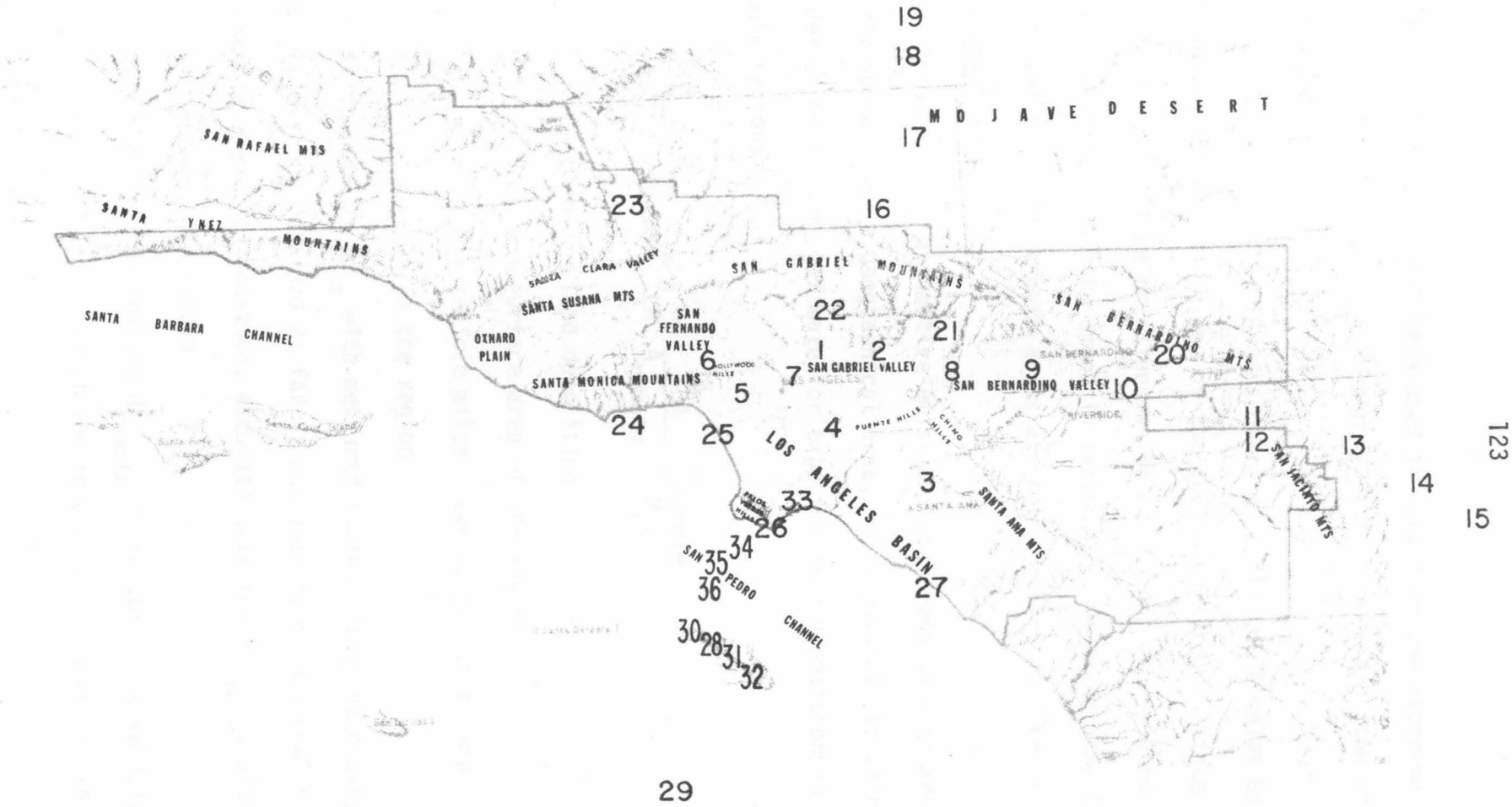

Figure A III-3 Deposition measurement sites.

A III-5. Some sites have been used in more than one experiment. For example, during most runs a "control" flat plate was placed on the roof of Keck Laboratory.

The data show that lead deposition in the Los Angeles Basin is considerably greater than in any of the contiguous areas. Since the sources of lead are automotive emissions which are roughly correlated with population density, this data trend is reasonable. However, the lead deposition values in the remote areas are higher than might be expected based on automobile traffic.

Assuming that automotive emissions and deposition fluxes are uniformly spread over a geographical area, it is possible to calculate an "order of magnitude" estimate for expected lead deposition in any of the remote regions:

$$J_{remote} = J_{LA} \frac{A_{LA}}{A_{remote}} \frac{M_{remote}}{M_{LA}} \qquad \text{(A III-1)}$$

where J = lead deposition

A = surface area of the region

M = vehicle miles traveled per unit time in the region.

To compare J_{remote} with measured fluxes, it is necessary that the measured data be obtained as far as possible from any local sources in the remote area. In addition, accurate data for M_{remote}, although difficult to obtain, are needed.

One method of estimating M_{remote} is to correlate vehicle-miles traveled with the population of the remote area. However, this was

TABLE A III-5

Deposition of lead, zinc, cadmium, nickel, and iron on flat teflon plates at several Southern California sites. Uncertainties are approximately 10% for lead and zinc, 25% for cadmium and iron, and >50% for nickel.

Region	Dates	Site Number	Deposition Fluxes, ng/cm^2 day Pb	Zn	Cd	Ni	Fe
Los Angeles Basin	July 17-24, 1974	1	42	13.7	-	2.6	252
		2	46	25.1	-	4.2	824
		3	81	33.7	-	3.2	546
		4	34	12.9	-	2.8	460
		5	32	7.3	-	2.0	174
		6	28	7.9	-	0.81	186
Central Los Angeles	May 7-14, 1973	1	70.4	17.9	0.080	3.22	-
		7a	2180	153	0.24	7.65	-
		7b	158	30.7	0.21	6.44	-
		7c	98	24.0	0.10	5.23	-
Eastern Suburbs	Dec. 2-9, 1974	1	34.0	9.38	0.251	4.27	-
		8	32.5	40.5	0.174	4.86	-
		9	5.73	4.61	0.157	4.90	-
		10	6.34	2.32	0.199	4.23	-
		11	5.85	2.72	0.111	4.92	-
		12	4.69	3.04	0.140	1.87	-
Coachella Valley	June 27-July 11, 1974	1	43.3	14.2	0.070	0.7	252
		11	13.3	3.2	-	1.5	301
		13	3.7	4.7	0.065	2.0	1070
		14	3.9	1.9	-	1.3	238
		15	1.4	1.4	-	1.0	145

TABLE A III-5 Continued

Region	Dates	Site Number	Deposition Fluxes, ng/cm^2 day				
			Pb	Zn	Cd	Ni	Fe
Antelope Valley	Aug. 3-16, 1974	1	51.7	18.0	0.356	1.10	244
		16	2.82	1.34	0.075	0	160
		17	2.23	1.21	0.038	0.248	192
		18	1.88	1.08	0.0108	0.129	127
		19	1.62	0.76	0	0.0862	149
San Gabriel Mountains	July 19-Aug. 20, 1974	1	50.0	17.9	0.072	1.5	320
		20	2.2	2.3	0.007	0.38	377
		21	3.8	2.3	0.106	0.50	197
		22	4.0	2.3	0.025	0.11	76
		23	4.3	2.5	0.019	0.81	229
Coast and Islands	July 24-Aug. 31, 1974	1	45.0	13.7	0.097	1.5	251
		24	11.2	4.5	0.084	1.7	361
		25	14.1	11.1	0.155	1.8	540
		26	8.11	6.5	0.150	1.3	299
		27	6.60	9.1	0.049	2.2	139
		28	2.89	16	0.027	0.70	95
		29	2.53	0.61	0	0.20	106
Catalina Island	Oct. 18-25, 1974	1	52.4	12.1	-	-	-
		28	68.9	171.4	-	-	-
		30	0.321	0.83	-	-	-
		31	0.366	0	-	-	-
		32	0.517	0.20	-	-	-

TABLE A III-5 Continued

Region	Dates	Site Number	Deposition Fluxes, ng/cm² day Pb	Zn	Cd	Ni	Fe
Buoy Experiment #1	May 2-9, 1975	34 *$	0.994	0.060	-	-	-
		34 *$	0.624	0.040	-	-	-
Buoy Experiment #2	May 16-23, 1975	33	7.29	2.74	-	-	-
		33 *	4.56	0.61	-	-	-
		34 $	2.62	1.41	-	-	-
		34 $	3.52	1.81	-	-	-
		34 *$	0.79	0.30	-	-	-
		34 *$	2.01	1.21	-	-	-
Buoy Experiment #3	May 29-June 10, 1975	33	4.99	2.00	0.0345	1.58	-
		33 *	0.83	0.25	0.0079	1.01	-
		34 *	0.62	0.46	0.0104	0.75	-
		35	2.28	1.24	0.0153	1.28	-
		35 *	0.41	0.17	0.0083	0.65	-
		36	2.83	0.67	0.0167	0.61	-
		36 *	0.91	0.12	0.0382	0.48	-

* Plates facing downward
$ Replicate samples

thought to be inaccurate due to the relatively great amount of automobile traffic from Los Angeles out to the deserts and mountains. Instead, data were obtained from the California State Highway Department (1972). The value of M_{LA} was obtained from Roberts et al. (1971), while the areas were measured from USGS Topographic Maps. The value of J_{LA} was obtained by averaging LA Basin data from Table A III-5.

Data for Equation A III-1 and calculated results are presented in Table A III-6. Note that the calculated lead fluxes are considerably smaller than the measured values for each region:

	Calculated	Measured (Averages)
Coachella Valley	1.89	5.47
San Gabriel Mountains	0.848	3.58
Antelope Valley	0.357	2.14

The excess deposition in the measured values over the calculated values is believed to represent the influence of Los Angeles on these contiguous areas.

The situation for the other trace metals is more complicated than for lead, since the sources are less well defined. However, there are general trends of decreasing zinc, cadmium, and nickel deposition with increasing distance from Los Angeles. Iron deposition is highly variable and does not correlate with distance from LA. This suggests that iron deposition is due to resuspended soil dust rather than due to industrial sources.

Results of the buoy experiments show that lead and zinc deposition decreases rapidly with distance from the coast. The small values of the

TABLE A III-6

Estimates of the lead flux in three regions contiguous to Los Angeles, due only to automotive traffic within each region. The excess between the measured lead fluxes of Table A III-5 and the above calculated values is believed to represent transport of lead out of the Los Angeles Basin.

Region	Area "A"	Vehicle miles/day "M"	J_{lead} (Eq. A III-1)
Los Angeles Basin	4430 km^2	1.18×10^8	46.9 ng/cm^2 day
Coachella Valley	1450	1.56×10^6	1.89
San Gabriel Mountains (incl. parts of the San Bernardino Mountains)	5400	2.60×10^6	0.848
Antelope Valley	6900	1.40×10^6	0.357

ratio $\frac{\text{bottom plate flux}}{\text{top plate flux}}$ at the coast (site 33) and at all three buoys suggests that sedimentation dominates flat surface deposition many kilometers from the source.

It should also be mentioned that resuspended soil dust or roof dust may have influenced the deposition data of Table A III-5. This is not believed to be a serious problem. Figure A III-1 shows that deposition values in the resuspension layer are less than a factor of two greater than deposition values above 150 cm. For the Table A III-5 measurements, the plates were usually located at least 10 cm above the ground or roof. Resuspension is discussed in Appendix IV.

Condensation Nuclei Concentration Data

The profile of condensation nuclei concentration in Figure I-3 represents the average values of several profile measurements. The individual data points are shown in Table A III-7. Average values of these points, which were used to construct Figure I-3, are also shown.

APPENDIX IV:

RESUSPENSION EXPERIMENTS

The concentrations of large particles as functions of height were measured over a field of short grass in December, 1976. The purpose of these experiments was to obtain profiles similar to the condensation nuclei profiles. From these data, information on large particle deposition could be obtained. However, no uniform profiles such as Figure I-4 were measured. Resuspension at ground level of the large particles, presumably soil dust, caused the concentration to decrease with height rather than increase. This region of decreasing concentration occurred between 6 cm and 30 cm. Above 30 cm, the profile increased with height, indicating a net downward flux at greater distances above the ground.

Detailed theories of resuspension have not yet been developed. At present, only rough empirical models exist. Bagnold (1941) and Chepil (1945) have discussed the physical aspects of resuspension. Sehmel (1976) and Sehmel and Lloyd (1976) have measured concentration profiles using Andersen impactors and have performed ZnS tracer studies to measure resuspension. Resuspension models have also been discussed (Energy Research and Development Administration, 1976).

For the present study, three cascade impactors (Scientific Advances, model CI-5) were placed at various heights above the ground and run approximately isokinetically at 1 liter per minute. The inlet airspeed was 34 cm/sec, while the average windspeeds ranged from 40 to 140 cm/sec during the experiments. Only the top stage was used (d_p > 4 μm aerodynamic diameter). Particles were collected on glass

cover slips onto which Vaseline had been lightly swabbed with a Q-tip. At the end of the sampling period, the particles were counted under the optical microscope using 100X magnification (10X micrometer eyepiece and 10X objective lens). Each sample was counted twice for better accuracy; the averages and standard deviations are given below. During one particular run, a sample of 300 particles were sized using the micrometer eyepiece. The geometric diameters ranged from 3 μm to 35 μm with and average of about 7 μm.

Simultaneously with each impactor run, wind profiles were measured to determine u*. Two hot wire anemometers were used (Datametrics model 800-LV). One unit was placed at the top height (which was either 323 cm or 268 cm for these runs) while the other anemometer was moved from height to height to obtain readings.

Five experiments were run. Experiment 1 was conducted on the roof of Keck Labs, on the SE corner, while subsequent runs took place on the Caltech athletic field. The field sampling location was about 50 feet north of the door on the north side of the pool enclosure. The winds were generally SW, which provided a considerable fetch.

The first experiment was performed in order to check similarity among the impactors. Sampling was for one hour. The particles counted on each impactor were (based on two countings):

Impactor 1	2458.5 ± 29.5
Impactor 2	2434.5 ± 8.5
Impactor 3	2447.5 ± 18.5

All subsequent data have been normalized to these values to account for differences among the impactors. Since a separate constricting orifice was used to control the flow rate on each impactor, small differences in flow rates were expected. Comparing the above data show that the differences were less than 1%.

For experiments 2 through 5, impactor 1 data were left unchanged. Impactor 2 data were multiplied by:

$$\frac{2458.5 \pm 29.5}{2434.5 \pm 8.5} = 1.0099 \pm 0.0126$$

while impactor 3 data were multiplied by:

$$\frac{2458.5 \pm 29.5}{2447.5 \pm 18.5} = 1.0045 \pm 0.0142$$

Table A IV-1 summarizes the experimental data. The concentration profiles are shown in Figure A IV-1. Wind profile measurements are presented in Appendix V.

It is seen that an apparent minimum in concentration exists at 30 cm above the ground. (This minimum may actually exist anywhere between 6 cm and 60 cm, but for present purposes, it is assumed to exist at 30 cm). Below this height, the concentration gradient is negative indicating an upward flux of material from the ground. Above 30 cm, the positive gradient implies a downward flux. The characteristic gradient is seen for both wet and dry grass conditions.

These data suggest that a resuspension layer exists, where the material close to the ground is continually moving about. The classical idea of deposition from the lower atmosphere onto a perfect sink surface

TABLE A IV-1

Concentrations of large particles as functions of height above a field of 2 cm tall grass.

Experiment Number	Date and Time	u*	State of grass	Impactor Number	Height above ground	Large Particle concentration (particles/cm^3
2	Dec. 3, 1976 8 AM-10 AM	5.4 cm/sec*	wet	3	323 cm	0.0299 ± 0.0016
				2	60	0.0332 ± 0.0018
				1	6	0.0299 ± 0.0016
3	Dec. 8, 1976 9:30 - 10:30 AM	3.2*	wet	3	62	0.0373 ± 0.0021
				2	31	0.0317 ± 0.0018
				1	6	0.0354 ± 0.0020
4	Dec. 10, 1976 1-2 PM	6.7	dry	3	62	0.0734 ± 0.0040
				2	31	0.0643 ± 0.0035
				1	6	0.0710 ± 0.0037
5	Dec. 12, 1976 10-10:30 AM	6.3	wet	3	60	0.0158 ± 0.0011
				2	31	0.0166 ± 0.0011
				1	6	0.0184 ± 0.0012

The wind during the first half of experiments 2 and 3 was calm. These u values represent the averages for the second half.

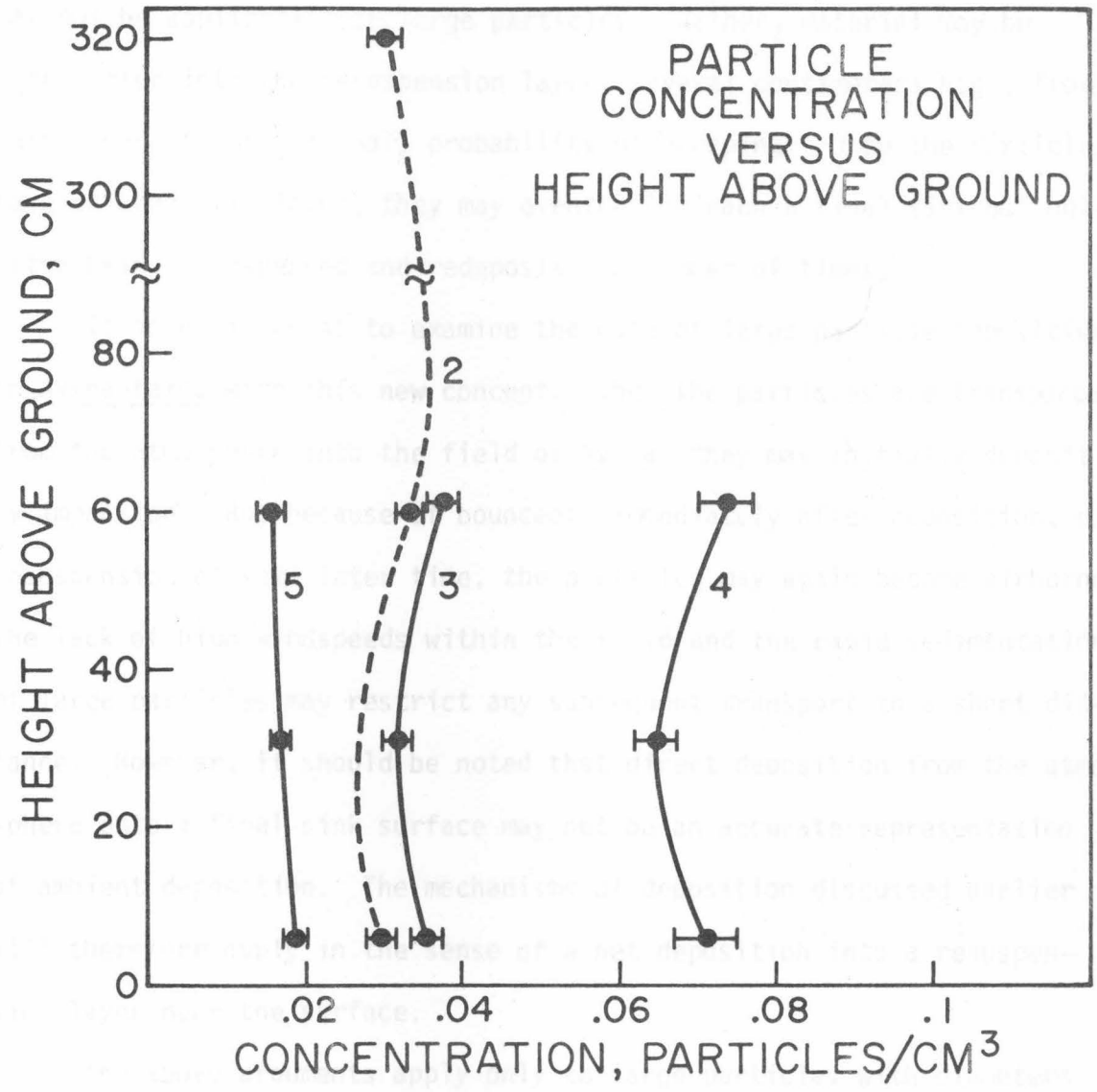

Figure A IV-1 Variations of large particle concentration with height above the Caltech althletic field. Below about 30 cm, there appears to be a net upward flux of particles from the ground. This resuspension layer is a function of surface conditions and wind conditions. Experiments 2, 3, 4, and 5 had u* values of 5.4, 3.2, 6.7, and 6.3 cm/sec respectively. The ground was wet due to a sprinkling system in experiments 2, 3, and 5. Experiment 4 was characterized by dry ground.

may not be applicable for large particles. Rather, material may be transported into the resuspension layer, several centimeters high, from which there is only a small probability of escaping. Once the particles have entered this layer, they may eventually reach a final sink but only after being resuspended and redeposited a number of times.

It is of interest to examine the case of large particle deposition on Avena fatua with this new concept. When the particles are transported from the atmosphere into the field of Avena, they may initially deposit by impaction. But because of bounceoff immediately after deposition, or resuspension at some later time, the particles may again become airborne. The lack of high windspeeds within the field and the rapid sedimentation of large particles may restrict any subsequent transport to a short distance. However, it should be noted that direct deposition from the atmosphere onto a final sink surface may not be an accurate representation of ambient deposition. The mechanisms of deposition discussed earlier will therefore apply in the sense of a net deposition into a resuspension layer near the surface.

The above arguments apply only to large particles with diameters of several microns or greater. Resuspension is not a significant mechanism for smaller particles.

APPENDIX V:

WIND PROFILES

Determinations of the friction velocity u* were made at four locations:

1. In a field of Avena fatua in a residential area of Los Angeles near Occidental College, where the condensation nuclei experiments were carried out.
2. In a field of Avena fatua in Ernest Debs Park, Los Angeles.
3. On the Caltech athletic field.
4. On the roof of Keck Laboratory, Caltech.

A profile for each of the above locations is presented in Figures A V-1, 2, 3, and 4, respectively. No attempt was made to correct these profiles for nonadiabatic conditions, hence they must be regarded as approximate.

The profiles were constructed using two Datametrics model 800-LV hot wire anemometers. One anemometer was positioned at the top height while the second anemometer was used to measure windspeeds at several lower heights.

Comparing Figures A V-1 and 2 shows that the first windfield needed no zero plane displacement correction, while the second profile necessitated a large displacement of 25 cm. This illustrates the difficulty in attempting to define an "average" windfield for deposition calculations. After making additional wind measurements and after examining the structure of Avena in several fields, it was decided that a zero plane displacement of about 25 cm was needed for typical conditions. Hence Figure A V-2 was scaled to the average windspeed in

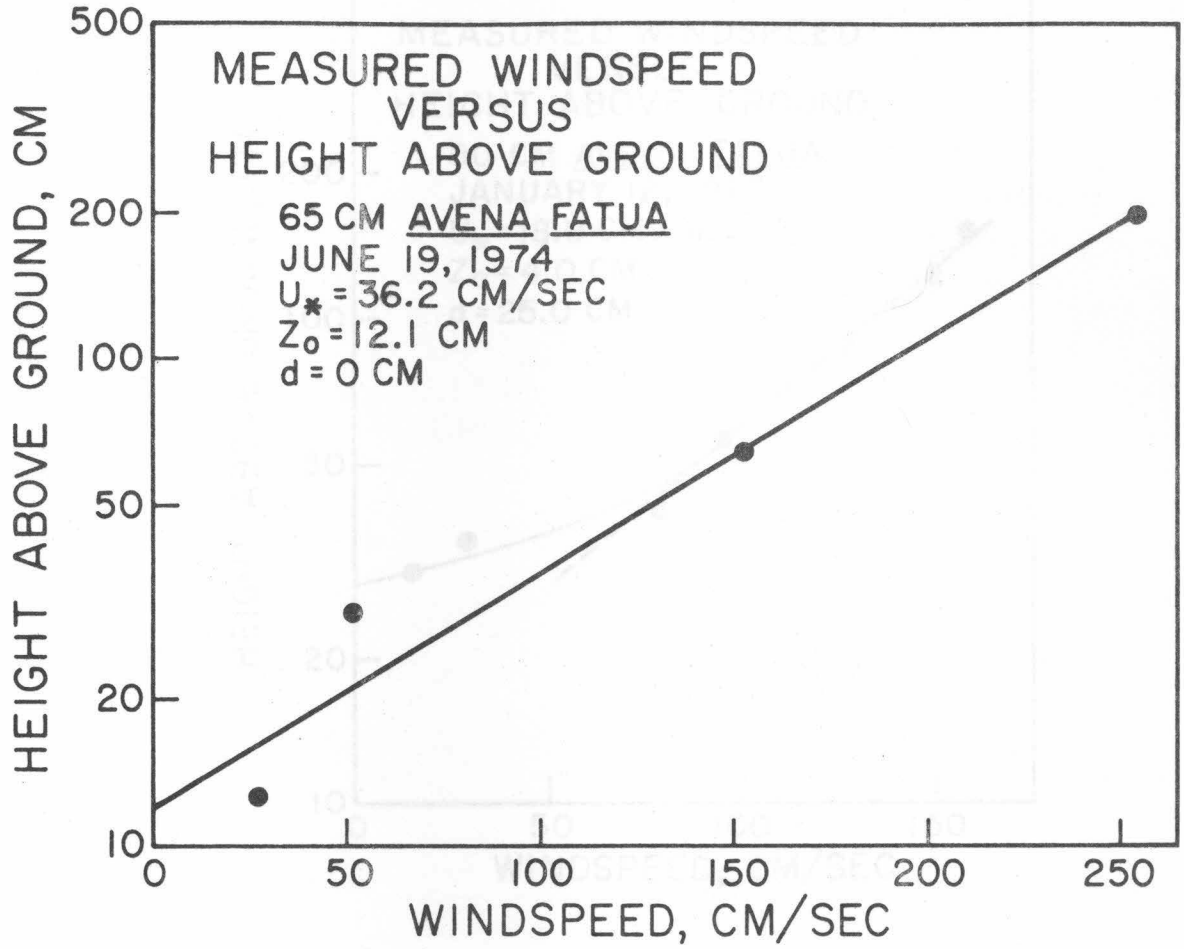

Figure A V-1 Wind profile above a field of 65 cm tall Avena fatua, located in a residential area of Los Angeles near Occidental College. This profile was obtained during a condensation nuclei experiment. The expression for the wind in this case is:

$$u(z) = \frac{u^*}{k} \ln \frac{z}{z_o} = \frac{36.2}{0.4} \ln \frac{z}{12.1}$$

An average profile for all condensation nuclei experiments in this field is:

$$u(z) = \frac{45.0}{0.4} \ln \frac{z}{12.1}$$

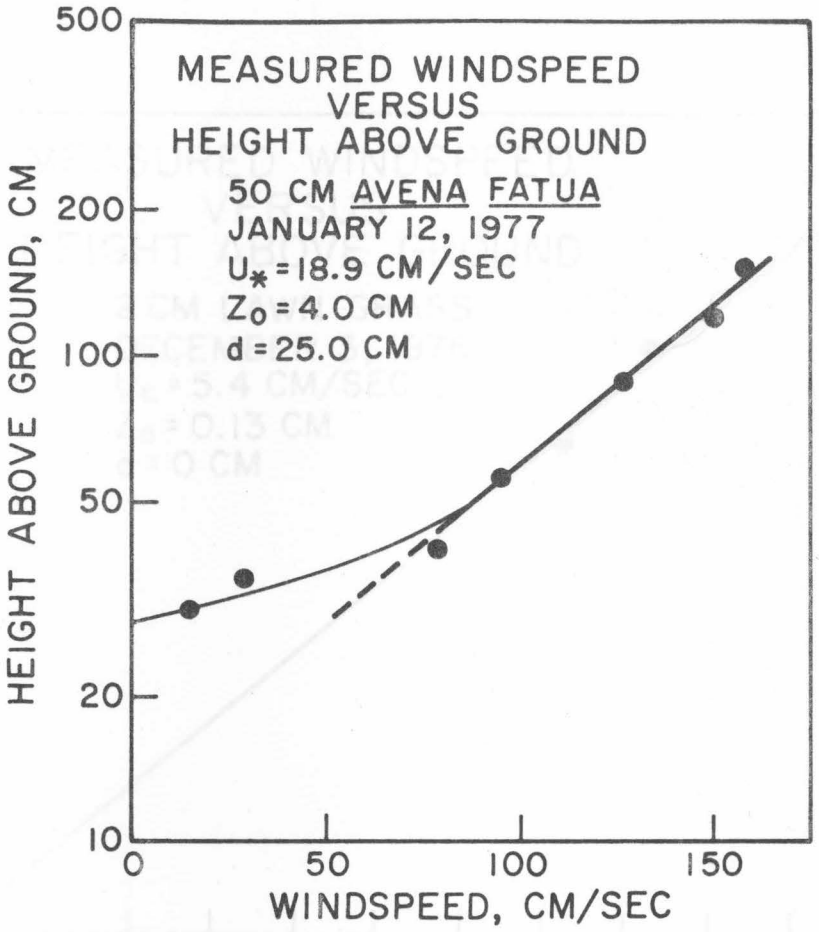

Figure A V-2 Wind profile above a field of 50 cm tall Avena fatua in Ernest Debs Park, Los Angeles. This profile is described by:

$$u(z) = \frac{u^*}{k} \ln \frac{z}{z_o} = \frac{18.9}{0.4} \ln \frac{z}{4.0}$$

The typical profile for Avena used in the filtration model is:

$$u(z) = \frac{21.2}{0.4} \ln \frac{z}{4.0}$$

Note that z=0 corresponds to a height of 25 cm above the ground due to the zero plane displacement.

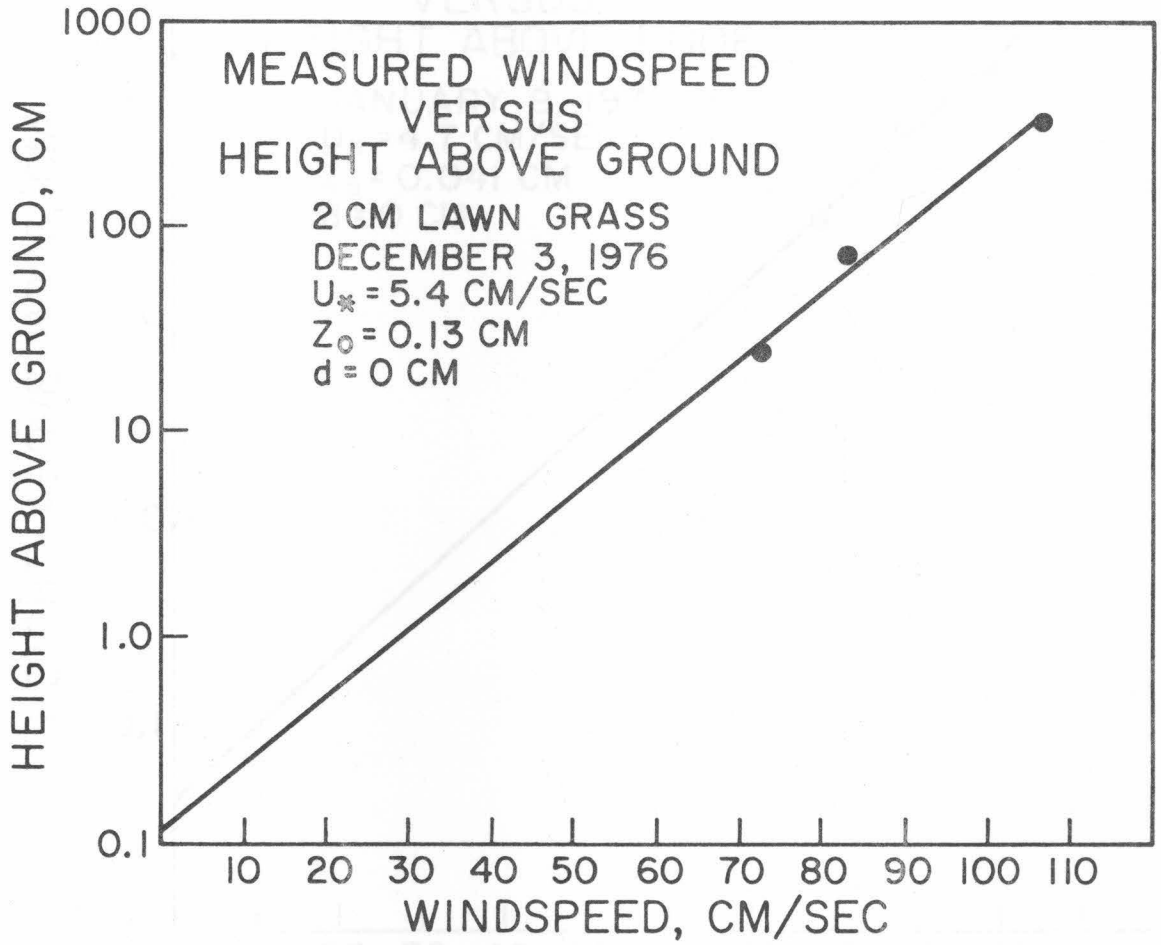

Figure A V-3 Wind profile above the Caltech athletic field, obtained during one of the resuspension experiments. The expression for this profile is:

$$u(z) = \frac{u^*}{k} \ln \frac{z}{z_o} = \frac{5.4}{0.4} \ln \frac{z}{0.13} \text{ cm/sec}$$

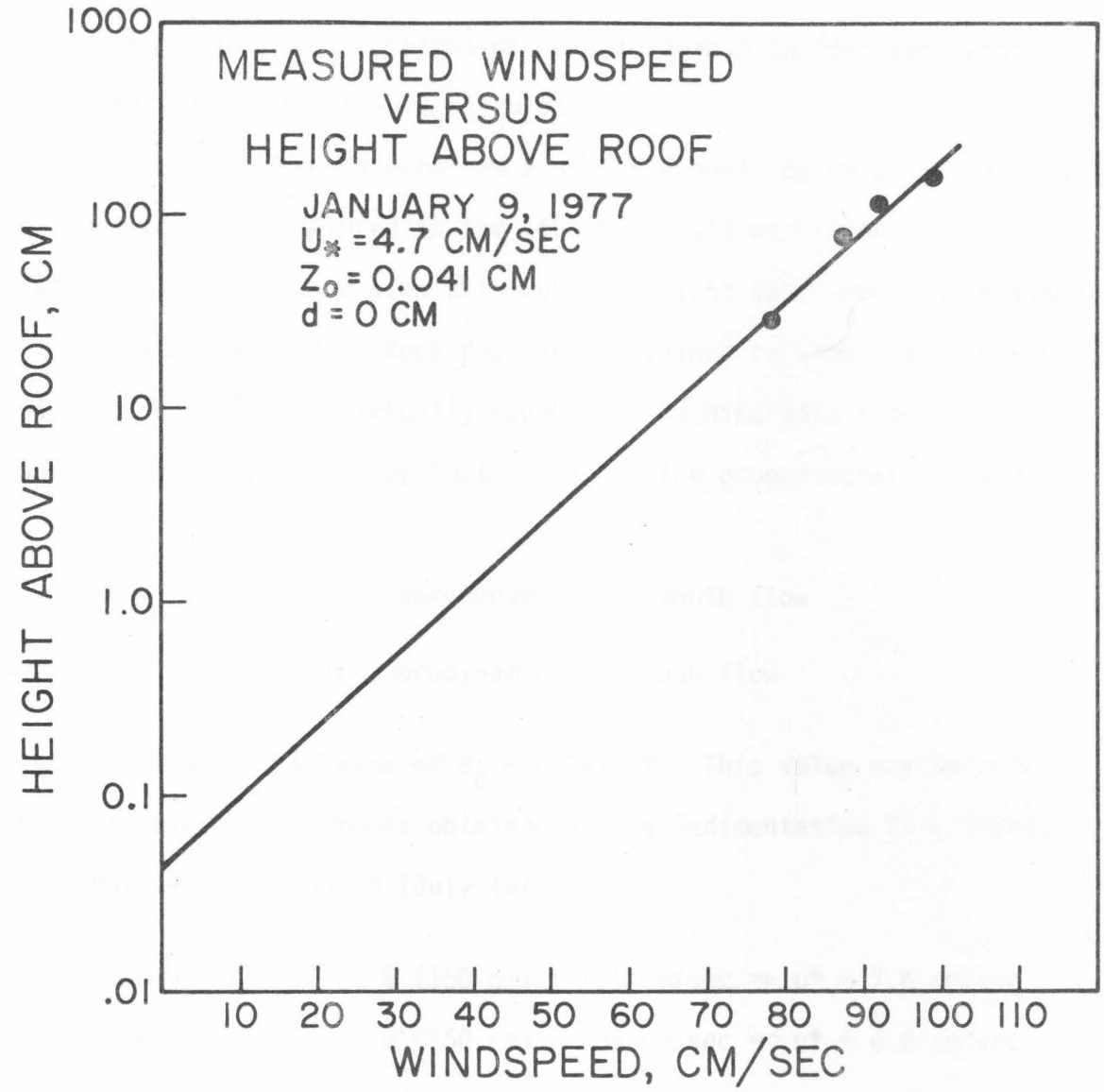

Figure A V-4 Wind profile above the roof of the Keck Laboratory penthouse. The wind flow over the roof was in the transition regime between aerodynamically rough and smooth flow during the sedimentation experiments. Since most windflows over natural surfaces are aerodynamically rough, deposition data obtained at this site represents a lower limit to expected deposition on natural surfaces. The expression for this profile is:

$$u(z) = \frac{u^*}{k} \ln \frac{z}{z_o} = \frac{4.7}{0.4} \ln \frac{z}{0.041}$$

Los Angeles (2 m/sec at a height of 2 m) to obtain an "average" wind profile for filtration theory calculations.

Figures A V-3 and 4 were not used for deposition calculations. Wind profiles were measured in the athletic field with hopes of correlating u* with resuspension although sufficient data were not obtained. The wind data measured on Keck roof were obtained to show that the roof windfield is not aerodynamically rough. Using Nikuradse's test for windflow smoothness given by Sutton (1953), the proper relations are:

$$\frac{u^* z_o}{\nu} < 0.13 \text{ for aerodynamically smooth flow}$$

and

$$\frac{u^* z_o}{\nu} > 2.5 \text{ for aerodynamically rough flow}$$

Figure A V-4 yields a value of $z_o = 0.041$ cm. This value may be combined with wind measurements obtained during Sedimentation Experiments No. 2 (May 1975) and No. 3 (July 1975):

Sedimentation Exp. 2 $\bar{u}$ (150 cm) = 156 cm/sec $\Rightarrow$ u* = 7.6 cm/sec

Sedimentation Exp. 3 $\bar{u}$ (150 cm) = 139 cm/sec $\Rightarrow$ u* = 6.8 cm/sec

Hence the smoothness test can be applied directly:

Sedimentation Exp. 2 $\frac{u^* z_o}{\nu} = 2.0$

Sedimentation Exp. 3 $\frac{u^* z_o}{\nu} = 1.8$

Thus the windfield was in the transition between smooth and rough flow for both experiments. Since windflow over nearly all natural surfaces is aerodynamically rough, (Sutton, 1953), the Keck roof deposition data represent a lower limit to trace metal deposition over natural surfaces.

APPENDIX VI:

EXPERIMENTAL ERRORS

All uncertainties in this thesis represent one standard deviation about the mean. The standard deviations have been compounded in the usual manner. That is, if f is a function of the variables x_1, x_2,..., x_n with standard deviations $\sigma_{x_1}, \sigma_{x_2}, \ldots \sigma_{x_n}$, then σ_f, the standard deviation of f, is given by:

$$\sigma_f = \left[\sum_{i=1}^{n} \left(\frac{\partial f}{\partial x_i}\right)^2 \sigma_{x_i}^2 \right]^{1/2} \qquad \text{(A VI-1)}$$

The standard deviations of individual measurements or sets of measurements have been determined in a variety of ways. A sample of n data points y_1, y_2, ..., y_n distributed over a range of values has a group standard deviation given by:

$$\sigma_y = \left[\frac{\sum_{i=1}^{n} (y_i - \bar{y})^2}{(n-1)} \right]^{1/2} \qquad \text{(A VI-2)}$$

$$\text{where } \bar{y} = \frac{\sum_{i=1}^{n} y_i}{n} \qquad \text{(A VI-3)}$$

If the standard deviation of the mean is desired rather than the standard deviation of the group, Equation A VI-4 applies:

$$\sigma_{\bar{y}} = \frac{\sigma_y}{\sqrt{n}} = \left[\frac{\sum_{i=1}^{n} (y_i - \bar{y})^2}{n(n-1)} \right]^{1/2} = \left[\frac{\sum_{i=1}^{n} y_i^2 - \frac{(\Sigma y_i)^2}{n}}{n(n-1)} \right]^{1/2} \quad \text{(A VI-4)}$$

This equation has been used to estimate the uncertainty in the mean value calculated from a distribution of data points.

In some cases the results of many measurements of a quantity, each with a separate known standard deviation, have been averaged. For n measurements z_1, z_2, ..., z_n with standard deviations σ_{z_1}, σ_{z_2}, ..., σ_{z_n}, the average and standard deviation of z is:

$$\bar{z} = \frac{\sum_{i=1}^{n} \frac{z_i}{\sigma_{z_i}^2}}{\sum_{i=1}^{n} \frac{1}{\sigma_{z_i}^2}} \quad \text{(A VI-5)}$$

$$\sigma_z = \left[\sum_{i=1}^{n} \frac{1}{\sigma_{z_i}^2} \right]^{1/2} \quad \text{(A VI-6)}$$

Uncertainties in the trace metal measurements include errors associated with the atomic absorption instrument, contamination problems in sample handling, and errors in reading the chart recorder output. The first of these was assumed to be negligible. Contamination was accounted for by assigning a 100% uncertainty to the blank value in each experiment. This was usually the most significant error. For most lead and zinc analyses, the blanks were small or negligible. Cadmium and iron had blanks which were a significant percent of the

sample value (20-50%), while nickel and vanadium had even greater blanks. The large nickel blanks were believed to be due to stainless steel sample handling equipment which contained nickel. The uncertainties in reading the chart recorder output were estimated by noting the signal to noise ratio and the precision in each set of measurements.

Additional errors occurred in the trace metal size distribution measurements. The uncertainties included in the error analysis were impactor nonideality (Table A I-1), statistical counting errors when calibrating the upper stages with atmospheric particles, and the uncertainty in the air flow rate through the impactor. Of these, impactor nonideality was the largest contributor to the size distribution uncertainties.

Errors due to nonisokinetic sampling, impactor wall losses, and the estimate of atmospheric particle density have not been included in the listed uncertainties, nor has the error in approximating the true distributions as stairstep functions. However, independent estimates of errors in sampling and in the stairstep approximations can be made.

The errors due to nonisokinetic sampling can be estimated from windspeed and wind direction data obtained during the impactor runs. For the July 1975 experiment, the average windspeed was 1.4 m/sec while the inlet airspeed was 1.8 m/sec. According to Watson (1954), the ratios of measured to actual airborne concentrations for these conditions are 96% for 12 μm, 90% for 31 μm and 84% for 37 μm equivalent diameter particles. Since the wind is gusty with speeds different from the average 1.4 m/sec, the true errors may be greater.

Errors due to the impactor not always facing into the wind can also be estimated. Frequent checks on the wind direction were made, and whenever the wind shifted by more than 20^{o}, the impactor was re-aligned. A record of these realignments show that the impactor could have been misaligned by about 30^{o} for as much as one fourth of the time during the run. For a windspeed equal to the inlet airspeed, Watson has predicted the ratios of measured to actual concentrations for a 30^{o} misalignment. His values are 92% for 12 μm and 85% for 37 μm equivalent diameter particles. The sampling errors for the May 1975 run are slightly smaller than for the July experiment.

Calculations of the flux have been based on the approximate stair-step distributions of Figures II-1 and II-2. By dividing each size range into several smaller stairsteps, so that the size distribution is closer to a smooth curve, an estimate of the error is obtained. This was done using the raw data from the particle size measurements which were accurate to ±0.4 μm, for $d_p > 4$ μm. The error was calculated to be less than 1%.

For the particles on the lower impactor stages, too small to be counted, the maximum error in calculating the flux was estimated. It was assumed that all of the mass was at one of the d_p endpoints of a stage, rather than uniformly distributed across the d_p range. The maximum error was calculated to be 3% of the total flux.

Another possible source of error is that the particles may change size as they deposit on the impactor plates. The assumption that the size distributions of trace metals based on aerodynamic equivalent

diameters is the same as the total distribution measured with the optical microscope may also be a source of error.

Uncertainties in the condensation nuclei data have not been examined in detail. However, one advantage of the profile method of obtaining flux information is that the method is not sensitive to errors in the absolute concentration values. Instrument biases do not affect the calculation since only relative concentrations are needed, ie, $\frac{\Delta c}{\Delta \text{ Ln } z}$. The high precision of the CNC measurements is shown by the small error bars in Figure I-4. Also, the signal-to-noise ratio of the chart recorder output was fairly high, and the concentration measurements were steady over short time periods (one minute). Because of these facts, the errors in the CNC flux data are believed to be small.

The wind profile measurements were subject to many of the same uncertainties as the previously discussed measurements: instrument error, errors in reading the chart recorder output, and difficulties in sampling the true wind. The anemometers were calibrated in a crude wind tunnel using a vacuum pump (Gast model 1022 103-G272x) and a 2-3/4" ID PVC pipe. A dry test meter measured the total volumetric flow through the pipe, while the anemometers measured the windspeed in the pipe. The flow rate through the system was controlled with a valve so several data points could be obtained. This calibration showed that the windspeeds indicated by the anemometers were within a few percent of the true windspeeds. Thus instrument error is not believed to be a serious problem.

Difficulties in reading the chart recorder output of the anemometers were more severe than in the CNC or trace metal experiments. The natural fluctuations in the wind resulted in rapidly changing chart

recorder output levels. Hand integrations of these outputs using a Keuffel and Esser Company model 7303 planimeter yielded values accurate to within about 10%.

Accurate sampling of the wind required that the hot-wire anemometer probes be oriented in the proper direction at all times. In this respect, direction-independent cup anemometers would have been better suited for these experiments. However, the relatively high threshold values for cup anemometers (about 1 m/sec) precluded their use in the profile measurements. Because the response of the hot-wire anemometers is not affected for wind direction variations less than $\pm 15^{o}$, and because the wind direction was monitored continuously during each profile run, the sampling errors for the profile experiments are not believed to be severe.

Uncertainties in the sulfate experiments were in general larger than in the other measurements described in this thesis. The two major difficulties in the sulfate analyses are believed to be inaccurate responses of the Meloy Sulfur Analyzer and poor recovery of sulfates by the strip flashing technique.

The Meloy sulfur analyzer was calibrated using an SO_2 permeation tube, and the response was considerably lower than expected under ideal operating conditions. The instrument problems were not adequately solved during the course of the sulfate experiments.

In order to prevent particle bounceoff from strips mounted in the low-pressure impactor, the strips were coated with a solution of silicon oil and hexane. When these strips were flashed, it was observed that

somewhat less than 100% of the deposited sulfate was recovered and detected by the Meloy Sulfur Analyzer. The recovery problem was not adequately resolved during these experiments.

The sulfate data must therefore be regarded as approximate. It is possible that if the errors associated with sulfate analysis had been reduced, reasonable agreement might have been obtained between calculated and measured sulfate deposition fluxes.

CONCLUSIONS

Particle deposition on Avena fatua can be predicted using filtration theory. The calculations show that the small fraction of large airborne particles controls the mass deposition of lead, zinc, and cadmium on Avena and also on smooth, flat surfaces. This implies that the traditional concept of a single deposition velocity based on total airborne concentration of a species might be inadequate to describe the deposition process. Rather, detailed isokinetic sampling for the entire size distribution may be needed in order to characterize the deposition accurately.

The importance of incorporating details of the surface structure into a predictive model has been illustrated by data in the literature. Such details have been included in the present study when vegetation was modelled as a fiber filter. Most previous deposition models have ignored the detailed surface structure and in doing so have omitted an important variable.

Resuspension is also an important part of the total deposition process. However, only limited data exist in the literature, and present models are inadequate. Resuspension was not considered as part of the filtration model described in this thesis. This is a major weakness of the model.

Turbulent inertial deposition has not been included in the model. This mechanism occurs when particles have sufficient inertia from turbulent wind eddies to be driven through the viscous sublayer and onto the surface. Particles larger than about one micron depositing on

smooth surfaces are often controlled by this mechanism unless sedimentation applies. Turbulent inertial deposition has not been thoroughly investigated in the free atmosphere. Like resuspension, this mechanism may be important. For the case of trace metals, however, impaction of large particles is likely to be far more significant than turbulent inertial deposition.

Research is needed in the areas of resuspension, turbulent inertial deposition, and incorporation of surface structure into deposition models. A larger data base would be useful for developing predictive models in all of these areas. Most important, a thorough physical understanding of all important deposition mechanisms should accompany development of the models.

REFERENCES

Aldaz, L.: Flux Measurements of Atmospheric Ozone Over Land and Water, J. Geophys. Res., 74, 6943, 1969.

Atkins, P. R.: Lead in a Suburban Environment, J. APCA, 19, 591, 1969.

Bagnold, R. A.: The Physics of Blown Sand and Desert Dunes, Methuen and Company, Ltd., London, 1941.

Beal, S. K.: Deposition of Particles in Turbulent Flow on Channel or Pipe Walls, Nucl. Sci. Eng., 40, 1, 1970a.

Beal, S. K.: Deposition of Polydisperse Aerosols in Turbulent Flow, Atmos. Envir., 4, 439, 1970b.

Best, A. C.: Transfer of Heat and Momentum in the Lowest Layers of the Atmosphere, Met. Office Geophys. Memoirs No. 65, 1935.

Brun, R. J., W. Lewis, P. J. Perkins and J. S. Serafini: NACA Report 1215, 1955.

Bullas, D. O.: 1953, data published by Chamberlain, A.C., 1960.

Bullock, J., and W. M. Lewis: The Influence of Traffic on Atmospheric Pollution, Atmos. Envir., 2, 517, 1968.

Businger, J. A., J. C. Wyngaard, Y. Izumi and E. F. Bradley: Flux-profile Relationships in the Atmospheric Layer, J. Atmos. Sci., 28, 181, 1971.

California. State of, 1972 Traffic Volumes on California State Highways, California Business and Transportation Agency, Department of Public Works, Division of Highways.

Cahill, T. A., and P. J. Feeney: "Contribution of Freeway Traffic to Airborne Particulate Matter," U. of Calif., Davis, UCD-CNL 169, Final Report to the Calif. ARB, 1973.

Cannon, H. L., and J. M. Bowles: Contamination of Vegetation by Tetraethyl Lead, Science, 137, 765, 1962.

Cardina, J. A.: Particle Size Determination of Tire-Tread Rubber in Atmospheric Dusts, Rubber Chem. and Tech., 47, 1005, 1974.

Chamberlain, A. C.: Aspects of Deposition of Radioactive and Other Gases and Particles, in Aerodynamic Capture of Particles, E. G. Richardson, Ed., Permagon Press, New York, 1960, p. 63.

Chamberlain, A. C.: Transport of Gases to and from Grass and Grass-like Surfaces, Proc. Roy. Soc. A, 290, 236, 1966a.

Chamberlain, A. C.: Transport of Lycopodium Spores and Other Small Particles to Rough Surfaces, Proc. Roy. Soc. A, 296, 45, 1966b.

Chamberlain, A. C.: Transport of Gases to and from Surfaces with Bluff and Wave-like Roughness Elements, Q. J. Roy. Met. Soc., 94, 318, 1968.

Chamberlain, A. C.: Mass Transfer to Bean Leaves, Boundary Layer Meteorology, 6, 477, 1974a.

Chamberlain, A. C.: "Travel and Deposition of Lead Aerosols," Environmental and Medical Sciences Division, UKAEA Research Group, Harwell, Feb. 1974b.

Chamberlain, A. C.: Pollution in Plant Canopies, in Heat and Mass Transfer in the Biosphere, D. A. deVries and N. H. Afgan, Eds., Hemisphere Publishing Co., Washington, D.C., 1975, p. 561.

Chamberlain, A. C., and R. C. Chadwick: Deposition of Spores and Other Particles on Vegetation and Soil, Ann. Appl. Biol., 71, 141, 1972.

Chepil, W. S.: Dynamics of Wind Erosion, Soil Science, 60, 475, 1945.

Cholak, J., L. J. Schafer, and D. Yeager: The Air Transport of Lead Compounds Present in Automobile Exhaust Gases, Amer. Ind. Hyg. Assoc. J, 29, 562, 1968.

Chow, T. J.: Lead Accumulation in Roadside Soil and Grass, Nature, 225, 295, 1970.

Daines, R. H., H. Motto, and D. M. Chilko: Atmospheric Lead: Its Relationship to Traffic Volume and Proximity to Highways, Env. Sci. and Tech., 4, 318, 1970.

Dannis, M. L.: Rubber Dust from the Normal Wear of Tires, Rubber Chem. and Tech., 47, 1011, 1974.

Davidson, C. I.: The Deposition of Trace Metal-Containing Particles in the Los Angeles Area, accepted for publication in J. Powder Tech, 1977.

Davidson, C. I., S. V. Hering, and S. K. Friedlander: The Deposition of Pb-Containing Particles from the Los Angeles Atmosphere, Proceedings of the Third International Conference on Environmental Sensing and Assessment, Volume 1, Las Vegas, Nevada, September, 1975.

Davidson, C. I., J. J. Huntzicker, and S. K. Friedlander: "The Flow of Trace Elements through the Los Angeles Basin: Impact on Nonurban Areas," Division of Environmental Chemistry, 167th Meeting, ACS, Los Angeles, CA, March 1974.

Davies, C. N.: Deposition from Moving Aerosols, in Aerosol Science, C. N. Davies, Ed., Academic Press, London, 1966, p.393.

Dedolph, R., G. Ter Haar, R. Holtzmann, and H. Lucas, Jr.: Sources of Lead in Perennial Ryegrass and Radishes, Env. Sci. and Tech., 4, 217, 1970.

Droppo, J. G., and J. M. Hales: Profile Methods of Dry Deposition Measurement, in Atmosphere-Surface Exchange of Particulate and Gaseous Pollutants (1974), Energy Research and Development Administration, NTIS No. CONF-740921, 1976, p.192.

Dyer, A. J., and B. B. Hicks: Flux-gradient Relationships in the Constant Flux Layer, Q. J. Roy. Met. Soc., 96, 715, 1970.

Energy Research and Development Administration, Atmosphere - Surface Exchange of Particulate and Gaseous Pollutants, (1974), NTIS no. CONF-740921, 1976.

Environment One Corp., Instruction Manual for Model Rich 100 Condensation Nuclei Counter, 1971.

Flesch, J. P., C. H. Norris, and A. E. Nugent, Jr.: Calibrating Particulate Air Samplers with Monodisperse Aerosols: Application to the Andersen Cascade Impactor, Amer. Ind. Hyg. Assoc. J., 28, 507, 1967.

Fowler, D., and M. H. Unsworth: Dry Deposition of Sulphur Dioxide on Wheat, Nature, 249, 389, 1974.

Friberg, L., M. Piscator, G. F. Nordberg, and T. Kjellstrom: Cadmium in the Environment, 2nd edition, CRC Press, Cleveland, Ohio, 1974, p.9.

Friedlander, S. K., and H. F. Johnstone: Deposition of Suspended Particles from Turbulent Gas Streams, Ind. Eng. Chem., 49, 1151, 1957.

Friedlander, S. K.: Smoke, Dust, and Haze: Fundamentals of Aerosol Behavior, John Wiley and Sons, New York, 1977, p.71 and p. 101.

Fuchs, N. A.: Mechanics of Aerosols, Permagon Press, MacMillan Co., New York, 1964, p.26 and p.164.

Garland, J. A., D. H. F. Atkins, C. J. Readings, and S. J. Caughey: Deposition of Gaseous Sulphur Dioxide to the Ground, Atmos. Envir., 8, 75, 1974.

Garland, J. A.: Dry Deposition of SO_2 and Other Gases, in Atmosphere-Surface Exchange of Particulate and Gaseous Pollutants (1974), Energy Research and Development Administration, NTIS no. CONF-740921, 1976, p.212.

Gillette, D. A., and J. W. Winchester: A Study of Aging of Lead Aerosols, Atmos. Envir., 6, 443, 1972.

Gregory, P. H.: Microbiology of the Atmosphere, Leonard Hill Books, Ltd., London, 1961, p.58.

Habibi, K.: Characterization of Particulate Lead in Vehicle Exhaust-Experimental Techniques, Env. Sci. and Tech., 4, 239, 1970.

Habibi, K.: Characterization of Particulate Matter in Vehicle Exhaust, Env. Sci. and Tech., 7, 223, 1973.

Harrison, P. R., W. R. Matson, and J. W. Winchester: Time Variations of Lead, Copper and Cadmium Concentrations of Aerosols in Ann Arbor, Michigan, Atmos. Envir., 5, 613, 1971.

Heichel, G. H., and L. Hankin: Particles Containing Lead, Chlorine, and Bromine Detected on Trees with an Electron Microprobe, Env. Sci. and Tech., 6, 1121, 1972.

Hering, S. V., R. C. Flagan, and S. K. Friedlander: "A New Low-Pressure Impactor: Determination of the Size Distribution of Aerosol Sulfur Compounds," 173rd National Meeting, American Chemical Society, Division of Environmental Chemistry, New Orleans, LA, March 20, 1977.

Hering, S. V.: Personal Communication, 1977.

Hidy, G. M.: Removal Processes of Gaseous and Particulate Pollutants, in Chemistry of the Lower Atmosphere, S.I. Rasool, Ed., Plenum Press, New York, 1972, P.121.

Hidy, G. M.: "Characterization of Aerosols in California," Interim Report for Phase I, State of California Air Resources Board Contract No. 358, 1973, p.254-264.

Hidy, G. M., and S. L. Heisler: Transport and Deposition of Flowing Aerosols, in Recent Developments in Applied Aerosol Technology, D. Shaw, Ed., John Wiley and Sons, New York, 1977.

Hirschler, D. A., L. F. Gilbert, F. W. Lamb, and L. M. Niebylski: Particulate Lead Compounds in Automobile Exhaust Gas, Ind. Eng. Chem., 49, 1131, 1957.

Hirschler, D. A., and L. F. Gilbert: Nature of Lead in Automobile Exhaust Gas, Arch. Env. Health, 8, 297, 1964.

Hitchcock, A. S.: Manual of Grasses of the United States, U. S. Department of Agriculture Publication no. 200, 1935, p.295.

Holman, J. P.: Heat Transfer, McGraw-Hill, New York, 1972, p.186.

Huntzicker, J. J., C. I. Davidson, and S. K. Friedlander: "The Flow of Trace Elements through the Los Angeles Basin: Zn, Cd, and Ni," Division of Environmental Chemistry, 167th Meeting, ACS, Los Angeles, CA, March 1974.

Huntzicker, J. J., S. K. Friedlander, and C. I. Davidson: Material Balance for Automobile-emitted Lead in Los Angeles Basin, Env. Sci. and Tech., 9, 448, 1975.

Huntzicker, J. J., and C. I. Davidson: Atmospheric Trace Metal Flows in the Los Angeles Basin: Zn, Cd, and Ni, in Air-Water-Land Relationships for Selected Pollutants in Southern California, J. J. Huntzicker, S. K. Friedlander, and C. I. Davidson, Eds., Final Report to the Rockefeller Foundation, W. M. Keck Laboratories, California Institute of Technology, Pasadena, CA, August, 1975, p.79.

Islitzer, N. F., and R. K. Dumbauld: Atmospheric Diffusion-deposition Studies Over Flat Terrain, Int. J. Air Water Poll., 7, 999, 1963.

Johnson, D. B.: Ultragiant Urban Aerosol Particles, Science, 194, 941, 1976.

Kitamoto, A., and Y. Takashima: Transport Theory of Aerosol in Turbulent Flow, Bull. Tokyo Inst. Tech., 121, 41, 1974a.

Kitamoto, A., and Y. Takashima: Deposition Rate of Aerosol Particles from Turbulent Flow Through Vertical Annuli, Bull. Tokyo Inst. Tech., 121, 67, 1974b.

Kloke, A., and K. Reibartsch: Verunreinigung von Kulturpflanzen mit Blei aus Kraftfahrzeugabgasen, Die Naturwissenshaften, 51, 367, 1964.

Lagerwerff, J. V., and A. W. Specht: Contamination of Roadside Soil and Vegetation with Cadmium, Nickel, Lead and Zinc, Env. Sci. and Tech., 4, 583, 1970.

Landahl, H. D., and R. G. Herrmann: Sampling of Liquid Aerosols by Wires, Cylinders, and Slides, and the Efficiency of Impaction of the Droplets, J. Coll. Int. Sci., 4, 103, 1949.

Lee, Jr., R. E., and S. S. Goranson: "Variations in the Size of Airborne Particulate Matter Over a Three Year Period," 68th Annual Meeting AIChE, Los Angeles, November 1975.

Lee, Jr., R. E., S. S. Goranson, R. E. Enrione, and G. B. Morgan: National Air Surveillance Cascade Impactor Network, II. Size Distribution Measurements of Trace Metal Components, Env. Sci. and Tech. 6, 1025, 1972.

Hudson, J. G.: "Surface Exchange of Cloud Condensation Nuclei," Ph.D. Thesis, University of Nevada at Reno, July 1976.

Lee, Jr., R. E., R. K. Patterson, and J. Wagman: Particle-size Distribution of Metal Components in Urban Air, Atmos. Envir., 2, 288, 1968.

Lee, Jr., R. E., R. K. Patterson, W. L. Crider, and J. Wagman: Concentration and Particle Size Distribution of Particulate Emissions in Automobile Exhaust, Atmos. Env., 5, 225, 1971.

Leh, H. O.: Verunreingungen von Kulturpflanzen mit Blei aus Kraftfahrzeugabgasen, Gesunde Pflanzen, 18, 21, 1966.

Lininger, R. L., R. A. Duce, J. W. Winchester, and W. R. Matson: Chlorine, Bromine, Iodine, and Lead in Aerosols from Cambridge, Massachusetts, J. Geophys. Res., 71, 2457, 1966.

Lundgren, D. A: Atmospheric Aerosol Composition and Concentration as a Function of Particle Size and Time, J. APCA, 20, 603, 1970.

Lundgren, D. A., and H. J. Paulus: "The Mass Distribution of Large Atmospheric Particles--and How It Relates to What a High Volume Sampler Collects," 66th Annual Meeting, Air Pollution Control Association, Chicago, Illinois, June 1973.

Lundgren, D. A., and H. J. Paulus: "Direct Determination of the Total Atmospheric Aerosol Mass Distribution," Division of Environmental Chemistry, 167th Meeting, ACS, Los Angeles, California, March 1974.

Marten, G. C., and P. B. Hammond: Lead Uptake by Bromegrass from Contaminated Soils, Agron. J., 58, 553, 1966.

May, K. R.: Calibration of a Modified Andersen Bacterial Aerosol Sampler, Applied Microbiology, 12, 37, 1964.

McCrone, W. C., and J. G. Delly: Particle Atlas, Edition 2, Volume 2, Ann Arbor Science Publishers, Inc., Ann Arbor, Mich., 1973.

Megaw, W. J., and R. C. Chadwick; 1957, data published by Chamberlain, A. C., 1960.

Motto, H. L., R. H. Daines, D. M. Chilko, and C. K. Motto: Lead in Soils and Plants: Its Relationship to Traffic Volume and Proximity to Highways, Env. Sci. and Tech., 4, 231, 1970.

Mueller, P. K., H. L. Helwig, A. E. Alcocer, W. K. Gong, and E. E. Jones, "Concentration of Fine Particles and Lead in Car Exhaust," ASTM Special Technical Publication No. 352, 1964.

Ninomiya, J. S., W. Bergman, and B. H. Simpson: "Proceedings of the Second International Clean Air Congress," H. M. Englund and W. T. Beery, Eds., Academic Press, New York, 1971, P.663.

Owen, P. R.: Dust Deposition From a Turbulent Airstream, Int. J. Air Poll., 3, 8, 1960.

Owen, P. R., and W. R. Thomson: Heat Transfer Across Rough Surfaces, J. Fluid Mech., 15, 321, 1963.

Page, A. L., T. J. Ganje, and M. S. Joshi: Lead Quantities in Plants, Soil and Air Near Some Major Highways in Southern California, Hilgardia, 41, 1, 1971.

Pasquill, F.: Atmospheric Diffusion, J. Wiley and Sons, New York, 1974, p.72.

Patterson, C. C.: unpublished data, 1975.

Patterson, C. C., and D. Settle: Contribution of Lead Via Aerosol Deposition to the Southern California Bight, J. Rech Atmospheriques, International Symposium on Chemistry of Sea/Air Exchange Processes, Nice, France, 1974.

Peirson, D. H.: 1973, published in Chamberlain, A. C., 1974.

Peirson, D. H., P. A. Cawse, L. Salmon, and R. S. Cambray: Trace Elements in the Atmospheric Environment, Nature, 241, 252, 1973.

Pierson, W. R., and W. W. Brachaczek: Airborne Particulate Debris from Rubber Tires, Rubber Chem. and Tech., 47, 1275, 1974.

Perry, R. H., and C. H. Chilton: Chemical Engineers' Handbook, McGraw-Hill, New York, 1973, p.5/22.

Pruitt, W. O., D. L. Morgan, and F. J. Lourence: Momentum and Mass Transfers in the Surface Boundary Layer, Q. J. Roy Met. Soc., 99, 370, 1973.

Rabinowitz, M.: Plant Uptake of Soil and Atmospheric Lead in Southern California, Chemosphere, 4, 175, 1972.

Rains, D. W., and J. Thornton: "Vegetation as an Indication of Long-Term Lead Pollution, Its Extent and Effect," Department of Agronomy and Range Science, University of California, Davis, CA, 1970.

Rao, A. K.: "An Experimental Study of Inertial Impactors," Ph.D. Thesis under K. T. Whitby, Particle Technology Laboratory, Mechanical Engineering Department, Univ. of Minnesota, June 1975, p.100.

Roberts, P. J. W., P. M. Roth, and C. L. Nelson: "Contaminant Emissions in the Los Angeles Basin," Appendix A of "Development of a Simulation Model for Estimating Ground Level Concentrations of Photochemical Pollutants," Rep. 71 SAI-6, Systems Applications, Inc., Beverly Hills, Calif., 1971.

Roberts, P. T.: "Gas-to-Particle Conversion: Sulfur Dioxide in a Photochemically-Reactive System," Ph.D. Thesis, California Institute of Technology, 1975.

Robinson, E., and F. L. Ludwig: Particle Size Distribution of Urban Lead Aerosols, J. APCA, 17, 664, 1967.

Rolfe, G. L., and A. Haney: "An Ecosystem Analysis of Environmental Contamination by Lead," Metals Task Force Research Report No. 1, Institute for Environmental Studies, University of Illinois at Urbana-Champaign, August, 1975.

Schlicting, H.: Boundary Layer Theory, McGraw-Hill, New York, 1960, p.79.

Sehmel, G. A.: Particle Deposition from Turbulent Airflow, J. Geophys. Res., 75, 1766, 1970.

Sehmel, G. A.: Particle Diffusivities and Deposition Velocities Over a Smooth Horizontal Surface, J. Coll. Int. Sci., 4, 891, 1971.

Sehmel, G. A.: Turbulent Deposition of Monodisperse Particles on Simulated Grass, in Assessment of Airborne Particles, T. T. Mercer, P. E. Morrow, and W. Stober, Eds., Charles C. Thomas, Springfield, Ill., 1972, p.48.

Sehmel, G. A.: Particle Eddy Diffusivities and Deposition Velocities for Isothermal Flow and Smooth Surfaces, J. Aerosol Sci., 4, 125, 1973.

Sehmel, G. A.: Particle Resuspension from an Asphalt Road Caused by Car and Truck Traffic, in Atmosphere-Surface Exchange of Particulate and Gaseous Pollutants (1974), Energy Research and Development Administration, NTIS no. CONF-740921, 1976, p.859.

Sehmel, G. A., and W. H. Hodgson: Predicted Dry Deposition Velocities, in Atmosphere-Surface Exchange of Particulate and Gaseous Pollutants (1974), Energy Research and Development Administration, NTIS no. CONF-740921, 1976, p.399.

Sehmel, G. A., S. L. Sutter, and M. T. Dana: Dry Deposition Processes, Battelle NW Laboratory Report 1751 Part 1, 1973, p. 43.

Sehmel, G. A., and F. D. Lloyd: Resuspension of Plutonium at Rocky Flats, in Atmosphere-Surface Exchange of Particulate and Gaseous Pollutants (1974), NTIS no. CONF-740921, 1976, p.757.

Sehmel, G. A., S. L. Sutter, and M. T. Dana: Dry Deposition Processes, Battelle NW Laboratory Report 1751 Part 1, 1973, p.43.

Servant, J.: Deposition of Atmospheric Lead Particles to Natural Surfaces in Field Experiments, in Atmosphere-Surface Exchange of Particulate and Gaseous Pollutants (1974), Energy Research and Development Administration, NTIS no. CONF-740921, 1976, p.87.

Shepherd, J. G.: Measurements of the Direct Deposition of Sulphur Dioxide onto Grass and Water by the Profile Method, Atmos. Envir., 8, 69, 1974.

Shuck, E. A., and J. K. Locke: Relationship of Automotive Lead Particulate to Certain Consumer Crops, Env. Sci. and Tech., 4, 324, 1970.

Slinn, W. G. N.: Dry Deposition and Resuspension of Aerosol Particles - A New Look at Some Old Problems, in Atmosphere-Surface Exchange of Particulate and Gaseous Pollutants (1974), Energy Research and Development Administration, NTIS no. CONF-740921, 1976, p.1.

Sutton, O. G.: Micrometeorology, McGraw-Hill, New York, 1953, p.82.

Ter Haar, G.: Air as a Source of Lead in Edible Crops, Env. Sci. and Tech., 4, 226, 1970.

Ter Haar, G., D. L. Lenane, J. N. Hu, and M. Brandt: Composition, Size and Control of Automotive Exhaust Particulates, J. APCA, 22, 39, 1972.

Tufts, B. J.: Determination of Particulate Lead Content in Air, Analytical Chem., 31, 238, 1959.

Turner, N. C., P. E. Waggoner, and S. Rich: Removal of Ozone From the Atmosphere by Soil and Vegetation, Nature, 250, 486, 1974.

Unsworth, M. H., and D. Fowler: Field Measurements of Sulphur Dioxide Fluxes to Wheat, in Atmosphere-Surface Exchange of Particulate and Gaseous Pollutants (1974), Energy Research and Development Administration, NTIS no. CONF-740921, 1976, p.342.

Watson, H. H.: Errors Due to Anisokinetic Sampling of Aerosols, Amer. Ind. Hyg. Assoc. J., 15, 5, 1954.

Wells, A. C., and A. C. Chamberlain: Transport of Small Particles to Vertical Surfaces, Brit. J. Appl. Phys., 18, 1793, 1967.

Wong, J. B., and H. F. Johnstone: "Collection of Aerosols by Fiber Mats," Technical Report 11, Eng. Exp. Station, University of Illinois, 1953.